University of Windsor
Scholarship at UWindsor

Electronic Theses and Dissertations Theses, Dissertations, and Major Papers

1974

Analytical and experimental investigations of flow around of a spur-dike.

Nabil Aly. Zaghloul
University of Windsor

Follow this and additional works at: https://scholar.uwindsor.ca/etd

Recommended Citation

Zaghloul, Nabil Aly., "Analytical and experimental investigations of flow around of a spur-dike." (1974). *Electronic Theses and Dissertations*. 1183.
https://scholar.uwindsor.ca/etd/1183

This online database contains the full-text of PhD dissertations and Masters' theses of University of Windsor students from 1954 forward. These documents are made available for personal study and research purposes only, in accordance with the Canadian Copyright Act and the Creative Commons license—CC BY-NC-ND (Attribution, Non-Commercial, No Derivative Works). Under this license, works must always be attributed to the copyright holder (original author), cannot be used for any commercial purposes, and may not be altered. Any other use would require the permission of the copyright holder. Students may inquire about withdrawing their dissertation and/or thesis from this database. For additional inquiries, please contact the repository administrator via email (scholarship@uwindsor.ca) or by telephone at 519-253-3000ext. 3208.

Analytical and Experimental Investigations
of
Flow Around A Spur-Dike

A Dissertation

Submitted to the Faculty of Graduate Studies in Partial
Fulfillment of the Requirements for the Degree
of Doctor of Philosophy in Civil Engineering
at the University of Windsor

by

Nabil Aly Zaghloul

Windsor, Ontario, Canada
1974

© Nabil Aly Zaghloul 1974

524130

To my Parents

ABSTRACT

A mathematical model simulating the local scour around a spur-dike is presented. The model predicts both the depth and shape of the scour hole, and consists of two relaxation stages: a) two dimensional relaxation in time; b) relaxation of the third dimension (depth). In the first stage, the Helmholtz-Poisson form of the Reynolds equations, with constant eddy viscosity, are solved by an alternating direction implicit finite difference scheme until a relatively stable separation pattern is obtained. In the second stage, the stream function and vorticity are relaxed in space only, and the depth is permitted to change on the basis of balancing the applied shear and bed resistance.

A stability analysis for the numerical technique is introduced. Confirmation of the model was obtained by several flume experiments. The experimental data were utilized to establish the important factors affecting the phenomenon, and an empirical formula for the maximum depth of scour was derived. High velocity and vorticity were observed in the region of the dike's nose and along the separation line. It was found that the vorticity, velocity and turbulence are the principal causes of erosion.

ACKNOWLEDGEMENTS

The writer wishes to express his gratitude to his advisor, Dr. S.P. Chee, for his guidance throughout the course of this study.

The writer is greatly indebted to his co-advisor, Dr. J.A. McCorquodale, for supervising the theoretical part of this project. His valuable suggestions as well as his generous financial contribution are sincerely appreciated.

Thanks are due to Mr. R. Patil of the Computer Center, at the University of Windsor, for his co-operation and assistance. Thanks are also due to the Civil Engineering laboratory technicians, Mr. G. Michalczuk and Mr. P. Feimer, for their help during the experimental programme.

Finally, the writer is grateful to the Department of Civil Engineering at the University of Windsor, and the National Research Council of Canada for the opportunity of carrying out this research.

TABLE OF CONTENTS

LIST OF FIGURES

Page

LIST OF PHOTOGRAPHS

LIST OF TABLES

CHAPTER I

INTRODUCTION

1.1. Objective

The purpose of this thesis is the development of a finite difference model to simulate the local scour phenomenon around a spur-dike in a granular bed material.

1.2 Definition of the Problem

A spur-dike is an obstruction, constructed at an angle to the flow direction, extending from the bank of an alluvial channel to the main flow. It serves one or more of the following functions: a) training of the stream flow; b) protection of the stream bank from erosion; c) improvement of depth for navigation; d) dam closures.

1.3 Motivation

The mechanism of local scour around an obstruction in a flowing stream is influenced by such factors as the local increase in stream velocity, the vortices produced by the obstruction, the turbulence of the flow and the bed material. The problem of local scour around a spur-dike is a complex phenomenon that involves interaction of fluid forces with a mobile bed material (see figure 1.1).

Model studies of such a phenomenon have often been used to predict the prototype scour depths and patterns, and numerous (1,3,5,15,16) data are available. Although model studies are subjected to uncertain scale effects, the writer has not found, in the literature, many theoretical attempts to evaluate the experimental findings. Numerical solutions have never been applied to the problem of scour around obstructions.

This thesis presents a numerical model for flow past a spur-dike to aid in the interpretation and scaling-up of model data.

1.4 The Approach in General

The flow around an obstruction in an alluvial channel is governed by unsteady flow conditions due to the erosion of the bed material. The phenomenon involves four dimensional parameters; the spacial coordinates x, y, z in addition to the time, t. Thus, it would be rather difficult to obtain a solution in a one stage model.

In order to tackle the problem the treatment was developed in two phases or stages which produce the final solution. The first phase is time dependent and involves the x and y dimensions and will be referred to as the two-dimensional phase. The mathematical model simulating this phase deals with the unsteady flow condition, past a sheet pile obstruction, resulting from flow separation. The usual stream function was introduced and the Reynolds equations were transformed to the form of a Helmholtz vorticity equation and a Poisson equation relating stream function to vorticity. A finite difference scheme with a regular computational grid consisting of about 1400 nodes was utilized in the solution. The Helmholtz and Poisson difference equations were solved alternately to obtain the variations in vorticity and stream function with time. The two-dimensional solution was continued until the flow pattern in the neighbourhood of the dike became relatively steady; thereafter the second, depth dependent, phase was started to deduce the scour depth, z. This phase is treated in a separate model which will be identified as the three-dimensional model. The stream function was redefined in terms of the depth-averaged velocity, and a bed shear function was computed from the local velocity, turbulence, and vorticity. The local depth was adjusted to reduce the difference between the local shear and the local bed resistance to zero.

An extensive experimental programme was conducted, to verify the numerical solution and obtain empirical correlations.

Computed scour patterns for different flow conditions and different opening ratios are presented and compared to experimental scour patterns.

The IBM 360/65 computer facilities, at the University of Windsor, were used in executing all the computations in the mathematical models.

CHAPTER II

BACKGROUND AND REVIEW OF LITERATURE

2.1 Definitions

Scour: may be defined as the enlargement of a flow section by the removal of material comprising the boundary through the action of the moving fluid. This phenomenon generally takes place when water flows on a movable bed. Implicit in this definition is the fact that the moving fluid exerts shearing and normal forces on the boundary particles, thereby causing their movement. The amount of material which the fluid can move or transport, in unit time, is termed the capacity of the flow.

Localized Scour: is regarded as the erosive action in a stream bed caused by an obstruction. A scour hole develops when the capacity of the water to carry sediment is greater than the incoming supply. Hence, the stream bed material is forced into motion by the local increase in transport capacity, which further disrupts the normal flow pattern. Therefore, localized scour occurs where the flow is being accelerated as it moves past the obstruction in the stream, or where large vortices are generated as the flow separates from the obstruction.

2.2 Types of Localized Scour

Local scour occurs under a variety of conditions in alluvial channels and rivers, and the following cases have been observed:

a) Scour in a Meandering River: Meandering channels usually occur on lower, gentler slopes towards a river mouth. Secondary currents occur at each meander loop and cause scouring of the outer bank and deposition on the inner bank. A consequence of this phenomenon is that the meandering loops extend outwards and gradually migrate downstream.

b) Scour Around the Foot of a Hydraulic Structure:

i) Scour around bridge piers and abutments: when designing a bridge to span a stream where the supporting material for the foundation is erodible, and where it is neither feasible nor justifiable to extend the foundation to bed rock, the engineer is confronted with the problem of designing foundations that must be economical and at the same time safe from washout due to scour. During floods, the scouring, or erosion, of the supporting material from the vicinity of the foundations may permit them to tilt or settle and cause partial or complete failure of the bridge. A number of analytical and laboratory investigations have been conducted in order to predict the maximum depth of scour according to different pier geometries (39), and different flow conditions (27,28,29,30,40,49). Also, other investigations were conducted in order to reduce the amount of scour around the pier base by using shields or arrestor devices (39,47,50).

ii) Scour Around Spur-Dikes: A spur-dike is an armored projection in an alluvial channel. Once the stream is obstructed by a spur-dike, a scour hole is developed in the vicinity of the dike.

c) Scour by Jets: This is the case in which there is no sediment supplied into the scour hole. The water jet may be classified under two conditions:

i) Two dimensional horizontal jet, as in the case of a water jet issuing underneath a sluice gate opening, the stilling basin of a spillway or a weir and the outlet of a culvert. The water jet will attack the erodible bed at the end of the solid floor. Local scour occurs downstream the solid floor and a scour hole is developed. Deep scour holes might result in undermining and failure of the solid floor.

ii) Vertical jet, as in the case of a water jet issuing from a solid (full) or hollow circular (annular) jet impinging vertically on a flat erodible boundary. Other typical examples are associated with free overfalls, flip buckets and ski-jump spillways.

2.3 Materials Composing the Stream Bed

Bed materials, from the point of view of erosivity, may be classified as:
i) non-cohesive sediments
ii) cohesive sediments

Non-Cohesive Sediments: are those of discrete particles, the movement of which, for given erosive forces, depends only on particle properties, such as shape, size and density, and on the relative position of the particle with respect to surrounding particles (7,17,19,38). Sands and gravels of stream beds or beaches that have been previously transported, or deposits laid down by wind or water, are included in this class.

Cohesive Sediments: are those for which the resistance to initial movement or erosion depends also on the strength of the cohesive bond between particles. This resisting force may far outweigh the influence of the characteristics of the individual particles. This class includes soils containing clay, as may be found in residual soils. In a broad sense, cohesionless sediments may be considered cohesive if soil bond is induced by a root network and/or a vegetative cover, either natural or cultivated (6,17). The property of cohesiveness, as related to erosion-resisting characteristics of a soil mass, introduces an important factor into the relationship between the erosive forces, inherent in the flow, and the physical properties of the soil particles that have not been evaluated (12). Because the forces required to erode or scour cohesive sediments are generally greater than those for non-cohesive sediments with approximately the same grain size, the rate and extent of scour depend on the property of cohesion rather than the characteristics of the particles. Once the bond has been broken, the individual particles become a part of the non-cohesive population. Further deposition, scour, or transport become functions of the properties of these separate particles.

2.4 Mechanism of Local Scour

2.4.1 Fundamental Principles of Scour

Laursen (27), in his paper "Observations on the Nature of Scour", has crystallized many of the scattered notions of scour into the following general principles:

1) The rate of scour will equal the difference between the capacity for transport out of the scoured area and the rate of supply of material to that area.

2) The rate of scour will decrease as the flow section is enlarged.

3) There will be a limiting extent of scour for given initial conditions.

4) The limit of scour will be approached asymptotically with respect to time.

These are the general principles which should be basic to any detailed analysis of local scour. The premise necessary to form the first principle is the conservation of matter, on the assumption that there is no distinction between the material supplied and the material scoured out of the scour area, and the rate of removal must equal the local capacity of the flow. The remaining principles can be deduced from the fact that, even if the bulk flow is constant with time (i.e. steady flow condition), the change in the boundary configuration, because of scour, results in unsteady flow conditions along the boundary. In general, the enlargement of the flow section will result in a reduction of the shear velocity along the boundary and therefore, the capacity for transport diminishes. The rate of scour must then decrease as the difference between the capacity and the rate of supply decreases. Implicit in the foregoing statement is the notion of a limiting extent for scour. The rate of scour will equal zero when the capacity is exactly equal to supply. That limit exists for the case in which material is supplied to the scoured area if the capacity decreases, as the flow section enlarges, until it equals the supply rate at a finite boundary position. For the case in which there is no supply to the hole, an additional assumption is needed - that below some critical velocity the capacity is zero. There must then be some finite boundary position for which the velocity decreases to this critical value and the rate of scour becomes zero. This position satisfies the notion of limit. Establishing the existence of a limit to the extent of scour gives no indication as to the time necessary to attain the limit. It can be shown that the limit must be approached asymptotically. If the limit were to be reached in a finite time, the scour must continue beyond the limit, or deposition (negative scour) must occur after the limit is reached, or the scour process must be described by two functions - one before and one after the limit. None of these possibilities is admissible. Deposition would require a two-valued relation between the capacity and the difference between the actual and the limiting boundary. Continued scour beyond the limit is not compatible with the concept of limit. Unless some new force is added there is no reason why the scour function should change at the limit. If the limit is approached asymptotically, however, no matter how small the difference between the actual and limiting boundary, there is always a small rate of scour so that the limiting position is approached more closely. Not until the limit is reached at infinite time does the rate of scour become zero. This process is orderly and continuous. It would appear that the above argument is only true for homogeneous materials; however, a bed material consists of discrete particles of random shape and size. Thus, as the scour progresses all the erodible particles which are of large but finite number could be eroded in a finite time; the remaining non-erodible larger particles would then form an armour layer.

2.4.2 Local Scour Equation

By using symbolic terms, the first general characteristic postulated by Laursen can be written as an equation of scour, in the form

$$\frac{d}{dt}\left[f(B)\right] = g(B) - g(S) \quad . \tag{2.1}$$

where B is a mathematical description of the boundary so that $\frac{d}{dt}\left[f(B)\right]$ is the rate of scour;

g(B) is the capacity of the flow to transport sediment out of the scour hole as a function of the boundary position;

and g(S) is the rate at which sediment is supplied to the scour hole by undisturbed flow.

Equation 2.1 describes not only the case of scour, but that of equilibrium, transport and deposition as well. The equation is interpreted as follows:

1) If the local rate of transport is greater than the rate of supply, $\frac{d}{dt}\left[f(B)\right]$ is positive and scour results.

Two cases can be considered:

a) clear water scour, i.e. $g(B) > 0$ and $0 = g(S) << g(B)$

b) scour with continuous sediment motion, i.e. $g(B) > g(S) > 0$.

2) If the local rate of transport is less than the rate of supply, deposition occurs, and $\frac{d}{dt}\left[f(B)\right]$ is negative.

3) When the local rate of transport is equal to the supply including the case in which they are both identically zero, $\frac{d}{dt}\left[f(B)\right]$ is equal to zero and the bed is stable.

For the longitudinal and cross-sectional equilibrium profiles of alluvial channels, two concepts are under consideration: one is termed the static equilibrium theory, or the tractive force theory; the other is termed the dynamic equilibrium theory, the live-bed theory, or the regime theory. The static equilibrium theory requires that the critical shear stress on the bed be constant at all points along the channel; the dynamic equilibrium theory requires that the sediment load passing through a cross-section of the upstream end be equal to that of all points along the channel. The application of equation 2.1, in general, depends on the establishment of mathematical functions to describe the bed geometry, the capacity, and supply, as functions of the flow conditions and time. Due to the difficulty in finding such descriptions, researchers resorted to experiments to determine these functions, and were compelled to manipulate different forms of equation 2.1 to obtain the maximum depth of scour.

2.5 Classification of Scour Hole Development

2.5.1 Clear Water Scour

This is the case in which no sediment is supplied into the scour hole and is usually connected with jets. Many attempts have been made to describe the change in bed configuration as a function of time and the limiting extent of scour for the case of a zero sediment supply. The pioneering investigation by Rouse (37), of the scour of a bed of non-cohesive sediment by a vertical jet of clear-water indicates the following facts:

a) The depth of scour in a uniform material is dependent primarily upon the size and velocity of the jet, the fall velocity of the sediment and the duration of the scour.

b) The relative rate of scour produced by a given jet at a given stage depends only upon the ratio of jet velocity to fall velocity, approaching zero as this ratio approaches unity.

c) Selective sorting of graded material occurs, so that with a wide variation in size of bed material the bottom of the hole gradually becomes paved with a progressively coarser material, thus decreasing the effective fall velocity of the sediment and reducing the scour rate.

d) If sediment is carried in by the jet at exactly the rate at which a clear jet would scour, the scour hole will be stabilized; by inference, an increase in rate of sediment inflow would cause a reversal in the scour process (i.e. deposition) and hence gradual filling of the hole until equilibrium is again established.

Laursen (27), showed that the scour pattern caused by submerged jets was similar in shape as the scour progressed and, hence, similarity of scour profiles was established by plotting dimensionless coordinates of the profiles using the horizontal distance from the inlet to the crest of the dune as a repeating variable. Except for the profiles representative of an initial transitory stage of scour, all the profiles of a run superpose if plotted in this manner. Moreover, the profile forms for all runs of any one sand were almost identical and the forms for the various sands differed only slightly.

Ahmed (2) in his research, "Mechanism of Erosion Below Hydraulic Works", confirmed Laursen's results by proving that, in case of concrete floors of sufficient lengths, such as are usually constructed for hydraulic works, the collective effect of the eddies on the erodible bed is such that scour profiles of equal depths, developed by different discharges, are similar irrespective of the sand sizes.

Experiments on scour by vertical solid and hollow jets and scour below a free overfall have been reported by Doddiah et al (9). Johnson (21), examined the scour pattern caused by the flow over an idealized spillway in which both the sizes of spillway and sediment were varied. Torapora (48), reported results of experiments on scour of sand bed by a horizontal jet. In all of these investigations, the scouring agency, the jet, was idealized so that the resulting flow pattern could be described by two parameters, the velocity and size of the jet.

2.5.2 Scour with Continuous Sediment

Scour around bridge piers, abutments and spur-dikes, and scour due to long constriction are typical examples of scour with continuous sediment. In such cases, sediment is continuously supplied to the scour area by the bed load movement upstream the scour hole. Investigations have been conducted in order to describe the variation of the extent of scour with time and the final equilibrium or limiting configuration when the sediment supply is not zero (15, 28, 44). The results show that the extent of scour is a function of time and the characteristics of the flow and the sediment; the same as for the case of clear water scour. The limiting configuration is reached if $\frac{d}{dt}\left[f(B)\right] = 0$, i.e. the rate of transport in the scoured region must be equal to the rate of supply. Equation 2.1 can be used to provide a solution at the limiting condition of scour. Straub (44,45,46), treated the special case of the equilibrium depth obtaining in long channel contractions. The procedure was equivalent to setting $\frac{d}{dt}\left[f(B)\right] = 0$ and solving for the limiting condition of scour. At the limit the capacity for transport in the contracted, scoured section must equal the rate of supply - which is equal to the capacity for transport in the uncontracted section. The contraction was sufficiently long that essentially uniform flow was established. The flow was described by Manning's formula with the same value of Manning's (n) in the contracted and uncontracted sections. Thus,

$$Q = \frac{1.49}{n} B_1 D_1^{2/3} S_1^{1/2} = \frac{1.49}{n} B_2 D_2^{2/3} S_2^{1/2} \tag{2.2}$$

The capacity was described by a sediment transport formula of the DuBoys type (10) with a coefficient, ϕ, experimentally determined as follows:

$$g(B) = \phi B_2 \tau_2 (\tau_2 - \tau_c) = \phi B_1 \tau_1 (\tau_1 - \tau_c) \tag{2.3}$$

where $\tau_1 = \gamma D_1 S_1$

$\tau_2 = \gamma D_2 S_2$

Upon combining Equations 2.2 and 2.3, a formula for the relative depth, D_2/D_1, can be written as:

$$\frac{D_2}{D_1} = \left[\frac{B_1}{B_2}\right]^{3/7} \left\{ \frac{-\tau_c/\tau_1 + \left[(\tau_c/\tau_1)^2 + 4(1-\tau_c/\tau_1)\ B_1/B_2\right]^{\frac{1}{2}}}{2(1-\tau_c/\tau_1)} \right\}^{3/7} \tag{2.4}$$

where τ_c is the critical tractive force for sediment;

τ is the tractive force;

D is the depth;

B is the width;

S is the slope;

the subscripts 1 and 2 refer to the uncontracted and contracted sections respectively;

n is the Manning roughness coefficient assumed to be the same in both sections; and

ϕ is the DuBoys transport parameter, the magnitude of which depends on the sediment size, and is the same in both sections.

Laboratory experiments confirmed this relationship very closely. Such confirmation could be expected since the coefficients in the transport equation were determined under similar conditions. Whether equation 2.4 will apply to field conditions depends not on equation 2.1, which must be valid, but on equation 2.2 and especially equation 2.3, which are approximate. Equation 2.4, shows that for the practical values of the contraction parameter, the relative depths are essentially independent of the ratio τ_c/τ_1. Thus, with τ_c very small compared to τ_1, or τ_c equal to 0, equation 2.4 is very nearly Griffith's equation (18),

$$\frac{D_2}{D_1} = \left[\frac{B_1}{B_2}\right]^{0.637} \tag{2.5}$$

which is based on field observations.

This agreement among analysis, laboratory data, and field observations, indicates that even an approximate knowledge of transport and flow conditions can lead to useful results.

A problem similar to the one of stream constrictions involves the equilibrium scour around bridge piers, abutments and spur-dikes. For such conditions, the scour is essentially localized so that the assumption of uniform flow is not valid. Recently, Gill (15), in his paper "Erosion of Sand Bed Around Spur-Dikes", proposed the so-called kinematic model to predict the equilibrium scour depth. Based on Straub's work, Gill modified equation 2.4, using another transport equation of the form

$$g(B) = CBq_S(\tau/\tau_c-1)^N \tag{2.6}$$

where

C = an empirical constant

$q_S = \sqrt{g(S_s-1)d^3}$

g = acceleration due to gravity

S_s = specific gravity of the bed material

d = mean size of bed material

N = a numerical exponent, that takes various values to produce various well known bed load equations.

Again, combining equations 2.2 and 2.6 and rearranging the parameters, an equation similar to equation 2.4 can be obtained. Thus.

$$\frac{D_2}{D_1} = \alpha_1 \left[\frac{B_1}{B_2}\right]^{6/7} \left\{\frac{1}{(B_1/B_2)^{1/N}(1-\tau_c/\tau_1) + \tau_c/\tau_1}\right\}^{3/7} \qquad (2.7)$$

Since equation 2.7 has been obtained from a simple case of long constriction, Gill proposed a coefficient, α_1, so that his equation can be used in the case of local erosion around spur-dikes. According to his experiments, this coefficient was found to depend on the upstream flow depth, D_1, and the size of bed material, d, and is given by the following empirical equation

$$\alpha_1 = 8.375(d/D_1)^{0.25} \qquad (2.8)$$

Schneible (39), conducted a model study in order to investigate the effect of bridge pier geometry on the relative depth of scour. A model study of scour around bridge piers and abutments was reported by Laursen and Toch (28), in which the depth of scour around a model bridge pier was measured for a rather wide range of velocities and sediment sizes. It was found that the effect, if any, of the velocity and the sediment size is so small as to be within the precision of the measuring instrument. The effect of the depth of flow is considerable, although the relationship is not one of direct proportionality. These experimental results can be rationalized in the light of the general characteristics of the scour process. For the velocity to have no effect on the equilibrium depth of scour, the capacity for transport of the spiral roller at the scour depth must always equal the rate of sediment supply as furnished by the bed-load movement in the flume. This can be true only if the capacity of the roller and the capacity in the flume bear the same relation to the mean velocity of flow. In the scour hole, the velocity at the grain level is a function of the velocity of the roller; in the flume, it is a function of the mean velocity. The velocity of the roller, as a first approximation, could be expected to bear a constant ratio to the mean velocity of flow. Therefore, the velocity at the level of the moving grains in the scour hole and in the flume should result in balanced capacities regardless of the absolute magnitude of the mean velocity. The lack of dependence of the depth of scour on sediment size was explained on a similar basis. If all depths and velocities are assumed the same, and the mean size of the bed is suddenly increased, so as to halve the rate of sediment transport upstream, velocities and shear stresses remain unchanged, but because of the increase in sediment size they are everywhere half as effective in moving the sediment as they were previously. It follows, therefore, that the rate of scour inside the scour hole will also be halved, and that the balance between sediment out and into the hole will remain unchanged. The scour hole will therefore remain in equilibrium without further scouring or filling. A similar analysis will show that the depth of scour should increase with the depth of flow. As a result of the vertical velocity distribution, the velocity at the level of the moving sand grains in the flume will decrease as the depth of flow increases. Since this velocity is the active agent of transport, the rate of sediment transport in the flume will also decrease. For an equilibrium depth of scour to be attained, the capacity of the roller must similarly decrease. The vertical velocity distribution has only a secondary influence on the roller velocity. The roller must, therefore, increase in size to be reduced sufficiently in velocity, and thereby in capacity - resulting in a greater depth of scour for greater depths of flow. Similar results were obtained by Ahmed (1), in model studies of spur-dikes. In a model of the Sutlej River, the spur projects into the channel one-third of the channel width. Two sands (mean diameters 0.354 mm and 0.695 mm) were used. The results show that: a) the ultimate scour was unaffected by changing the grade, and b) the rate of development of scour was much more rapid with the finer sand. In conclusion, considering the case of scour with continuous sediment motion (i.e. the rate of supply is not equal to zero), the limiting or equilibrium depth of scour depends only on the depth of flow. The velocity and sediment size do not have any appreciable effect on the equilibrium depth. In the case of clear water scour, (i.e. the rate of supply is zero), the scour hole will deepen until the shear stress on the walls of the hole drops to the threshold value appropriate to the bed material. There is then no movement of sediment into or out of the hole. The finer the sediment the lower is this threshold stress and the deeper the hole must become in order to lower the velocity and shear inside the hole to the correct value. In the clear water scour, therefore, the depth of scour is greater for fine sediments than for coarse. In terms of this discussion, clear water flow means any flow in which the bed material upstream of the obstruction is undisturbed, even though the water may contain a heavy suspended load of a material finer than the bed material. Grade, et al (16), reported on their study of scour around spur-dikes, that the size of sediment has an influence both on the rate of scour and the maximum scour depth. They represent that effect by the drag coefficient of the sediment particle. It is the writer's conviction that the use of the drag coefficient as a measure of sediment properties is not a valid criterion. The drag coefficient formula as it stands in Grade's paper is derived for a drag flow around a single sphere in a laminar flow condition. However, according to Einstein (11), the flow near the bed is turbulent and the bed load movement depends on both the lift and drag forces. In addition, the authors have stated that the equilibrium scour depth depends on the sediment size and they do not agree with Laursen's conclusion (29). Upon investigation of both works, the writer concluded that there is a serious error in Grade's statement due to the fact that Laursen's experiments are extremely accurate because he used a transport flume which provided the condition of scour with continuous sediment motion. On the other hand, the authors are quoted in the following statements:

> "The flume being a non-recirculating type, clear water flowed over the upstream portion of the sand bed from which it picked up some sediment. This scoured material supplied the necessary sediment in the downstream portion of the flume where the spur-dike model was introduced. In a few runs, in which the sediment transport rate was high, sediment was fed manually at the upstream end. The use of a recirculating system would have been better for this investigation, however, it was thought that much

> valuable information could be obtained with the simple non-recirculating system that was available to the writers."

Based on the preceding statement, it would appear that their experiments were conducted under a clear water condition or nearly a clear water condition. This explains, why the sediment size appeared to be an important parameter in their analysis.

A similar argument can be extended to Gill's work (15), who in analyzing his experimental data, mixed the data of the clear water condition with those of the continuous sediment supply condition, which gave rise to the importance of the sediment size as a factor affecting the depth of scour. A closer look on his data for the continuous sediment supply condition, one can find that the equilibrium scour depth is almost identical for two of his experiments, conducted under the same flow conditions and the same dike length; with two different material sizes, (see reference (15), table 1, experiment no. 24, and table 2, experiment no. 13). Also, Gill postulated that for the purpose of design, the distinction between clear water scour and scour caused by bed load transporting flow, can be ignored. The writer cannot agree with Gill, since for the design purposes, the clear water condition is the critical criterion due to the fact that it provides a deeper scour hole as illustrated by Laursen (30) for a relief bridge scour problem, and also by Shen et al (40).

Shen et al (40), emphasized the fact that a blunt-nosed pier induces a strong horseshoe vortex system, which they thought to be the main reason for scour around obstructions. In the case of spur-dikes, the scour is influenced by other factors which appear to be more important than the horseshoe vortex as will be discussed in Chapter III.

CHAPTER III

THEORETICAL DEVELOPMENTS

3.1 General Comment

The developments in this chapter are treated in two parts:

a) The Two-Dimensional Model: which constitutes the time dependent phase and is developed utilizing the Reynolds equations with a constant eddy viscosity.

b) The Three-Dimensional Model: which constitutes the depth dependent phase and is developed from a special treatment of the continuity equation and a stream function based on the depth averaged velocity.

3.2 The Two-Dimensional Model

This model treats the development of the separation pattern around an obstruction in a two-dimensional flow field.

3.2.1 The Equations of Motion for Turbulent Flow

It is assumed, in this analysis, that the fluid is incompressible and follows a Newtonian behaviour with constant viscosity and constant eddy viscosity for a given flow condition.

Considering the external forces acting on an elemental volume of fluid, d$\forall$, the net force due to the stress tensor, σ_{ji}, is $\left[\frac{\partial \sigma_{ji}}{\partial x_j}\right] dV$.

Applying Newton's second law to the volume dV, then

$$\vec{F} = m\,\vec{a} \tag{3.1}$$

or

$$df_i + \left[\frac{\partial \sigma_{ji}}{\partial x_j}\right] dV = m\,a_i = m\,\frac{dU_i}{dt} \tag{3.2}$$

where $m = \rho_f\, dV$

$F_i = \frac{df_i}{dV}$ = external body force per unit volume

Therefore,

$$\rho_f\,\frac{dU_i}{dt} = F_i + \frac{\partial \sigma_{ji}}{\partial x_j} \tag{3.3}$$

The nine stress components, σ_{ji}, form a second-order tensor. This stress tensor can be divided into two parts as follows:

a) $\sigma_{ji} = \mu\, D_{ji}$

where $D_{ji} = \frac{\partial U_i}{\partial x_j} + \frac{\partial U_j}{\partial x_i}$ = the deformation tensor

μ = dynamic viscosity

b) $\sigma_{ji} = -P\,\delta_{ji}$

where P is the normal stress or pressure

δ_{ji} is the Kronecker delta or unit second-order tensor.

Combining both components, the total stress is then

$$\sigma_{ji} = -P\ \delta_{ji} + \mu\ D_{ji} \tag{3.4}$$

Substituting equation 3.4 into equation 3.3 yields

$$\rho_f \frac{dU_i}{dt} = \frac{\partial}{\partial x_j}(-P\ \delta_{ji}) + \frac{\partial}{\partial x_j}(\mu\ D_{ji}) + F_i$$

or

$$\rho_f \left(\frac{\partial U_i}{\partial t} + U_j \frac{\partial U_i}{\partial x_j} \right) = - \frac{\partial P}{\partial x_i} + \mu \frac{\partial D_{ji}}{\partial x_j} + F_i \tag{3.5}$$

For an incompressible fluid, the equation of continuity is

$$\frac{\partial U_i}{\partial x_i} = 0 \tag{3.6}$$

Using equation 3.6, the deformation tensor term of equation 3.5 reduces to

$$\frac{\partial D_{ji}}{\partial x_j} = \frac{\partial^2 U_i}{\partial x_j^2}$$

and hence, equation 3.5 reads (20)

$$\rho_f \left(\frac{\partial U_i}{\partial t} + U_j \frac{\partial U_i}{\partial x_j} \right) = - \frac{\partial P}{\partial x_i} + \mu \frac{\partial^2 U_i}{\partial x_j^2} + F_i \tag{3.7a}$$

or in vector notation

$$\rho_f\left(\frac{\partial}{\partial t} + \vec{U}.\nabla\right)\vec{U} = -\nabla P + \mu\nabla^2\vec{U} + \vec{F} \qquad (3.7b)$$

Equations 3.7a and 3.7b are forms of the general expression for the Navier-Stokes equation for incompressible fluid with a constant viscosity. These equations apply to non-turbulent as well as instantaneous conditions in turbulent flows.

In order to illustrate the turbulent motion and its influence on the mean motion more explicitly, the procedure of Reynolds (20) is invoked. At every point the flow obeys equations 3.6 and 3.7 in which U_i is the instantaneous velocity in the direction i. For laminar flow, U_i corresponds to the local average or the ensemble velocity, $\overline{U}_i$, but in turbulent flow, U_i is made up of an average component, $\overline{U}_i$, and a random component, u_i, i.e.

$$U_i = \overline{U}_i + u_i \qquad (3.8)$$

Similarly, the pressure is expressed as

$$P = \overline{P} + p \qquad (3.9)$$

Introducing equations 3.8 and 3.9 into 3.6 and taking the time average of all terms

$$\frac{\partial}{\partial x_i}\overline{(\bar{U}_i + u_i)} = \frac{\partial \bar{U}_i}{\partial x_i} + \frac{\partial \bar{u}_i}{\partial x_i} = 0 \qquad (3.10)$$

but $\frac{\partial \bar{u}_i}{\partial x_i} = 0$, therefore $\frac{\partial \bar{U}_i}{\partial x_i} = 0$.

Applying the same operation on equation 3.7a yields

$$\rho_f \frac{d}{dt}\overline{(\bar{U}_i + u_i)} = - \frac{\partial}{\partial x_i}(\bar{P} + p) + \mu \frac{\partial^2}{\partial x_j^2}\overline{(\bar{U}_i + u_i)} + \bar{F}_i \qquad (3.11)$$

or

$$\rho_f \left[\frac{\partial \bar{U}_i}{\partial t} + \frac{\partial \bar{u}_i}{\partial t} + \overline{(\bar{U}_j + u_j)\frac{\partial}{\partial x_j}(\bar{U}_i + u_i)}\right] = - \frac{\partial \bar{P}}{\partial x_i} - \frac{\partial \bar{p}}{\partial x_i}$$

$$+ \mu \frac{\partial^2 \bar{U}_i}{\partial x_j^2} + \mu \frac{\partial^2 \bar{u}_i}{\partial x_j^2} + \bar{F}_i \qquad (3.12)$$

Since,

$$\frac{\partial \bar{u}_i}{\partial t} = 0 , \quad \frac{\partial \bar{p}}{\partial x_i} = 0 , \quad \mu \frac{\partial^2 \bar{u}_i}{\partial x_j^2} = 0 , \text{ and}$$

$$\overline{(\bar{U}_j + u_j)\frac{\partial}{\partial x_j}(\bar{U}_i + u_i)} = \bar{U}_j \frac{\partial \bar{U}_i}{\partial x_j} + \frac{\partial}{\partial x_j}(\overline{u_j u_i}) ,$$

therefore equation 3.12 can be expressed as

$$\rho_f \left(\frac{\partial \overline{U}_i}{\partial t} + \overline{U}_j \frac{\partial \overline{U}_i}{\partial x_j} \right) = - \frac{\partial \overline{P}}{\partial x_i} + \frac{\partial}{\partial x_j} \left(\mu \frac{\partial \overline{U}_i}{\partial x_j} - \rho_f \overline{u_j u_i} \right) + \overline{F}_i \tag{3.13}$$

which is the form of the Reynolds equation.

Comparing equation 3.13 with the Navier-Stokes equation 3.7a, it can be concluded that the turbulence term, $\rho\overline{u_j u_i}$, may be interpreted as stresses on an element of the fluid in addition to the stresses determined by the pressure, P, and the viscous stresses. With these turbulence stresses, the complete stress components read

$$\sigma_{ji} = -\overline{P}\delta_{ji} + \mu \overline{D}_{ji} - \rho_f \overline{u_j u_i} \tag{3.14}$$

where $\overline{P}\delta_{ji}$ is the normal stress due to average pressure;
$\mu\overline{D}_{ji}$ is the viscous stress due to average motion;
$\rho_f\overline{u_j u_i}$ is the turbulent or Reynolds stress.

In general, the Reynolds stresses are both normal and tangential; the normal stress components, $-\rho\overline{u}_n^2$, are obtained by putting i = j, and the tangential stresses, $-\rho\overline{u_j u_i}$, are deduced when $i \neq j$. Boussinsq (20), assumed that the Reynolds stresses act like viscous stresses and proposed an eddy viscosity, λ, such that

$$\sigma_{ji} = -\overline{P}\delta_{ji} + (\mu + \lambda)\overline{D_{ji}} \tag{3.15}$$

where λ is assumed to be scalar and approximately constant within the flow field.

With equation 3.15 in mind, equation 3.13 can be manipulated to

$$\rho_f \left(\frac{\partial \overline{U}_i}{\partial t} + \overline{U}_j \frac{\partial \overline{U}_i}{\partial x_j} \right) = - \frac{\partial \overline{P}}{\partial x_i} + (\mu + \lambda) \frac{\partial^2 \overline{U}_i}{\partial x_j^2} + \overline{F}_i \qquad (3.16a)$$

or in a vector notation

$$\rho_f \left(\frac{\partial}{\partial t} + \vec{U} \cdot \nabla \right) \vec{U} = -\nabla P + (\mu + \lambda) \nabla^2 \vec{U} + \vec{F} \qquad (3.16b)$$

Now equation 3.16b is considered in the form

$$\frac{\partial \vec{U}}{\partial t} + \tfrac{1}{2} \nabla \vec{U}^2 - \vec{U} \times (\nabla \times \vec{U}) = - \frac{\nabla P}{\rho_f} + (\nu + \xi) \nabla^2 \vec{U} + \vec{g} \qquad (3.17)$$

where $\nu = \mu/\rho_f$ = kinematic viscosity
$\xi = \lambda/\rho_f$ = kinematic eddy viscosity
$\vec{g} = \vec{F}/\rho_f$ = gravitational acceleration.

The vorticity, ω, is defined as (36)

$$\vec{\omega} = \nabla \times \vec{U} \qquad (3.18)$$

Taking the curl of equation 3.17 leads to

$$\frac{\partial \vec{\omega}}{\partial t} + \nabla \times \vec{\omega} \times \vec{U} = -\nabla \, 1/\rho_f \times \nabla P + (\nu + \xi) \, \nabla^2 \vec{\omega} \qquad (3.19)$$

It is noted that $\vec{g}$ has been taken as a conservative force and hence it does not appear in equation 3.19. If the density is everywhere the same, equation 3.19 becomes

$$\frac{\partial \vec{\omega}}{\partial t} + \nabla \times \vec{\omega} \times \vec{U} = (\nu + \xi) \, \nabla^2 \vec{\omega} \qquad (3.20)$$

Equation 3.20 is a Helmholtz type vorticity equation.

3.2.2 Two-Dimensional Forms of the Equations Using Cartesian Coordinates

The basic equations to be considered in the application to follow are the continuity equation $\nabla . \vec{U} = 0$, the vorticity equation $\vec{\omega} = \nabla \times \vec{U}$, and the Helmholtz type vorticity equation. The velocity components in the x and y directions are defined in terms of the stream function, ψ, as

$$u = \frac{\partial \psi}{\partial y} \qquad (3.21)$$

and

$$v = -\frac{\partial \psi}{\partial x} \qquad (3.22)$$

which together automatically satisfy continuity.

Also equation 3.18 in two dimensions becomes

$$\omega = -\frac{\partial u}{\partial y} + \frac{\partial v}{\partial x} \qquad (3.23)$$

or in terms of the stream function

$$\frac{\partial^2\psi}{\partial x^2} + \frac{\partial^2\psi}{\partial y^2} = -\omega \qquad (3.24)$$

which is a Poisson type equation.

The time dependent Helmholtz type vorticity equation in two dimensions becomes

$$\frac{\partial \omega}{\partial t} + \frac{\partial}{\partial x}\left(u\omega - (\nu + \xi)\frac{\partial \omega}{\partial x}\right) + \frac{\partial}{\partial y}\left(v\omega - (\nu + \xi)\frac{\partial \omega}{\partial y}\right) = 0 \qquad (3.25)$$

This represents a two-dimensional non-linear second order partial differential diffusion-convection equation.

3.2.3 The Numerical Solution of the Differential Equations

The equations governing the phenomenon under consideration may be solved numerically by either a finite difference scheme or a finite element method. Neither one of these two methods has ever been applied to solve the problem of flow around spur-dikes. In the present study, the finite difference method was chosen as it has the following advantages over the finite element method:

a) it requires less computer storage;

b) the treatment is considerably simpler for rectangular geometries;

c) it provides a more convenient procedure for adjusting the depth.

The Poisson equation 3.24 and the Helmholtz vorticity equation 3.25 were solved numerically by a finite difference scheme. The derivatives were approximated with central differences both in space and time.

The flow field was discretized by a square mesh (cell) over a sufficient length of the channel (figure 3.1). Different mesh sizes were tested and computer time versus accuracy was the criterion used in selecting the mesh size. The scheme used involves a total of about 1400 points. The spur-dike extends perpendicularly from the upper wall to the desired opening. The velocity components in the x and y directions were evaluated at the square cell mid-lengths, while the stream function and the advanced vorticity values were evaluated at the cell nodes.

The finite difference forms of the velocity components u and v are given respectively, by

$$u_{i,j+\frac{1}{2}} = \frac{\psi_{i,j+1} - \psi_{ij}}{a} \tag{3.26}$$

$$v_{i+\frac{1}{2},j} = \frac{\psi_{ij} - \psi_{i+1,j}}{a} \qquad (3.27)$$

where a is the cell size.

The vorticity equation 3.23 is discretized using central difference in space as follows

$$\omega_{ij} = \frac{u_{i,j-\frac{1}{2}} - u_{i,j+\frac{1}{2}} + v_{i+\frac{1}{2},j} - v_{i-\frac{1}{2},j}}{a} \qquad (3.28)$$

The Poisson equation, 3.24, using central difference in space, has the form

$$\psi_{ij} = \frac{1}{4}\left[\psi_{i+1,j} + \psi_{i-1,j} + \psi_{i,j+1} + \psi_{i,j-1} + a^2\omega_{ij}\right] \qquad (3.29)$$

Equation 3.29 was solved numerically using an iterative scheme, as will be described later.

The Helmholtz type vorticity equation may be discretized, adopting the alternating direction technique of Peaceman and Rachford (34) but with modifications. Peaceman and Rachford showed that their technique was considerably more efficient than either explicit or implicit methods. They applied their technique to the heat flow equation

$$\frac{\partial T}{\partial t} = \frac{\partial^2 T}{\partial x^2} + \frac{\partial^2 T}{\partial y^2} \qquad (3.30)$$

where T is the temperature.

Assuming that the solution is known for time $t = n\,\delta t$, their method consists of replacing only one of the second-order derivatives, $\partial^2 T/\partial x^2$ say, by an implicit difference approximation in terms of the unknown pivotal values at the (n+1)th time level, while the other second order derivative, $\partial^2 T/\partial y^2$, is replaced by an explicit finite difference approximation. The solution advances to the (n+2)th time level by replacing $\partial^2 T/\partial y^2$ by an implicit finite difference approximation and $\partial^2 T/\partial x^2$ by an explicit one. On the basis of this discussion, equation 3.25 was formulated in the following finite difference form

$$\frac{\omega_{ij}^{n+1} - \omega_{ij}^{n-1}}{2\delta t} = \frac{1}{a}\left[(u\omega)_{i-\frac{1}{2},j}^{n} - (u\omega)_{i+\frac{1}{2},j}^{n} + (v\omega)_{i,j-\frac{1}{2}}^{n} - (v\omega)_{i,j+\frac{1}{2}}^{n}\right] + \frac{\nu + \xi}{a^2}\left\{\omega_{i-1,j}^{n+1} + \omega_{i+1,j}^{n+1} - 2\omega_{ij}^{n+1} + \omega_{i,j-1}^{n} + \omega_{i,j+1}^{n} - 2\omega_{ij}^{n}\right],\qquad (3.31)$$

Replacing ω_{ij}^{n} by the average term $\frac{1}{2}\left[\omega_{ij}^{n+1} + \omega_{ij}^{n-1}\right]$, equation 3.31 reduces to

$$-r\omega^{n+1}_{i-1,j} + (1 + 3r)\,\omega^{n+1}_{ij} - r\omega^{n+1}_{i+1,j}$$

$$= r(\omega^{n}_{i,j-1} + \omega^{n}_{i,j+1}) + (1-r)\omega^{n-1}_{ij}$$

$$+ r_1 \left[(u\omega)^{n}_{i-\frac{1}{2},j} - (u\omega)^{n}_{i+\frac{1}{2},j} + (v\omega)^{n}_{i,j-\frac{1}{2}} - (v\omega)^{n}_{i,j+\frac{1}{2}}\right] \quad (3.32a)$$

along the x-axis

$$-r\omega^{n+2}_{i,j-1} + (1 + 3r)\,\omega^{n+2}_{ij} - r\omega^{n+2}_{i,j+1}$$

$$= r(\omega^{n+1}_{i-1,j} + \omega^{n+1}_{i+1,j}) + (1-r)\omega^{n}_{ij}$$

$$+ r_1 \left[(u\omega)^{n+1}_{i-\frac{1}{2},j} - (u\omega)^{n+1}_{i+\frac{1}{2},j} + (v\omega)^{n+1}_{i,j-\frac{1}{2}} - (v\omega)^{n+1}_{i,j+\frac{1}{2}}\right]. \quad (3.32b)$$

along the y-axis

where $r = \dfrac{2(\nu + \xi)\delta t}{a^2}$

$$r_1 = \frac{2\,\delta t}{a}$$

It is emphasized that Peaceman and Rachford utilized forward time differencing for equation 3.30; however, the use of the forward time difference for equations 3.32 led to instability. The use of central time difference and the replacement of ω_{ij}^{n} by the average term $\frac{1}{2}(\omega_{ij}^{n+1} + \omega_{ij}^{n-1})$ were necessary for stability considerations as will be discussed in Chapter VI.

The transport or convection term in the Helmholtz equation was linearized by defining it in terms of the velocities and vorticities at the beginning of each computational step. To obtain the difference values for the transport term, which are not positioned at the node points, the averages of the adjacent values were used. Experimentation with the model indicated the following are the best forms for convergence as will be illustrated in Chapter VI.

$$(u\omega)_{i+\frac{1}{2},j} = \left[\frac{u_{i+1,j+\frac{1}{2}} + u_{i,j+\frac{1}{2}} + u_{i,j-\frac{1}{2}} + u_{i+1,j-\frac{1}{2}}}{4}\right] \times \left\{\frac{\omega_{i+1,j} + \omega_{ij}}{2}\right\} \tag{3.33a}$$

$$(v\omega)_{i,j+\frac{1}{2}} = \left[\frac{v_{i+\frac{1}{2},j+1} + v_{i-\frac{1}{2},j+1} + v_{i-\frac{1}{2},j} + v_{i+\frac{1}{2},j}}{4}\right] \times \left\{\frac{\omega_{i,j+1} + \omega_{ij}}{2}\right\} \tag{3.33b}$$

The additional values $(u\omega)_{i-\frac{1}{2},j}$ and $(v\omega)_{i,j-\frac{1}{2}}$ can be obtained by permutation of the indices of these equations. Equations 3.29 and 3.32 were solved alternately to obtain the variations in vorticity and stream function with time. A master flow chart indicating the successive steps of the procedure is presented in figure 3.2.

It is worthwhile mentioning at this point that Fromm (14), introduced an explicit finite difference technique to solve the Helmholtz vorticity equation without the inclusion of the eddy viscosity term, ε. However, it was confirmed that the use of the proposed method of this analysis gave a more stable solution.

3.2.4 Dimensionless Difference Equations

The previous equations can be formulated in dimensionless forms in terms of the approaching velocity, V_∞, and the channel width, B. By definition, the stream function is given by

$$\psi = \int u \, dy$$

which indicates the discharge per unit depth. Thus, the values of ψ ranges from zero on the lower boundary to a maximum of $V_\infty B$ on the upper boundary. The dimensionless stream function is obtained by dividing the ψ values in the domain of solution by the stream function on the upper wall boundary, $\psi_{max} = Q$. Thus, the appropriate dimensionless stream function values vary from $\psi' = 0$ on the lower boundary to $\psi' = 1$ on the upper boundary.

The dimensionless velocity is

$$u' = \frac{u}{V_\infty} = \frac{\Delta\psi}{a} \times \frac{1}{V_\infty} = \frac{\Delta\psi' \times V_\infty B}{\lambda B \times V_\infty} = \frac{\Delta\psi'}{\lambda} \qquad (3.34)$$

Hence,

$$u'_{i,j+\frac{1}{2}} = \frac{\psi'_{i,j+1} - \psi'_{ij}}{\lambda} \qquad (3.35)$$

and

$$v'_{i+\frac{1}{2},j} = \frac{\psi'_{ij} - \psi'_{i+1,j}}{\lambda} \qquad (3.36)$$

where $\lambda = a/B$

$\psi' = \psi/\psi_{max} = \psi/V_\infty B$

The dimensionless vorticity is then

$$\omega' = \omega \times B/V_\infty \qquad (3.37)$$

The Poisson equation is written in a dimensionless difference form as

$$\psi'_{ij} = \frac{1}{4}\left[\psi'_{i-1,j} + \psi'_{i+1,j} + \psi'_{i,j-1} + \psi'_{i,j+1} + \lambda^2\omega'_{ij}\right] \qquad (3.38)$$

If the dimensionless time interval is taken as

$$\delta t' = \delta t \times V_\infty/B \quad , \qquad (3.39)$$

equation 3.32 can be reduced to the following dimensionless form

$$-r'\omega'^{n+1}_{i-1,j} + (1+3r')\,\omega'^{n+1}_{ij} - r'\omega'^{n+1}_{i+1,j} = r'(\omega'^{n}_{i,j-1} + \omega'^{n}_{i,j+1})$$

$$+ (1-r)\omega'^{n-1}_{ij} + r'_1 \Big[(u'\omega')^{n}_{i-\frac{1}{2},j} - (u'\omega')^{n}_{i+\frac{1}{2},j}$$

$$+ (v'\omega')^{n}_{i,j-\frac{1}{2}} - (v'\omega')^{n}_{i,j+\frac{1}{2}} \Big] \qquad (3.40a)$$

and

$$-r'\omega'^{n+2}_{i,j-1} + (1+3r')\,\omega'^{n+2}_{ij} - r'\omega'^{n+2}_{i,j+1} = r'(\omega'^{n+1}_{i-1,j} + \omega'^{n+1}_{i+1,j})$$

$$+ (1-r')\,\overline{\omega}'^{n}_{ij} + r'_1 \Big[(u'\omega')^{n+1}_{i-\frac{1}{2},j} - (u'\omega')^{n+1}_{i+\frac{1}{2},j}$$

$$+ (v'\omega')^{n+1}_{i,j-\frac{1}{2}} - (v'\omega')^{n+1}_{i,j+\frac{1}{2}} \Big] \qquad (3.40b)$$

where

$r' = 2\delta t'/R_N \times \lambda$

$r'_1 = 2\delta t'/\lambda$

$R_N = V_\infty B/(\nu + \xi)$ = a dimensionless number.

It is noted that the eddy viscosity, ξ, may be calculated using Kalinske's formula (38)

$$\xi = \frac{y}{15}\sqrt{\tau/\rho_f} \qquad (3.41)$$

where

y = distance from the boundary (half the channel width in this case);

τ = shear stress (γRS)

ρ_f = fluid density

The energy slope, S, can be calculated using Manning or Chezy formulas.

3.2.5 Systematic Iterative Procedure for Solving Poisson's Equation

Finite difference methods for solving elliptic differential equations often lead to tens of thousands of algebraic equations and the~~ir~~ solution is a major problem in itself. Large sets are generally solved iteratively and small sets by direct elimination methods. Iterative methods for solving large sets of elliptic finite difference equations are more efficient than the direct method in that they take advantage of the large number of zero coefficients.

Of the available iterative schemes, the extrapolated Liebmann method was adopted in the solution of the finite difference Poisson equation because of its fast rate of convergence. The form of the equation is

$$\psi_{ij}^{k+1} = \psi_{ij}^{k}(1-w) + w \times \bar{\psi} \qquad (3.42)$$

where $\bar{\psi}$ is the Gauss-Seidel solution, given by

$$\bar{\psi} = \frac{1}{4}\left[\psi_{i-1,j}^{k+1} + \psi_{i+1,j}^{k} + \psi_{i,j+1}^{k+1} + \psi_{i,j}^{k}+1 + a^2\omega_{ij}\right] \qquad (3.43)$$

and w = over relaxation factor.

If the value of w is such that $1 < w < 2$, the method is termed successive over relaxation (S.O.R.) while for $0 < w < 1$, it is a successive under relaxation (S.U.R.).

In this study, S.O.R. was used in the iterative process which was terminated within a specified tolerance of 0.0002 as indicated by Equation 6.3.

3.2.6 Boundary Conditions

The boundary conditions pertinent to the present problem are illustrated in figure 3.1.

a) Inflow and Outflow Boundaries: These boundaries were chosen at considerable distances upstream and downstream of the obstacle where a steady, uniform irrotational flow condition can be assumed. Along these boundaries, the following two conditions were met:

i) $\omega = 0$ at all times

ii) ψ varies linearly with y.

Laboratory observations and experimentation with the mathematical model showed that a distance of about 2 ft. upstream of the dike and a distance of about 3.5 ft. downstream from the dike are the minimum distances at which the flow pattern can be considered to be steady and uniform. As a result, the above two conditions were applied at a distance of 25 inches upstream of the dike and 44 inches downstream of the dike; by the choice of these

4

7

minimum distances a saving in computational time is gained.

b) Upper and Lower Wall Boundaries: The wall boundaries were treated as streamlines; it follows that a natural condition on the wall boundary is that of a constant ψ. Theoretically, a no slip condition applies at the wall, i.e. a vorticity of $\omega = - \partial u/\partial y$ exists at the walls. However, in the present analysis due to considerations that will be elaborated on in Chapter VI, the walls are treated as frictionless. Hence a zero vorticity condition was imposed at the two wall boundaries. Thus, on the upper wall,

$$\psi = Q \quad , \quad \omega = 0$$

and on the lower wall

$$\psi = 0 \quad , \quad \omega = 0$$

c) The Dike's Boundary Conditions: In treating flow around obstructions, an essential requirement is that the periphery of the obstacle must be a stream line. Therefore, ψ must be everywhere the same on that periphery and is equal to ψ on the upper wall. In addition, a no-slip condition was assumed along the dike. Thus, the boundary conditions for the dike are

$$\psi = Q \text{ , and } v = 0$$

The presence of the dike, with the no-slip condition, introduces vorticity that causes separation. Experimentation with the model showed that the best representation of the singularity of the dike's nose could be obtained by the use of a sheet pile dike and neglecting the velocity gradient $\partial u/\partial y$, indicating that the separation line emerges, from the nose, tangential to the upstream face of the dike. This, however, will be discussed in detail in Chapter VI.

3.3 Three-Dimensional Model

This model deals with the development of the scour hole after the flow separation pattern has reached a relatively steady condition.

3.3.1 The Governing Differential Equation of Motion

The Dupuis assumption (8) of negligible vertical velocity was adapted to the present problem in order to simplify the solution and satisfy continuity requirements. Referring to the fluid cell shown in figure 3.3 and applying the principle of conservation of mass, the following continuity equation is arrived at

$$u \frac{\partial z}{\partial x} + v \frac{\partial z}{\partial y} + z\left(\frac{\partial u}{\partial x} + \frac{\partial v}{\partial y}\right) = 0 \qquad (3.44)$$

where z = the average water depth.

The velocities in this phase are depth dependent. The depth-averaged components, u" and v", can be redefined in terms of a new stream function, ψ'', as follows

$$u'' = \frac{1}{z}\frac{\partial \psi''}{\partial y} \tag{3.45}$$

$$v'' = -\frac{1}{z}\frac{\partial \psi''}{\partial x} \tag{3.46}$$

Equations 3.45 and 3.46 were combined with equation 3.23 to yield another Poisson type equation of the form

$$\frac{\partial^2 \psi''}{\partial x^2} + \frac{\partial^2 \psi''}{\partial y^2} = u''\frac{\partial z}{\partial y} - v''\frac{\partial z}{\partial x} - \omega z \tag{3.47}$$

It is noted that since at the deepest part of the scour hole the bed is nearly horizontal, therefore, the gradients $\partial z/\partial y$ and $\partial z/\partial x$ would approach zero at this part.

It should be emphasized that, the inclusion of the convective and diffusion terms in calculating the vorticity in the three-dimensional model would greatly complicate the solution. Therefore, equation 3.23 was applied to calculate the vorticity during the adjustment of the depth.

3.3.2 Bed Shear Function

The shear stress acting on the bed near the dike's vicinity depends on the local velocity, vorticity, and turbulence. The following functional form is proposed to express these factors.

$$\underset{\substack{\vdots\\ \text{shear}\\ \text{stress}}}{\tau} = \phi \left\{ \underset{\substack{\vdots\\ \text{average}\\ \text{velocity}}}{v_R} \left[1 + \underset{\substack{\vdots\\ \text{vorticity}\\ \text{correction}}}{f(\omega)} + \underset{\substack{\vdots\\ \text{turbulence}\\ \text{correction}}}{f(\eta)} \right] \right\}^2 \qquad (3.48)$$

An empirical equation, based on the above function, was derived and is given by

$$\tau = \frac{\gamma}{c^2} v_R^2 \left(1 + k_1 \frac{\omega}{\omega_o} + k_2\right)^2 \qquad (3.49)$$

where τ = the shear stress acting on the bed

γ = the specific weight of water

c = Chezy's coefficient

v_R = the resultant velocity

k_1, k_2 = constants

ω_o = reference vorticity

3.3.3 Scour Depth Calculation

The local depth was adjusted to reduce the difference, between the local shear and the local bed resistance, to zero. Therefore, a function for the increment in eroded depth, Δz, was formulated as

$$\Delta z = k_3 \, (\tau - \tau_c) \qquad (3.50)$$

where k_3 = constant to satisfy stability conditions as will be shown in Chapter VI.

τ_c = critical shear stress for the bed material.

3.3.4 Solution of the Differential Equation by Finite Difference Schemes

Equations 3.45 and 3.46 in difference forms yield

$$u''_{i,j+\frac{1}{2}} = \frac{2}{(z_{i,j+1} + z_{ij})} \times \frac{\psi''_{i,j+1} - \psi''_{ij}}{a} \qquad (3.51)$$

$$v''_{i+\frac{1}{2},j} = \frac{2}{(z_{i+1,j} + z_{ij})} \times \frac{\psi''_{ij} - \psi''_{i+1,j}}{a} \qquad (3.52)$$

which are the velocity components evaluated at the cell midlength.

Equation 3.47 was discretized, using central differences, as follows

$$\psi''_{ij} = \left[\frac{\psi''_{i-1,j}}{(z_{i-1,j} + z_{i,j})} + \frac{\psi''_{i+1,j}}{(z_{i+1,j} + z_{i,j})} + \frac{\psi''_{i,j-1}}{(z_{i,j-1} + z_{i,j})} + \frac{\psi''_{i,j+1}}{(z_{i,j+1} + z_{i,j})} + \frac{a^2}{2}\,\omega_{ij}\right] \Bigg/ \left\{\frac{1}{(z_{i-1,j} + z_{i,j})} + \frac{1}{(z_{i+1,j} + z_{i,j})} + \frac{1}{(z_{i,j-1} + z_{i,j})} + \frac{1}{(z_{i,j+1} + z_{i,j})}\right\}$$

(3.53)

An iterative procedure was applied to solve equation 3.53 for the stream function, ψ''. The stream function values were used to compute the velocity components, u'' and v'', and adjust the vorticity, ω, for the stretching of the stream tube area. These values produced the local shear stress, τ, utilizing equation 3.49. Finally, the local depth was adjusted by equation 3.50.

The boundary conditions governing the stream function and vorticities in the two-dimensional model were maintained as the solution progressed downward in the z-direction.

Figure 3.4 presents the Master flow chart for the three-dimensional solution.

CHAPTER IV

EXPERIMENTAL SET UP AND PROCEDURE

4.1 Test Flume and Laboratory Facilities

The experiments were conducted in a 36 ft. long, 1.5 ft. wide and 2 ft. deep aluminum flume with plexiglass walls (figure 4.1). The head tank is 9 ft. long by 9 ft. high and is provided with a screen to help filter the air bubbles, dissipate the excess energy of the incoming flow, and maintain a uniformly distributed flow over the width of the flume. The water is supplied to the system by a centrifugal low head pump driven by a 50 H.P. D.C. motor; the pump can deliver a maximum discharge of 3000 USGPM. A graded gravel bed was set 6 ft. downstream of the entrance, and extended 12 ft. with a thickness of 10 inches. The flow was channelized over the bed by means of a 4:1 ramp. The discharge was measured by an electronic flow meter calibrated in USGPM against a pitot-tube, and time was recorded by an electric clock. A point gauge mounted on a sliding wooden frame was utilized to measure water and bed surface elevations. Plywood plates, ½ inch thick, were used to model different spur-dikes. The flume is equipped with a tail-gate to control flow depth.

The graded gravel passed a No. 4 (Tyler) sieve and was retained by a No. 8 sieve; thus its geometric mean diameter was calculated and found to be 0.177 inch. The specific gravity and the angle of repose for the bed material are respectively 2.65 and 30°.

4.2 Procedure

a) The spur-dike was fixed to the side wall of the flume, and the gravel bed was then levelled. The sliding point-gage was used to check the horizontal bed surface at different locations.

b) The runs started by slowly allowing the water to flow over the horizontal bed. The tail gate of the flume was used to adjust the water depth until the proper conditions were attained. During that time, a steel screen was laid on the bed, in the vicinity of the dike, to prevent any scour before achieving the desired discharge and water depth; thereafter the screen was removed and the timer was switched on.

c) The scour was observed to develop near the dike's nose, and the bed level was recorded at various time intervals. The experiment was continued until the bed level at the dike's nose virtually indicated no measurable change. The equilibrium state was typically reached after about 2.5 hours.

d) Having recorded the maximum depth of scour, the flow was gradually decreased to avoid disturbing the scour pattern. The water level within the scour hole was lowered by 1 inch increments and wet strings were used to trace the intersections of the water surface with the sloping sides of the scour hole. This procedure was carried out until the hole was completely drained. Contour maps were drawn, and photographs were taken for the scour holes.

The experiments were conducted under a clear-water condition, i.e. there was no sediment supplied into the scour hole. In most experiments, the scoured material, deposited downstream the scour hole, was continuously removed. Under such a condition, the experiments resemble what is occurring in natural streams, due to the fact that a continuous flow will transport away this deposited material leaving, thus, the scour hole unprotected.

4.3 Conditions Tested

Different sets of experiments were conducted to deduce the effect of the following parameters on the maximum depth of scour:

a) flow rate;

b) upstream water depth;

c) opening ratio;

d) Fround number upstream of the dike;

e) Angle of inclination of spur-dike w.r.t. the main flow;

f) Prolonged running time.

4.4 Rigid Bed Experiment

After the spur-dike experiments were completed, the bed material was removed from the test flume. An experiment was then conducted for the purpose of measuring velocities, using a pitot-tube, in order to trace the separation line. In this experiment, the discharge was 620 USGPM and the depth was maintained at about 8 inches; an opening ratio of 0.667 was used. The velocities were recorded at various cross-sections at 0.2 and 0.8 of the depth. Along each section, measurements were made at different points. The spacings between these points were closer, in the separation zone than in the other areas, to achieve better accuracy of the separation line. In the wake zone, near the wall, the velocity of the reversed flow was also recorded. The reattachment of the separation line to the wall was detected by introducing a dye on the water surface, near the wall, and determining the zone at which the dye started to flow in the forward direction. The depths, at all the points where the velocity was taken, were measured using the piezometric reading of the manometer connected to the pitot-tube. Also, the depths at some selected points were measured by means of a point gauge.

4.5 Results

The data of the different sets of experiments conducted are documented in tables 4.1 to 4.4.

Table 4.1 lists the results of the experiments with a constant depth, H, of 0.667 ft. and discharges ranging from 0.67 to 1.48 ft^2/sec. and opening ratios ranging between 0.5 to 0.90.

Table 4.2 shows the results of the experiments with a constant α of 0.667. Four sets of 3 experiments each are given; in each set the velocity was kept constant by maintaining a constant q/H ratio.

The variation in α which ranged between 0.5 to 0.9 is given in table 4.3 for experiments conducted with a constant upstream Fround No.

In table 4.4, the results of varying the angle of inclination, θ, of the spur-dike between 30° to 150° are presented. In these experiments the values of q, H, and α were kept constant at 0.89 ft^2/sec., 0.667 ft. and 0.667 respectively.

Figures 4.2 to 4.19 present few typical contour maps for the different conditions tested. Also, some examples are shown in photographs 4.1 to 4.6.

For the rigid bed experiment, figure 4.20 illustrates the velocity values, based on the average of the measurements taken at 0.2 and 0.8 of the depth. The corresponding pitot-tube values of the depth, averaged in the same way, are shown in figure 4.21. The depth values measured by the point gauge are given in figure 4.22.

CHAPTER V

ANALYSIS OF THE EXPERIMENTAL DATA

5.1 Influencing Variables

From the first set of experiments, listed in table 4.1, a plot of D_s against q can be obtained. The plot, on a log-log graph, is shown in figure 5.1, which indicates a straight line relationship with a constant slope of 2/3. Thus, an equation of the form,

$$\frac{D_s}{q^{2/3}} = \text{constant} \qquad (5.1)$$

may be fitted for different values of α. This equation suggests that the regime theory is applicable to the phenomenon under consideration as will be shown later.

The data of the second set of experiments (table 4.2) were used to plot D_s versus H for different approaching velocities. A set of parallel straight lines, with a constant slope of 2/3, were obtained as illustrated in figure 5.2. Consequently, the D_s-H relationship can be described by the expression

$$\frac{D_s}{H^{2/3}} = \text{constant} \qquad (5.2)$$

Utilizing the values of tables 4.1 and 4.2, for a constant value of $\alpha = 0.667$, the variation of D_s with the product of H and V can be plotted. Again, the plot, presented in figure 5.3, displays a straight line relationship of a constant slope of 2/3. From figure 5.3, the effect of the approaching velocity, V, and the upstream water depth, H, can be expressed in a generalized equation as follows

$$\frac{D_s}{H^{2/3}\ V^{2/3}} = \text{constant} \qquad (5.3)$$

From the above equation, it follows that

$$\frac{D_s}{H\ F^{2/3}} = \text{constant} \qquad (5.4)$$

where F is the Froude No.

Equation 5.4 indicates the dependence of the scour depth on the Froude number. Figure 5.4 illustrates the variation of D_s/H with F for different values of α; as can be seen, the curve confirms equation 5.4.

In order to deduce the effect of the opening ratio on the scour depth, the values of table 4.3 were used to plot D_s/H against α. The relationship is represented by a straight line of an adverse slope of 1 as shown in figure 5.5. Thus,

$$\frac{D_s}{H} = \text{constant} \times \left(\frac{1}{\alpha}\right) \qquad (5.5)$$

Finally, the relation between D_s/H and the angle of inclination of the spur-dike, θ, is plotted in figure 5.6 with the aid of table 4.4. A straight line of a very mild negative slope of -0.043 was obtained; then

$$\frac{D_s}{H} = \text{constant} \times \left(\frac{1}{\theta}\right)^{0.043} \qquad (5.6)$$

Equations 5.1 to 5.6 may be pooled in the general form

$$\frac{D_s}{H} = f'(F, \alpha, \theta) \qquad (5.7)$$

which emphasizes the important variables affecting the maximum depth of scour.

5.2 The Solution of the Local Scour Equation by Dimensional Analysis

It was shown in chapter II that the scour process could be represented by the relationship

$$\frac{d}{dt}\Big[f(B)\Big] = g(B) - g(s) \qquad (2.1)$$

The integral form of this equation may be written, functionally, as

$$f(B) = \phi \ (g(B), g(s), t) \tag{5.8}$$

which indicates that the bed configuration is a function of the local rate of transport, rate of supply, and time. It may be assumed that the rate of transport depends on the flow pattern and the properties of the sediment. The flow pattern, in turn, will depend on the boundary geometry, including the bed configuration, which is a function of time, the characteristic velocities, and the fluid properties.

Utilizing the procedures of dimensional analysis, the variables entering the problem can be grouped into the following categories:

variables describing the geometry of the channel and obstruction

width of channel, B;
size of obstruction, b;
angle of attack, θ;
channel slope, S.

variables describing the flow

mean approaching velocity, V;
upstream flow depth, H;
maximum scour depth, D_s.

variables describing the fluid

mass density of water, ρ_f;
specific weight of water, γ;
dynamic viscosity, μ.

variables describing the sediment

mean size, d;
standard deviation, σ;
particle fall velocity, v_s;
critical shear stress, τ_c;
specific gravity, S_s.

Hence, the following functional relationship is formulated

$$g(B) = \phi_2(B, b, \theta, S, V, H, D_s, \rho_f, \gamma, \mu, d, \sigma, v_s, \tau_c, S_s) \tag{5.9}$$

Substituting equation 5.9 into equation 5.8 yields

$$f(B) = \phi_3(B, b, \theta, S, V, H, \rho_f, \gamma, \mu, d, \sigma, v_s, \tau_c, S_s, g(s), t) \tag{5.10}$$

Applying the Buckingham π - theorem (26,36), with V, H and ρ_f as the repeating variables, the following equation is arrived at

$$f_1(B) = \phi_4 \left(\frac{B}{H}, \frac{b}{H}, \theta, S, \frac{V}{\sqrt{gH}}, \frac{VH}{\nu}, \frac{d}{H}, \frac{\sigma}{H}, \frac{V}{v_s}, \frac{V}{\sqrt{\tau_c/\rho_f}}, S_s, g(s), \frac{Vt}{H}\right) \tag{5.11}$$

in which $f_1(B)$ is a dimensionless function of the bed configuration. The fluid properties are embedded in the characteristic Reynolds number and Froude number. The non-cohesive sediment properties are reflected by the critical tractive force, τ_c, settling velocity, v_s, specific gravity, S_s, and standard deviation, σ. The supply function, g(s), is a dimensionless parameter that depends on the rate at which sediment, if any, enters the scour area. It should be realized that the terms descriptive of the flow pattern may also be functions of time, and that the particular meaning assigned to each independent variable must be determined for each situation.

In this analysis, a somewhat simpler form of equation 5.11 may be used to provide the necessary parameters. The supply rate of sediment is zero and the scour hole does reach an equilibrium condition. The flow regime is in the fully turbulent zone and has a negligible effect on the phenomenon. The non-cohesive sediment may be described by the mean diameter, the settling velocity and the specific gravity. Hence, equation 5.11 can be simplified to

$$f_1(B) = \phi_5\left(\frac{B}{H},\frac{b}{H},\theta,S,\frac{V}{\sqrt{gH}},\frac{d}{H},\frac{V}{v_s},S_s\right) \quad . \tag{5.12}$$

The expression $f_1(B)$ may be represented by the relative depth of scour, D_s/H. With certain manipulation, permissible within the theory of dimensional analysis, equation 5.12 can be written as

$$\frac{D_s}{H} = \phi_6\left(\frac{B}{H},\frac{B-b}{H},\theta,S,\frac{V}{\sqrt{gH}},\frac{d}{H},\frac{V}{v_s},S_s\right) \tag{5.13}$$

In all the experiments conducted, the bed material and the bed slope were kept constant. Accordingly, the terms S, d/H, V/v_s and S_s in equation 5.13 can be omitted. Assuming that B/H is of secondary importance, equation 5.13 reduces to

$$\frac{D_s}{H} = \phi_7(\alpha,\theta,F) \qquad (5.14)$$

which has the same form as equation 5.7.

The above functional relation can be written as

$$\frac{D_s}{H} = K\left[(\alpha)^{a_1}\ (\theta)^{a_2}\ (F)^{a_3}\right] \qquad (5.15)$$

where a_1, a_2, a_3 and K are to be found by statistical methods.

Multilinear regression (7,32) was applied to fit the data, and the following empirical formula was derived.

$$\frac{D_s}{H} = 2.62\left[(\alpha)^{-1} \times (\theta)^{-0.043} \times (F)^{2/3}\right] \qquad (5.16)$$

Equation 5.16 gave a correlation coefficient of 0.95.

In order to illustrate the scatter in the data, a plot of the calculated versus the observed scour depths is presented in figure 5.7. The coefficient K has an average value of 2.62 and was found to be independent of the Reynolds number as can be seen from figure 5.8. Equation 5.16 may be transformed to

$$D_s = 0.825 \times \left(\frac{1}{\alpha}\right) \times \left(\frac{1}{\theta}\right)^{0.043} \times (q)^{2/3} \qquad (5.17)$$

The regime methods of Lacey and Blench (4,25), use the enhanced discharge intensity, q_c, through the clear channel; thus, equation 5.17 may be modified to

$$D_s = 0.825 \times \left(\frac{1}{\alpha}\right)^{1/3} \times (C_c)^{2/3} \times \left(\frac{1}{\theta}\right)^{0.043} \times (q_c)^{2/3} \qquad (5.18)$$

in which $q_c = q/\alpha \times C_c$

C_c = coefficient of contraction.

Based on the ranges covered in the experiments, the average values of $\alpha^{1/3}$, $\theta^{0.043}$, and $C_c^{2/3}$ were found to be respectively 0.88, 1.0, and 0.78. With these average values, equation 5.18 may be approximated to

$$D_s = 0.68\, q_c^{2/3} \qquad (5.19)$$

Khosla (22), from Lacey's regime formula has related the scour depth to the discharge intensity by the expression

$$D_s = 0.90\, \frac{q_c^{2/3}}{f^{1/3}} \qquad (5.20)$$

where f is Lacey's silt factor, a function of the grain size, d, that is given by $f = 8\sqrt{d}$. Thus, for the material used equation 5.20 becomes

$$D_s = 0.62\, q_c^{2/3} \qquad (5.21)$$

Using the Blench regime formula (4), the maximum scour depth relative to the water surface can be expressed as

$$D_s = \frac{1}{f_b^{1/3}} q_c^{2/3} \tag{5.22}$$

where f_b is the bed factor $= 9.6\sqrt{d}$.

Therefore, equation 5.22 yields

$$D_s = 0.65\, q_c^{2/3} \tag{5.23}$$

As can be seen, the experimentally derived equation is identical in form to the regime equations 5.21 and 5.23.

5.3 Scour Hole Development and Limiting Scour Depth

As the scour hole develops and increases in depth, the side material of the depression as well as that reaching the upstream edge by general transport, if any, slide towards the bottom of the depression and are removed by a concentrated shearing stress action. The greatest rate of scour will occur where the shear stress due to fluid velocity, turbulence and vorticity was greatest; at this location the scour hole will be deepest. Downstream from this position, the shear stress decreases with distance, thereby causing the capacity for pick-up and transport to diminish, and as a result some of the scoured sediment will deposit on the downstream slope of the scour hole. As the scour hole deepens, the lateral limit of the hole is moved further from the flow disturbance. Hence, the rate of transport out of the hole can be expected to decrease drastically as the depth of scour increases.

The change in bed configurations, as a function of time and the limiting extent of scour, was investigated. The effect of time was deduced by utilizing the settling velocity, v_s, as a defining property for the non-cohesive medium and by examining equation 5.11 for each experiment. Thus, for the one experiment

$$f_1(B) = \phi_8 \left(\frac{V}{v_s}, \frac{Vt}{H}\right) \qquad (5.24)$$

Equation 5.24 shows that the extent of scour is a function of time and the characteristics of the flow and sediment. Figure 5.9 shows plots of D_s versus the logarithm of time for different values of V/v_s with constant upstream water depth and opening ratio. The curves illustrate that the extent of scour increases linearly, over the range shown, with the logarithm of time and that the larger the value V/v_s, the steeper the curves and the greater the rate of scour. Rouse (37), and Doddiah et al (9), stated that the scour depth is directly proportional to a geometric progression of time. In other words, the state of equilibrium in the process of scour cannot be expected either at any depth or after any period of time. Also, according to [illegible]u and Skinner (31), the scour depth increases indefinitely in the absence of sediment supply to the scour hole from the upstream. This hypothesis is in direct contradiction with Laursen's third principle, indicated in Chapter II. It is the writer's conviction that the interpretation of Laursen is valid and in order to confirm it, an experiment was conducted for a sufficiently long time to show that the limiting extent of scour is actually reached. The experiment was run for 3 days, and the scour hole did stabilize and no further change in its size was observed. The results of this experiment are presented in figure 5.10, which illustrates that a practical equilibrium is attained after a relatively short time. The limit of scour is presumed to have resulted after the continuous enlargement of the hole and the subsequent decrease of velocity along the bottom of the hole reached a stage at which the velocity was less than the critical velocity.

5.4 Geometry of Scour Hole

From the experiments, it was observed that the upstream portion of the scour hole has the approximate form of an inverted cone with its surface maintaining an angle higher than the angle of repose of the material. The vertex of the cone represents the greatest depth of scour and is displaced slightly from the spur-dike's nose. The downstream portion of the hole is elongated in the downstream direction and has a milder slope. The sloping sides of the hole in the upstream portion are higher than the angle of repose of the material due to the following reasons:

a) The bed is composed ~~of a~~ granular flaky type material, which under a slight amount of compaction will be arranged in stratified layers increasing, thus, the angle of repose.

b) The shape of the scour hole as an inverted cone produces a bridging effect which increases the angle of repose.

c) As a result of the scour hole, the flow separates from the original boundary and a horizontal roller is developed inside the scour hole. The horizontal roller will compact the material on the sloping face of the hole. Also the horizontal roller is rotating such that the velocity component at the sloping face is upward, which prevents the material from sliding. When the flow is stopped, this slope will not be dynamically stable and any vibration will cause it to slide downwards.

A prolonged experiment was carried out in which no removal of the scoured sediment took place in order to detect the effect of the stacked material on the shape of the scour hole. The experiment was first stopped after

2½ hours and a contour map for the scour hole was obtained. The experiment was restarted again, carefully, to avoid disturbing the pattern, and the procedure was repeated after 43 hours. The final contour map was obtained after 72 hours. The successive maps are presented in figure 5.11. The figure shows that the stacked material moves downstream as time progresses, leaving the scour hole without protection which results in enlarging the hole. Since this is indicative of what happens in nature, a fairly proper simulation of the phenomenon requires the continuous removal of the stacked material; this results in saving a considerable amount of run time.

5.5 Rigid Bed Analysis

The velocity and depth values, given in figures 4.20 and 4.21, were integrated over the appropriate cross sections to yield the stream function, ψ; consequently, the shape and location of the separation line could be obtained as shown in Fig. 5.12. As can be seen from this figure, the section of maximum contraction is about 12 inches downstream from the dike. The coefficient of contraction was deduced based on the average of the pitot-tube depths along both the contracted and clear opening sections; a value of $C_c = 0.68$ was found. The depth values, obtained by means of the point gauge, were also utilized to give a value of 0.64 for C_c. The discrepency between the two calculated values of C_c is attributed to the fact that the pitot-tube depth measurements at the clear opening section might have been affected by the main vortex which would tend to lower the piezometric head. Thus, an average value of $C_c = 0.66 \pm .02$ was considered.

The reattachment of the separation line to the wall is observed, from figure 5.12, to be at a distance ranging between 39 inches to 42 inches downstream from the dike.

5.6 Experimental Errors

The possible errors that might have occurred in performing the experiments are summarized as follows:

a) The errors in reading the flow meter. The flow chart is graduated in 50 USGPM divisions, and by interpolation the discharge could be read within an accuracy of about ± 10 USGPM.

b) The errors in measuring elevations. The point gauge is provided with a vernier that permits readings within an accuracy of ± 1/100 inch. Also, the fluctuations in water level introduces an error in reading the depths estimated at about ± 0.2 inches.

c) Errors in time measurements due to human reaction. This error is estimated to be ± 0.5 seconds.

d) Errors in placing the strings within the scour hole and errors in tracing the contours. The combined error in this case is estimated to be ± 0.15 inches both in the horizontal and vertical directions.

e) The error due to considering the initial bed perfectly horizontal.

CHAPTER VI

EVALUATION OF THE NUMERICAL TECHNIQUE

In this chapter the order of calculations and methods of solution are emphasized. The numerical techniques used in the two-dimensional and three-dimensional models are discussed and evaluated. The computed coefficient of contraction was verified experimentally; the jet theory and the experimental data reported by the U.S. Geological Survey were also used to confirm the results.

The contour maps for the scour holes as predicted by the mathematical model are given and compared to the experimental ones.

A detailed stability analysis as well as a series truncation error analysis for the numerical technique are presented.

The computer programmes are given in appendix (D).

6.1 Evaluation of the Two-Dimensional Model

6.1.1 Solution of the Poisson Equation

As mentioned in Chapter III the extrapolated Liebmann method was adopted in the solution of the Poisson difference equation. The method uses the latest iterative values as soon as they are obtained and scans the mesh points systematically from left to right along successive columns. Since constant values of ψ should be maintained along the dike and walls, the iterative process was not applied to the boundary ψ values. A few initial runs of the programme were made to establish the optimum value of the over relaxation factor, w, based on the minimum number of iterations. The optimum value of w was found to be 1.75 as indicated by figure 6.1. Frankel (13), gives the optimum value of w for a maximum rate of convergence as

$$w_{opt} = 2 - \frac{2\pi}{\sqrt{2}} \left[\frac{1}{p^2} + \frac{1}{q^2} \right]^{\frac{1}{2}} \tag{6.1}$$

for a regular grid $i = o,p$

$j = o,q$

An alternative form of equation 6.1 is

$$w_{opt} = \frac{2}{1 + \sqrt{1-\lambda_1^2}} \tag{6.2}$$

where $\lambda_1 = \frac{1}{2}(\cos \frac{\pi}{p} + \cos \frac{\pi}{q})$

In the present study P=18 and q=69, and upon substitution with these values, equations 6.1 and 6.2 yield respectively w_{opt} of 1.74 and 1.77. These results agree very closely with the value obtained from figure 6.1. Since the iterative procedure consumes the major part of the computing time, a block iterative scheme, in the vicinity of the dike, was utilized in addition to the use of the optimum over relaxation factor. A block (figure 6.2) is characterized by a region where a drastic change in the flow pattern warrants extra improvement of the values compared to the value outside the block. Within the block, more sweeps were performed to improve the ψ values than in the rest of the solution domain.

Experimentation with the model showed that the minimum computer time was achieved by applying the iterative procedure in the following arrangement:

i) three sweeps covering the whole region;
ii) two sweeps covering the block region alone;
iii) one sweep for the complete region.

Step (i) was only performed once to start the solution, then steps (ii) and (iii) were repeated alternately.

The iterative procedure was terminated when the following condition was satisfied

$$\frac{\left|\psi_{ij}^{k+1} - \psi_{ij}^{k}\right|_{\max}}{\psi_0} \leq 0.0002 \qquad (6.3)$$

where ψ_0 is a reference value taken as the upper wall value. If, for some reason, convergence to the desired accuracy was not reached after 150 sweeps, the problem was terminated with the realization that some error must have induced that problem.

6.1.2 Solution of the Helmholtz Vorticity Equation

The Helmholtz vorticity difference equation was solved by an alternating direction implicit scheme as illustrated in chapter III. The eddy viscosity, ξ, was computed by means of equation 3.41; the energy slope, s, was found from Manning's equation using a value of 0.015 for the roughness. Hence an average value of 0.007 ft^2/sec for ξ was obtained.

For the problem under consideration, the main vorticities affecting the phenomenon are caused by the presence of the obstruction while the wall vorticities are strictly confined to the wall zone and do not play a significant role in shaping the flow separation pattern. Simulation of this behaviour in the numerical model necessitates the prevention of the wall vorticities from disturbing the main system to avoid an erroneous solution and avoid excessive instability. Thus, the zero vorticity boundary condition was imposed on the walls. This argument can easily be verified by analogy to the situation of figure 6.3, which illustrates flow around two symmetrical obstacles. The upper wall resembles line AB while the lower wall is similar to CD. Essentially, these boundaries are regarded as frictionless.

The vorticities generated along the dike-fluid interface were calculated using equation 3.28 instead of equation 3.32. This implies that the vorticity values along the dike were always lagging by one time step behind the other advanced vorticity values in the solution domain. The order of calculations, therefore, is to let the obstacle take a ψ value equal to the maximum discharge, and iterate keeping ψ fixed at the obstacle. The velocity components are then calculated and the vorticities are finally updated by equation 3.28. This is a legitimate procedure since equations 3.28 and 3.29 are equivalent. It can easily be seen that if the resulting vorticities are introduced as a source function to equation 3.29, the end result would be the same even though the ψ values were not held fixed on the obstacle. The vorticities, prescribed on the obstacle in the above described manner, are affected by the transport and diffusion properties of ω in the sense that transport and diffusion may take place between the interface and adjacent points in the fluid. This occurs through the normal time advancement of ω, using equation 3.32 at the adjacent points. The solution of the Helmholtz equation, along either direction, produces a set of simultaneous equations with (N-1) internal points. The coefficient matrix gives rise to a tri-diagonal system which can be solved by a special case of Gauss elimination method (43). This method was found to consume less computer time than the iterative procedures or the Gauss-Jordan method for solving simultaneous equations.

6.1.3 Order of Calculations

The iterative solution for the stream function, ψ, was initiated by assuming a zero vorticity. Velocity components corresponding to the obtained ψ values were calculated and used to determine the vorticity values along the dike-fluid interface, and compute the convective term in the Helmholtz vorticity equation. Time was advanced, and ω was calculated at each time increment at all mesh points except those on the obstacle-fluid interface. The time increment was based on a stability versus computer time criterion. Thus, a value of $\delta t' = 0.0134$ was found to satisfy stability requirements and save computational time. The Poisson and Helmholtz difference equations were solved alternately to obtain the variations in stream functions and vorticities with time. With progression of time the separation pattern develops and extends downstream until eventually it reaches a relatively steady condition. Experimentation with the programme indicates that the relatively steady separation pattern is attained after about 500 iterations in time; thereafter the final Poisson solution can be obtained. Figures 6.4 to 6.7 show dimensionless plots of the initial Laplace solutions and the fully developed separation patterns as obtained from the final Poisson solutions for different opening ratios ranging between 0.5 to 0.833. The experimental curve, fig. 5.12, is in general agreement for $\alpha = 0.667$. The numerically computed coefficient of contraction due to flow separation can also be found from these figures. Figure 6.8 shows a comparison between the computed coefficient of contraction and a) the values reported by Von Mises on the jet theory (38); b) the experimental results of flow through constrictions presented by the U.S. Geological survey (23,24,51) and c) University of Windsor experimental results. Von Mises, in his work, neglected the effects of gravity, viscosity and compressibility. The comparison, with a non-viscous flow separation is justifiable due to the fact that the wall vorticity was found to have an insignificant effect in the present analysis.

From a qualitative flow visualization study using a bi-refringent fluid the writer noted that the wall boundary layer did not grow and its maximum thickness was about 0.5 inch. This implies that the vorticity generated at the boundary was not transported by diffusion and convection to the main flow field. Also, it was observed that the vorticity, generated in the system, tended to create a vertical vortex at the dike's nose and a trail of vortices travelling downstream along the separation line. This behaviour is illustrated by photographs 6.1 and 6.2.

Figures 6.9 and 6.10 present dimensionless plots of iso-velocity and iso-vorticity patterns as obtained from the Poisson solution with an opening ratio of 0.667. These figures indicate that values of high velocity and vorticity exist in the region of the dike's nose and along the separation line. These local velocities along with the vorticities and turbulence are the principal causes of erosion.

6.2 Evaluation of the Three-Dimensional Model

6.2.1 The Shear Stress Function

As mentioned before the local shear stress function may be generated from the local velocity, turbulence, and vorticity as described by equation 3.49. The Chezy coefficient in this equation was calculated based on the Simons and Albertson (35,42) empirical formula for a plane bed with little or no sediment movement. Thus

$$\frac{C}{\sqrt{g}} = 5.9 \log(H/d_{85}) + 5.44 \tag{6.4}$$

where H = average depth of flow

d_{85} = fall diameter (85% finer by weight).

In this analysis, an average value of 91.5 for C was obtained by equation 6.4. The resultant velocities on the node points were computed by averaging the adjacent values of u and v. Thus,

$$VR_{i,j} = \sqrt{\left[\frac{u_{i,j-\frac{1}{2}} + u_{i,j+\frac{1}{2}}}{2}\right]^2 + \left[\frac{v_{i-\frac{1}{2},j} + v_{i+\frac{1}{2},j}}{2}\right]^2} \tag{6.5}$$

It is to be emphasized that applying this averaging process to points lying in the separation region would lead to underestimation of the resultant velocities, due to the discontinuity of the flow and the presence of jet action and high velocity gradients. This difficulty was overcome by taking the maximum resultant velocity at a point in the separation region as the maximum resultant velocity of the four surrounding mid-cell points. In addition, the resultant velocities at the points adjacent to the dike's nose were further increased by 15% to account for the existance of high velocity gradients in this vicinity.

It is noted that a portion of the vertical vortex generated at the nose of the dike sheds and is transported along the separation line. Since the numerical equations tend to suppress the shedding mechanism (i.e. artificial stability is introduced), a shedding effect was superimposed on the average vorticity pattern. This was achieved by using the following empirical decay function

$$\Delta\omega_{ij} = 0.5 \cdot \omega_{nose} \cdot \left[1 - x/L \right]^2 \qquad (6.6)$$

where $\Delta\omega_{ij}$ are additions to the local vorticity values for the nodes along the separation line;

x is the distance, along the x-axis, from the local mesh point to the dike's location;

L is the extent of the separation line in the x-direction.

The net vorticity value was incorporated in the term $k_1\omega/\omega_o$. The value of k_1 was taken equal to 0.5, based on experimentation with the model, and the reference vorticity, ω_o, was chosen as the vorticity at the dike's nose before the beginning of erosion.

The continuous momentum transfer from the acceleration region to the wake region creates a turbulence or entrainment zone around the separation line. This zone was simulated in the model by a free jet expanding along the separation line with a slope of 5:1. In this zone, different correction values were assigned to the constant k_2. Based on experimentation with the model, k_2 was taken equal to 0.2 in the first 10 inches downstream of the dike, 0.1 in the next 15 inches and then zero, in remaining part of the zone.

6.2.2 Calculation of the Eroded Depth

The increment in the eroded depth, Δz, was given in chapter III as

$$\Delta z = k_3(\tau-\tau_c) \tag{3.50}$$

The critical shear stress, τ_c, was calculated from Shield's formula (41).

A value of $\tau_c = 0.075$ lb/ft^2 was obtained for plane level beds and utilized in the numerical model. Furthermore, the critical shear stress was adjusted according to the orientation of the downstream local slope of the scour hole with respect to the local average velocity vector. Hence,

$$\tau_c' = \tau_c \times \left[\frac{\tan \phi}{\tan \theta} + 1\right] \qquad (6.7)$$

where ϕ is the local adverse slope of the scour hole;

θ is the angle of internal friction for the bed material.

In order to ensure convergence, the discretization in the z-direction was controlled by adjusting the constant k_3 to yield a maximum value of $\Delta z < 0.05$ ft.

The increased shear stress due to the horseshoe vortex (figure 1.1) generated in the dike's vicinity was accounted for, in the model, by introducing the maximum value of the shear stress evaluated at the tip of the dike at the diagonal mesh point upstream from the nose of the dike. This has the effect of increasing the area of bed subjects to maximum shear. The three-dimensional model is governed by the following conditions:

a) no deposition is allowed;

b) the slope of the scour hole sides must not exceed the angle of repose of the bed material. This was controlled by an inverted cone, having surface slopes equal to the angle of repose, placed with its vertex at each eroded point successively. The positions of all points lying inside the enveloping surface of the cone were adjusted.

6.2.3 The Depth-Averaged Stream Function

The difference form of the three-dimensional Poisson type equation 3.53 may be solved by iterative procedures. The adopted difference equation, in the linearized form, is analogous to that utilized for unbalanced finite difference grids, often applied to Laplace and Poisson's equations (43,52,53,54,55). In this analysis the Gauss-Seidel iterative scheme was used to solve the equation, and the solution was terminated when the specified tolerance as given by equation 6.3 was satisfied or the number of iterations exceeded 150. The use of a large Δz may introduce an error that hinders convergence because of the non-linear nature of equation 3.53.

6.2.4 Order of Calculations and Numerical Results

The final two-dimensional Poisson solution was utilized in the three-dimensional model to provide the initial values for a flat bed. The local shear stress at every node was calculated with proper allowance for the horseshoe vortex, and taking into account the appropriate corrections and adjustments of velocities, vorticities, turbulence and shedding mechanism. The eroded depth, Δz, was computed from the difference between the computed local shear stress and the adjusted local bed resistance. The excavations and adjustments of the bed levels and slopes were made using the previously mentioned inverted cone technique. The stream function was readjusted by the iterative solution, and the corresponding depth-averaged velocity components and local vorticities were calculated.

The bed adjustments were continued until the difference between the local shear and the local bed resistance was within a tolerance of 0.001 at every point, and no more scour was considered to occur. Different scour contour maps were obtained from the mathematical model for different discharges, upstream water depths, and opening ratios. Figures 6.11 to 6.16 show the computed and experimental scour patterns. Figure 6.17 illustrates a typical contour map for the scour hole predicted by the numerical model and the corresponding experimental patterns obtained after 2½ hours and 24 hours of run time. As mentioned in chapter V, when the same experiment was allowed to continue for a long time, a larger and slightly deeper hole developed. The comparison between the 24 hours experimental pattern and the computed one indicates a marked improvement in the agreement; it appears that the computed scour pattern represents the limiting condition.

A comparison plot of the maximum depths of scour obtained from the numerical model versus the experimental maximum scour depths and the ones calculated by equation 5.16 gives the correlation shown in figure 6.18. Shown also is a comparison of the predicted and observed maximum length, L, of the scour hole over its maximum width, w.

6.3 Stability Analysis

If it were possible to carry out all calculations of the finite difference equations to an infinite number of decimal places, their exact solution would be obtained. In practice, however, each calculation is carried out to a finite number of decimal places or signigicant figures, a procedure that introduces a "round-off" error every time it is used, and the solution actually computed is not the exact one; it is termed the numerical solution. Generally, a set of finite difference equations is stable when the cumulative effect of all the rounding errors is negligible.

6.3.1 The Two-Dimensional Model

The equations, solved in this model, are the Poisson difference equation, and the Helmholtz vorticity difference equation.

The stability of the Poisson difference equation: This equation is analyzed by a procedure very similar to that used by O'Brien et al (33), assuming that there exists an error, ε_{ijk}, at each mesh point. The manner in which errors are propagated can easily be seen by applying the finite difference equation to the errors themselves.

Because ε obeys both the difference equation and the boundary conditions, it may be expanded in a finite double series of orthogonal functions that also satisfy both the difference equation and the boundary conditions, namely

$$\varepsilon_{ijk} = \sum_{p=0}^{M} \sum_{q=0}^{N} A_{pqk} \cos \beta_p \Delta x \cos \beta_q \Delta y \tag{6.8}$$

where $\beta_p = p\pi$; $\beta_q = q\pi$; M = the number of intervals in the x-direction; N = the number of intervals in the y-direction.

Since a square mesh is used in this analysis, $\Delta x = \Delta y = a = 1/N$. Substituting equation 6.8 in the Poisson difference equation 3.42 and examining each term in the series separately shows that

$$\begin{aligned} A_{pq_{k+1}} = (1-w)\, A_{pq_k} + w \Big\{ & A_{pq_{k+1}} \cos \beta_p \Delta x \\ & + A_{pq_k} \cos \beta_p \Delta x + A_{pq_{k+1}} \cos \beta_q \Delta y \\ & + A_{pq_k} \cos \beta_q \Delta y + a^2 \omega_{ij} \Big\} \end{aligned} \tag{6.9}$$

Dividing by A_{pq_k} and rearranging the terms, then

$$R = \frac{4 - 2w - 2w(S_1+S_2) + \left[\frac{a^2\omega_{ij}}{A_{pq_k}}\right] w}{4 - 2w + 2w(S_1+S_2)} \tag{6.10}$$

where $R = A_{pq_{k+1}}/A_{pq_k}$

$$S_1 = \sin^2 \frac{\beta_p \Delta x}{2} = \sin^2 \frac{p\pi}{2N}$$

$$S_2 = \sin^2 \frac{\beta_q \Delta y}{2} = \sin^2 \frac{q\pi}{2N}$$

The arbitrarily defined error amplitude, A_{pq_k}, is assumed to have a large value, therefore, the term $(a^2\omega_{ij}/A_{pq_k})$ will be negligible. For stability, R must have an absolute value less than or equal to unity for all values of p and q. For a large A_{pq_k} the stability condition is guaranteed.

<u>The stability of the proposed Helmholtz difference equation</u>: Let the error ε_{ijn} satisfy the difference equation 3.32 and appropriate boundary conditions. The error may be represented by

$$\varepsilon_{ijn} = \sum_{p=0}^{M} \sum_{q=0}^{N} A_{pq_n} \cos \beta_p \Delta x \cos \beta_q \Delta y \tag{6.11}$$

The convective term in equations 3.32 can be re-stated in the form

$$\frac{1}{2} r_1 \left\{ u^n_{i-\frac{1}{2},j} (\omega^n_{ij} + \omega^n_{i-1,j}) - u^n_{i+\frac{1}{2},j}(\omega^n_{ij} + \omega^n_{i+1,j}) \right.$$

$$\left. + v^n_{i,j-\frac{1}{2}}(\omega^n_{ij} + \omega^n_{i,j-1}) - v^n_{i,j+\frac{1}{2}}(\omega^n_{ij} + \omega^n_{i,j+1}) \right\} \tag{6.12}$$

The Taylor series expansion is used to evaluate the velocity components, u and v, so that

$$\left.\frac{\partial u}{\partial x}\right|_{ij} = \frac{u_{i+\frac{1}{2},j} - u_{i-\frac{1}{2},j}}{a} \tag{6.13}$$

$$\left.\frac{\partial v}{\partial y}\right|_{ij} = \frac{v_{i,j+\frac{1}{2}} - v_{i,j-\frac{1}{2}}}{a} \tag{6.14}$$

From the continuity equation

$$\left.\frac{\partial u_o}{\partial x}\right|_{ij} + \left.\frac{\partial v_o}{\partial y}\right|_{ij} = 0 \tag{6.15}$$

therefore,

$$\frac{u_{i+\frac{1}{2},j} - u_{i-\frac{1}{2},j}}{a} + \frac{v_{i,j+\frac{1}{2}} - v_{i,j-\frac{1}{2}}}{a} = 0 \tag{6.16}$$

Combining equation 6.12 and 6.16 yields

$$\tfrac{1}{2} r_1 \left[u^n_{i-\frac{1}{2},j}\omega^n_{i-1,j} - u^n_{i+\frac{1}{2},j}\omega^n_{i+1,j} + v^n_{i,j-\frac{1}{2}}\omega^n_{i,j+1} - v^n_{i,j+\frac{1}{2}}\omega^n_{i,j+1} \right] \tag{6.17}$$

Replacing the convective term of equations 3.32 by the above expressions and substituting equation 6.11 into the modified equations 3.32 then

$$A_{pq_{n+1}}(-2r\cos\beta_p\Delta x + 1 + 3r) = A_{pq_n}\Big(2r\cos\beta_q\Delta y - \tfrac{1}{2}r_1\cos\beta_q\Delta y\,\frac{\partial v_o}{\partial y}\,a - \tfrac{1}{2}r_1\cos\beta_p\Delta x\,\frac{\partial u_o}{\partial x}\,a\Big) + (1-r)\,A_{pq_{n-1}} \qquad (6.18)$$

and

$$A_{pq_{n+2}}(-2r\cos\beta_q\Delta y + 1 + 3r) = A_{pq_{n+1}}\Big(2r\cos\beta_p\Delta x - \tfrac{1}{2}r_1\cos\beta_q\Delta y\,\frac{\partial v_o}{\partial y}\,a - \tfrac{1}{2}r_1\cos\beta_p\Delta x\,\frac{\partial u_o}{\partial x}\,a\Big) + (1-r)\,A_{pq_n} \qquad (6.19)$$

Dividing equation 6.18 and 6.19 by r and rearranging the terms, gives respectively

$$A_{pq_{n+1}}(1+\rho+4S_1) = A_{pq_n}\Big[2-4S_2-C_1(1-2S_2)-C_2(1-2S_1)\Big] + (\rho-1)\,A_{pq_{n-1}} \qquad (6.20)$$

and

$$A_{pq_{n+2}}(1+\rho+4S_2) = A_{pq_{n+1}}\left[2-4S_1-C_1(1-2S_2)-C_2(1-2S_1)\right]$$

$$+ (\rho-1)\,A_{pq_n} \qquad (6.21)$$

where $C_1 = \frac{a^2}{2(\nu+\xi)} \times \frac{\partial v_o}{\partial y}$

$$C_2 = \frac{a^2}{2(\nu+\xi)} \times \frac{\partial u_o}{\partial x}$$

$$\rho = \frac{1}{r} = a^2/2\delta t(\nu+\xi)$$

Figure 6.19 illustrates the advancement of the solution from time n. R_1, R_2, R_3 ... R_{NN} represent the ratios of the successive A_{pq}'s for half the time step while RA_1, RA_3, ... RA_{NN} and RR_2, RR_4 ... RR_{NN-1} are the ratios of successive A_{pq}'s for the full time step. In the initial set up of the solution the vorticity values at (n-1) and (n) were assumed equal. Hence R_1 = $A^{n-1}/A^n = A^0/A^1 = 1$. Equation 6.20 was used for the advancement along the x-axis and for the calculation of the ratios R_2, R_4, ... R_{NN} and the ratios RA_1, RA_3, ... RA_{NN}, whereas the ratios R_3, R_5, ... R_{NN-1} and the ratios RR_2, RR_4, ... RR_{NN-1} were computed by equation 6.21 which was also used for the advancement along the y-axis.

Based on the preceding analysis and by manipulating equations 6.20 and 6.21, the following expressions can be deduced.

$$R_1 = A^{n-1}/A^n = 1$$

$$R_2 = A^n/A^{n+1} = \frac{1 + \rho + 4S_1}{\left[2-4S_2-C_1(1-2S_2)-C_2(1-2S_1)\right] + (\rho-1) \times R_1} \tag{6.22}$$

$$R_3 = A^{n+1}/A^{n+2} = \frac{1 + \rho + 4S_2}{\left[2-4S_1-C_1(1-2S_2)-C_2(1-2S_1)\right] + (\rho-1) \times R_2} \tag{6.23}$$

These expressions indicate that each half step ratio is always dependent on the previous one; this forms a chain process that can be traced back to the ratio $R_1 = 1$.

The full step ratios can also be derived using equations 6.20 and 6.21 as follows -

$$RA_1 = A^{n+1}/A^{n-1} = \frac{(1/R_1)\left[2-4S_2-C_1(1-2S_2)-C_2(1-2S_1)\right] + (\rho-1)}{1 + \rho + 4S_1} \tag{6.24}$$

and

$$RR_2 = A^{n+2}/A^n = \frac{(1/R_2)\left[2-4S_1-C_1(1-2S_2)-C_2(1-2S_1)\right] + (\rho-1)}{1 + \rho + 4S_2} \tag{6.25}$$

These equations show that the full step ratios are computed from the corresponding half step ratios.

The solution is stable if the absolute values of all the ratios, in at least one of the groups comprising the full step ratios, lie in a range less or equal to one over many advancements. The stability should be tested at every point in the S_1-S_2 plane. The difficulty still to be overcome arises in the impossibility of predicting the velocity gradients embedded in the terms C_1 and C_2. The problem is first approached by taking $C_1 = C_2 = 0$ which eliminates the convective term from the Helmholtz equation. Figure 6.20 shows a contour map for the values of ρ. Any value of ρ equal or less than the appropriate contour value will induce instability. Therefore, for the solution to be stable over the entire domain, ρ must exceed the highest contour value.

Since the flow is mainly in the x-direction, the velocity gradient in the y-direction was assumed negligible; thus C_1 was eliminated. The velocity gradient in the x-direction was then utilized to represent the acceleration and decceleration flow zones which result from the contraction and expansion of flow as induced by the separation line. For the cases of gradual contraction and expansion, the corresponding values of C_2 were taken as 1 and -1 respectively. Figures 6.21 and 6.22 present the ρ values for the two cases. Values for C_2 of 10 and -10 were used to represent the conditions of rapid contraction and expansion respectively, and the corresponding contour maps are shown in figures 6.23 and 6.24.

Furthermore, the value of ρ = 170, used in the mathematical model, was kept constant and the variation in C_2 was obtained. Figures 6.25 and 6.26 show respectively positive and negative C_2-contours which indicate zones of instability. The C_2-contours therefore, are of an opposite nature to that of the ρ-contours, i.e. in order to ensure overall stability, the value of C_2 should be less than the minimum C_2 contour value.

As can be seen from figure 6.22, a region of high instability is encountered at the point of coordinates (0,0). Also, when the expansion is rapid, the region of high instability spreads from this point to extend over approximately 1/3 of the domain (see figure 6.24). This supports the use of a zero vorticity boundary condition at the walls.

Experimentation with the model indicated that the velocity gradients in the acceleration and decceleration zones never yielded a value of C_2 greater than unity. Moreover, the velocity gradients along the dike itself were restricted by the special treatment described in section 6.1.2. Consequently, the rapid contraction and expansion are hypothetical cases which are not faced in the problem under consideration.

6.3.2 The Three-Dimensional Model

The stability of the numerical solution in this case was investigated by examining the iterative procedure used to solve the three-dimensional Poisson difference equation 3.53. This equation may be rewritten as

$$\psi''_{ij} = \frac{\psi''_{i-1,j}/\lambda_1 + \psi''_{i+1,j}/\lambda_2 + \psi''_{i,j-1}/\lambda_3 + \psi''_{i,j+1}/\lambda_4 + \frac{a^2}{2}\,\omega_{ij}}{1/\lambda_1 + 1/\lambda_2 + 1/\lambda_3 + 1/\lambda_4} \tag{6.26}$$

in which $\lambda_1 = 1/(z_{i-1,j} + z_{ij})$

$\lambda_2 = 1/(z_{i+1,j} + z_{ij})$

$\lambda_3 = 1/(z_{i,j-1} + z_{ij})$

$\lambda_4 = 1/(z_{i,j+1} + z_{ij})$

A procedure similar to the one used for the two-dimensional Poisson equation was applied to the above equation to give

$$R = \frac{(1/\lambda_2 + 1/\lambda_4) - 2S_1/\lambda_2 - 2S_2/\lambda_4 + (a^2\omega_{ij}/2A_{pq_k})}{(1/\lambda_2 + 1/\lambda_4) + 2S_1/\lambda_1 + 2S_2/\lambda_3} \tag{6.27}$$

This expression reveals that for a large A_{pq_k} the term $(a^2\omega_{ij}/2A_{pq_k})$ can be neglected and the remaining terms will always yield a value of R less than unity, which indicates a stable solution.

This analysis ignores the change in z. However, as mentioned before, it was found by experimentation with the model, that the change in z should be kept small in order for the solution to converge.

6.4 Series Truncation Error Analysis

A possible error in the numerical solution could result from the discretization of the flow field. The finite-difference solution is said to be convergent when the numerical solution tends to the exact solution of the partial differential equation as Δx, Δy, and Δt approach zero. In the following two sections the Poisson difference equation and the Helmholtz difference equation are examined.

6.4.1 The Poisson Difference Equation

When a function ψ and its derivatives are single-valued, finite, and continuous functions of x and y, then by Taylor's theorem

$$\psi(x+\Delta x,y) = \psi(x,y)+\frac{\partial\psi}{\partial x}\Delta x+\frac{1}{2}\frac{\partial^2\psi}{\partial x^2}\Delta x^2+\frac{1}{6}\frac{\partial^3\psi}{\partial x^3}\Delta x^3+0(\Delta x^4)$$

$$\psi(x-\Delta x,y) = \psi(x,y)-\frac{\partial\psi}{\partial x}\Delta x+\frac{1}{2}\frac{\partial^2\psi}{\partial x^2}\Delta x^2-\frac{1}{6}\frac{\partial^3\psi}{\partial x^3}\Delta x^3+0(\Delta x^4)$$

$$\psi(x,y+\Delta y) = \psi(x,y)+\frac{\partial\psi}{\partial y}\Delta y+\frac{1}{2}\frac{\partial^2\psi}{\partial y^2}\Delta y^2+\frac{1}{6}\frac{\partial^3\psi}{\partial y^3}\Delta y^3+0(\Delta y^4)$$

$$\psi(x,y-\Delta y) = \psi(x,y)-\frac{\partial\psi}{\partial y}\Delta y+\frac{1}{2}\frac{\partial^2\psi}{\partial y^2}\Delta y^2-\frac{1}{6}\frac{\partial^3\psi}{\partial y^3}\Delta y^3+0(\Delta y^4)$$

(6.28)

Substituting these relations into the Poisson difference equation 3.29 and taking $\Delta x = \Delta y = a$, yields

$$\psi(x,y) = \frac{1}{4}\left[4\psi(x,y) + \left\{\frac{\partial^2\psi}{\partial x^2} + \frac{\partial^2\psi}{\partial y^2}\right\} a^2 + a^2\omega + 0(a^4)\right] \tag{6.29}$$

or

$$\frac{\partial^2\psi}{\partial x^2} + \frac{\partial^2\psi}{\partial y^2} + \omega + 0(a^2) = 0 \tag{6.30}$$

When $a \rightarrow 0$, the above equation reduces to the form

$$\frac{\partial^2\psi}{\partial x^2} + \frac{\partial^2\psi}{\partial y^2} = -\omega \tag{3.24}$$

Thus, the solution converges to the original partial differential equation 3.24 with a 2nd order accuracy.

6.4.2 The Helmholtz Difference Equation

The Taylor theorem was used to expand the velocity components u and v in the x and y directions and the vorticity in the x, y and t directions. The following relationships are obtained, assuming $\Delta x = \Delta y = a$.

$$\begin{aligned}
u(x-a,y+a/2) &= u_o-\frac{\partial u}{\partial x}\,a + \frac{\partial u}{\partial y}\,a/2 + 0(a^2)\\
u(x-a,y-a/2) &= u_o-\frac{\partial u}{\partial x}\,a - \frac{\partial u}{\partial y}\,a/2 + 0(a^2)\\
u(x\quad,y-a/2) &= u_o-\ 0\ - \frac{\partial u}{\partial y}\,a/2 + 0(a^2)\\
u(x\quad,y+a/2) &= u_o-\ 0\ + \frac{\partial u}{\partial y}\,a/2 + 0(a^2)\\
u(x+a,y+a/2) &= u_o+\frac{\partial u}{\partial x}\,a + \frac{\partial u}{\partial y}\,a/2 + 0(a^2)\\
u(x+a,y-a/2) &= u_o+\frac{\partial u}{\partial x}\,a - \frac{\partial u}{\partial y}\,a/2 + 0(a^2)
\end{aligned}\qquad (6.31)$$

$$\begin{aligned}
v(x-a/2,y-a) &= v_o-\frac{\partial v}{\partial x}\,a/2 - \frac{\partial v}{\partial y}\,a + 0(a^2)\\
v(x+a/2,y-a) &= v_o+\frac{\partial v}{\partial x}\,a/2 - \frac{\partial v}{\partial y}\,a + 0(a^2)\\
v(x+a/2,y\quad) &= v_o+\frac{\partial v}{\partial x}\,a/2 +\ 0\ + 0(a^2)\\
v(x-a/2,y\quad) &= v_o-\frac{\partial v}{\partial x}\,a/2 +\ 0\ + 0(a^2)\\
v(x-a/2,y+a) &= v_o-\frac{\partial v}{\partial x}\,a/2 + \frac{\partial v}{\partial y}\,a + 0(a^2)\\
v(x+a/2,y+a) &= v_o+\frac{\partial v}{\partial x}\,a/2 + \frac{\partial v}{\partial y}\,a + 0(a^2)
\end{aligned}\qquad (6.32)$$

$$\begin{aligned}
\omega(x-a,y\quad,t) &= \omega_o - \frac{\partial \omega}{\partial x}\,a + 0(a^2)\\
\omega(x+a,y\quad,t) &= \omega_o + \frac{\partial \omega}{\partial x}\,a + 0(a^2)\\
\omega(x\quad,y-a,t) &= \omega_o - \frac{\partial \omega}{\partial y}\,a + 0(a^2)\\
\omega(x\quad,y+a,t) &= \omega_o + \frac{\partial \omega}{\partial y}\,a + 0(a^2)
\end{aligned}\qquad (6.33)$$

$$\begin{aligned}
\omega(x\quad,y\quad,t+\Delta t) &= \omega_o + \frac{\partial \omega}{\partial t}\,\Delta t + 0(\Delta t^2)\\
\omega(x\quad,y\quad,t-\Delta t) &= \omega_o - \frac{\partial \omega}{\partial t}\,\Delta t + 0(\Delta t^2)
\end{aligned}\qquad (6.34)$$

$$\omega(x-a,y\quad,t+\Delta t) = \omega_o - \frac{\partial\omega}{\partial x} a + \frac{\partial\omega}{\partial t}\Delta t + 0(\Delta t^2) + \tfrac{1}{2}\frac{\partial^2\omega}{\partial x^2} a^2$$

$$- \frac{1}{6}\frac{\partial^3\omega}{\partial x^3} a^3 + 0(a^4)$$

$$\omega(x+a,y\quad,t+\Delta t) = \omega_o + \frac{\partial\omega}{\partial x} a + \frac{\partial\omega}{\partial t}\Delta t + 0(\Delta t^2) + \tfrac{1}{2}\frac{\partial^2\omega}{\partial x^2} a^2$$

$$+ \frac{1}{6}\frac{\partial^3\omega}{\partial x^3} a^3 + 0(a^4) \qquad (6.35)$$

$$\omega(x\quad,y-a,t+\Delta t) = \omega_o - \frac{\partial\omega}{\partial y} a + \frac{\partial\omega}{\partial t}\Delta t + 0(\Delta t^2) + \tfrac{1}{2}\frac{\partial^2\omega}{\partial y^2} a^2$$

$$- \frac{1}{6}\frac{\partial^3\omega}{\partial y^3} a^3 + 0(a^4)$$

$$\omega(x\quad,y+a,t+\Delta t) = \omega_o + \frac{\partial\omega}{\partial y} a + \frac{\partial\omega}{\partial t}\Delta t + 0(\Delta t^2) + \tfrac{1}{2}\frac{\partial^2\omega}{\partial y^2} a^2$$

$$+ \frac{1}{6}\frac{\partial^3\omega}{\partial y^3} a^3 + 0(a^4) \qquad (6.36)$$

Substituting the previous relationships into the Helmholtz difference equation 3.32 leads to

$$2\Delta t\,\frac{\partial\omega}{\partial t} - a^2 r\left[\frac{\partial^2\omega}{\partial x^2} + \frac{\partial^2\omega}{\partial y^2}\right] + a\, r_1\left[\frac{\partial}{\partial x}(u\omega) + \frac{\partial}{\partial y}(v\omega)\right]$$

$$= r0(\Delta t^2) + r\ 0(a^4) + r_1\ 0(a^2) \qquad (6.37)$$

Dividing by 2Δt and substituting the values of r and r_1, the above equation can be rearranged to

$$\frac{\partial\omega}{\partial t} - (\nu+\xi)\left[\frac{\partial^2\omega}{\partial x^2} + \frac{\partial^2\omega}{\partial y^2}\right] + \frac{\partial}{\partial x}(u\omega) + \frac{\partial}{\partial y}(v\omega)$$

$$= \frac{r}{2}\, 0(\Delta t) + (\nu+\xi)\; 0(a^2) + 0(a) \qquad (6.38)$$

If Δt and $a \rightarrow 0$ with r = constant, then

$$\frac{\partial\omega}{\partial t} + \frac{\partial}{\partial x}\left(u\omega - (\nu+\xi)\frac{\partial\omega}{\partial x}\right) + \frac{\partial}{\partial y}\left(v\omega - (\nu+\xi)\frac{\partial\omega}{\partial y}\right) = 0 \qquad (3.25)$$

Thus, the solution converges to the original partial differential equation 3.25 with a 1st order accuracy for both a and t, provided that r is a real finite value, i.e. Δt should approach zero faster than a.

CHAPTER VII

CONCLUSIONS

The conclusions of this thesis are considered in two parts:

a) Those relating to the numerical models.

b) Those relating to the experimental studies.

7.1 Conclusions Based on the Numerical Models

a) In the vicinity of the spur-dike and along the separation line regions of high velocity and vorticity exist. It was found by experimentation with the model that the local velocity, vorticity and turbulence are the main causes of erosion.

b) The alternating direction implicit scheme, used with central time differencing, has the advantage of averaging the error between successive time advancements and was proved to yield stable solutions.

c) The use of an optimum over relaxation factor along with a block iterative scheme in solving the two-dimensional Poisson's equation results in a considerable saving of computation time.

d) The numerically computed values of the coefficient of contraction gave good agreement with those obtained by the jet theory and the data of the U.S.

Geological Survey. Experimental confirmation was obtained for an opening ratio of 0.667, using pitot-tube measurements.

e) The finite difference formulation used for the depth-averaged stream function ensures the stability of the solution.

f) The proposed technique predicts both the depth and shape of the scour hole, and there is good agreement between the numerical solution and experiment.

g) The comparison between the predicted scour pattern and the experimental one, obtained after a prolonged run time indicates that the former represents the limiting scour condition.

7.2 Conclusions Based on the Experimental Studies

a) The maximum depth of scour is significantly affected by the channel's Froude number and the opening ratio at the spur-dike's location.

b) The derived empirical formula, for the maximum depth of scour, is identical in form to the regime equations of Lacey and Blech. The formula gave a good correlation coefficient, and may be used to predict the maximum scour depth for conditions similar to those covered in this study.

c) The depth of scour progresses linearly with the logarithm of time during the development of the hole. The greater the ratio of the disturbing force to the resisting force, the greater the rate of scour.

d) The experiments indicate that the limiting extent of scour is reached when the velocity has been reduced to its critical value due to the enlargement of the scoured section.

e) The continuous removal of the material deposited downstream of the scour hole provides proper simulation of prototype conditions and has the advantage of considerably saving experimental run time.

f) The clear water condition, under which the experiments were conducted, yields deeper and larger scour holes, which confirms the fact that this condition is more critical regarding design criteria.

CHAPTER VIII

RECOMMENDATIONS FOR FUTURE STUDIES

The present analysis gives rise to a number of interesting points that warrant further research. Thus, the following investigations are recommended for further work:

1) More experiments using a variety of sediment sizes are required in order to check the validity of the empirical formula for the maximum depth of scour. Field data should also be collected and used for the same purpose.
2) The proposed numerical model can be applied to the case of scour with a continuous sediment supply. In this case, a bed load function is required along with the shear stress function.
3) The problems of two opposing dikes and a series of dikes can be investigated and solved by the proposed technique.
4) The finite element method can be used to solve the phenomenon of scour around spur-dikes and check the proposed model. By means of the finite element method it is possible to tackle the problem of scour around bridge piers and

inclined spur-dikes. Also, confirmation of the proposed model should be obtained by prototype data.

5) A more rational approach should be applied to evaluate the following parameters:

   a) horseshoe vortex;

   b) turbulence effect;

   c) vorticity shedding mechanism;

   d) eddy viscosity distribution;

   e) the boundary condition at the dike's nose.

6) It may be possible through a careful study to evaluate the convection and diffusion terms and include their effects in obtaining the vorticity in the three-dimensional case.

APPENDIX A

Figures

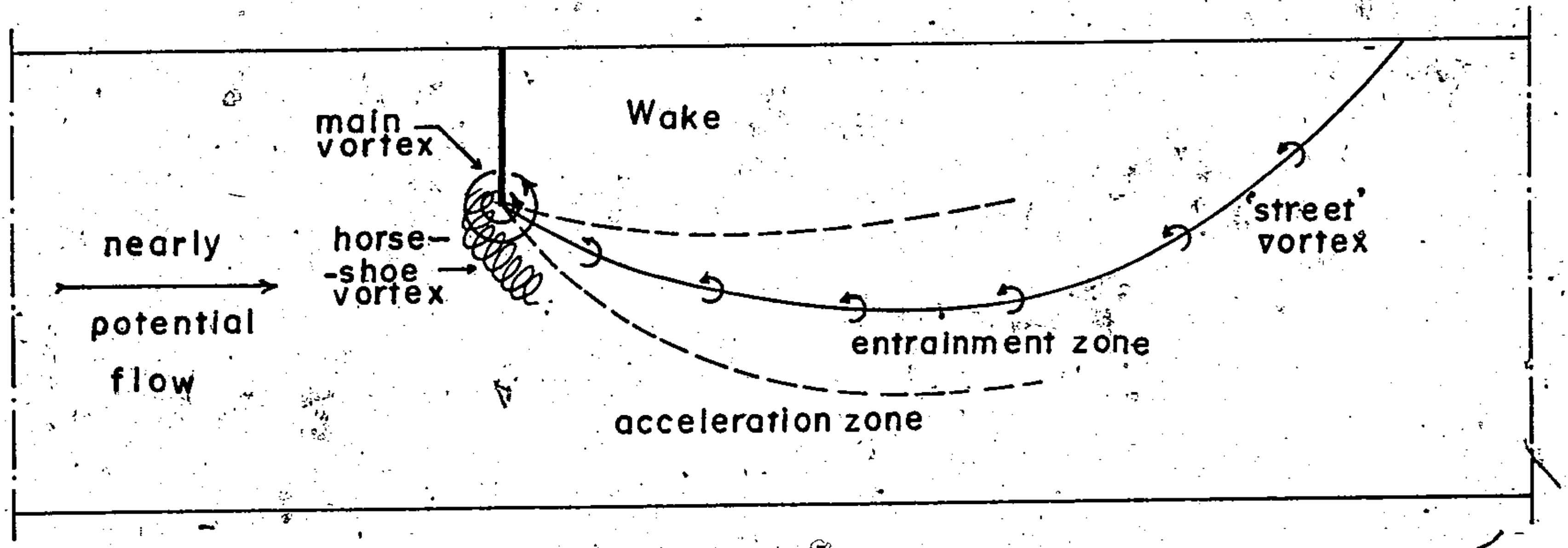

Figure 1.1. Mechanisms of scour.

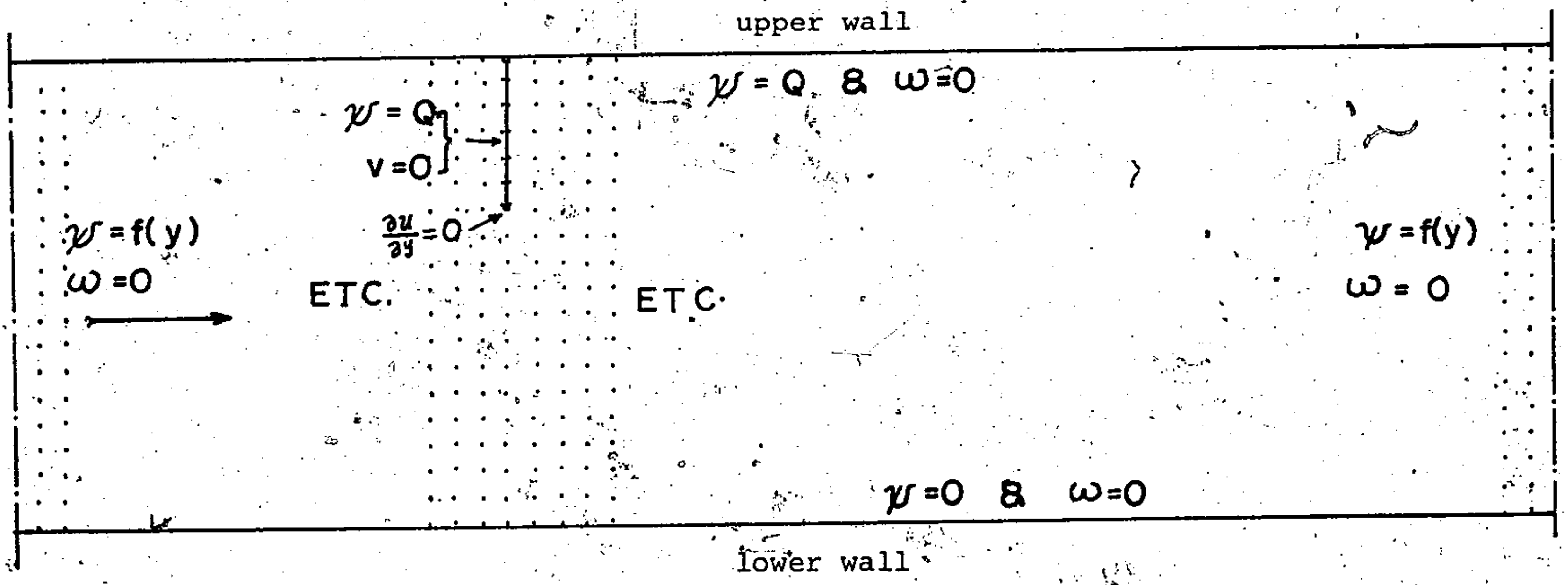

Figure 3.1. Discretization and Boundary Conditions.

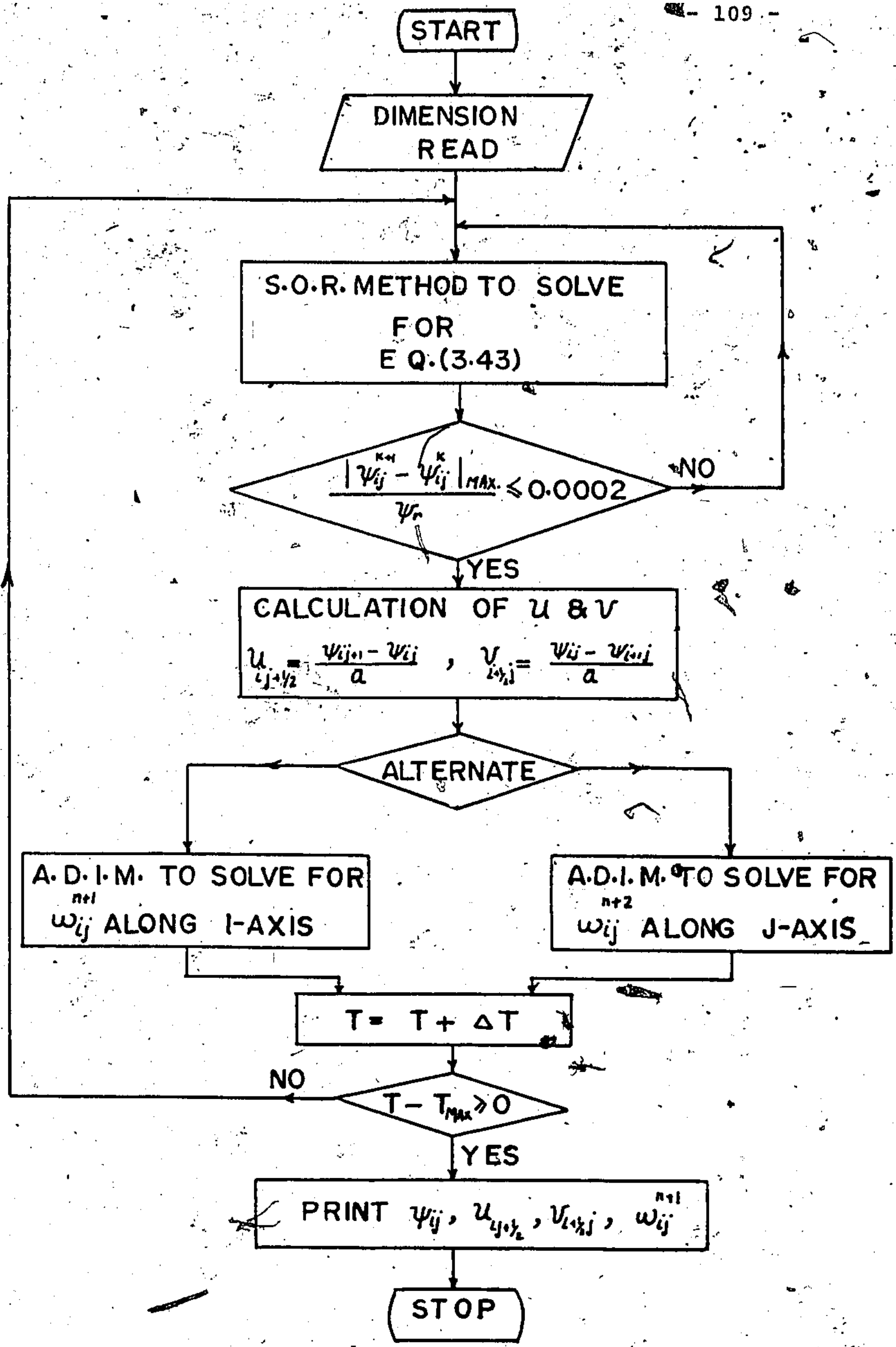

Figure 3.2. Master Flow Chart for Two-Dimensional Flow.

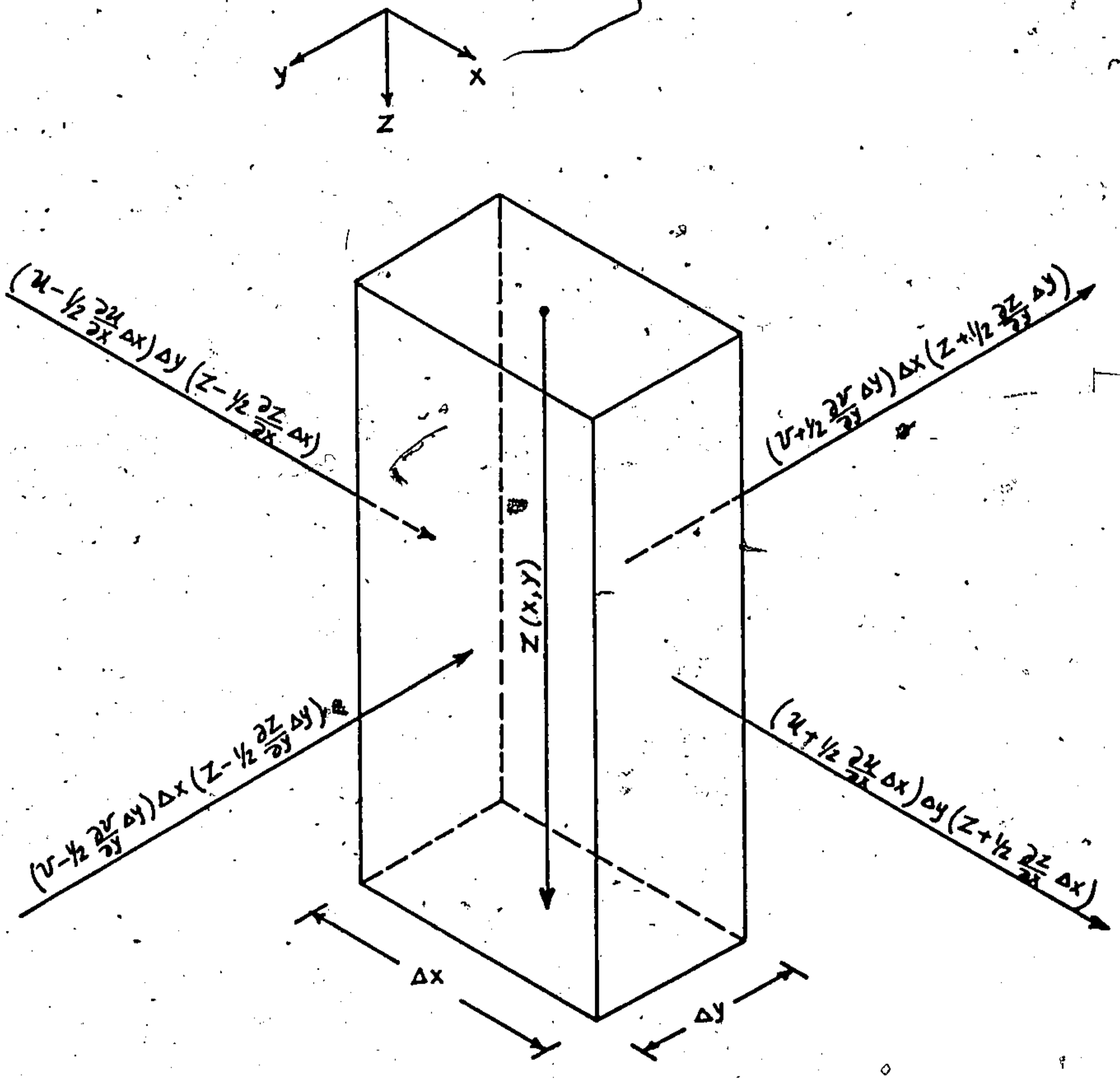

Figure 3.3. Fluid Element.

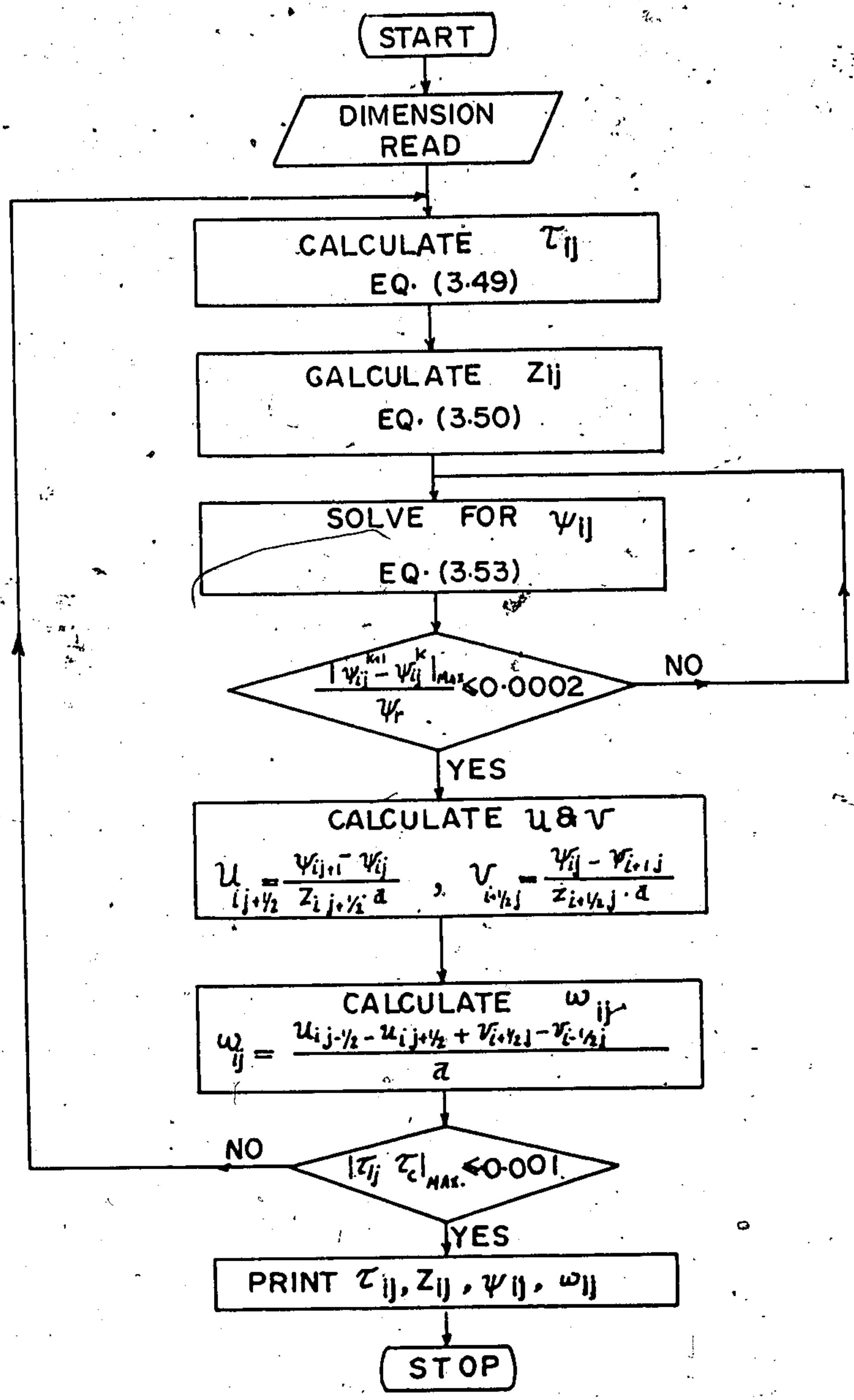

Figure 3.4. Master Flow Chart for Three-Dimensional Flow.

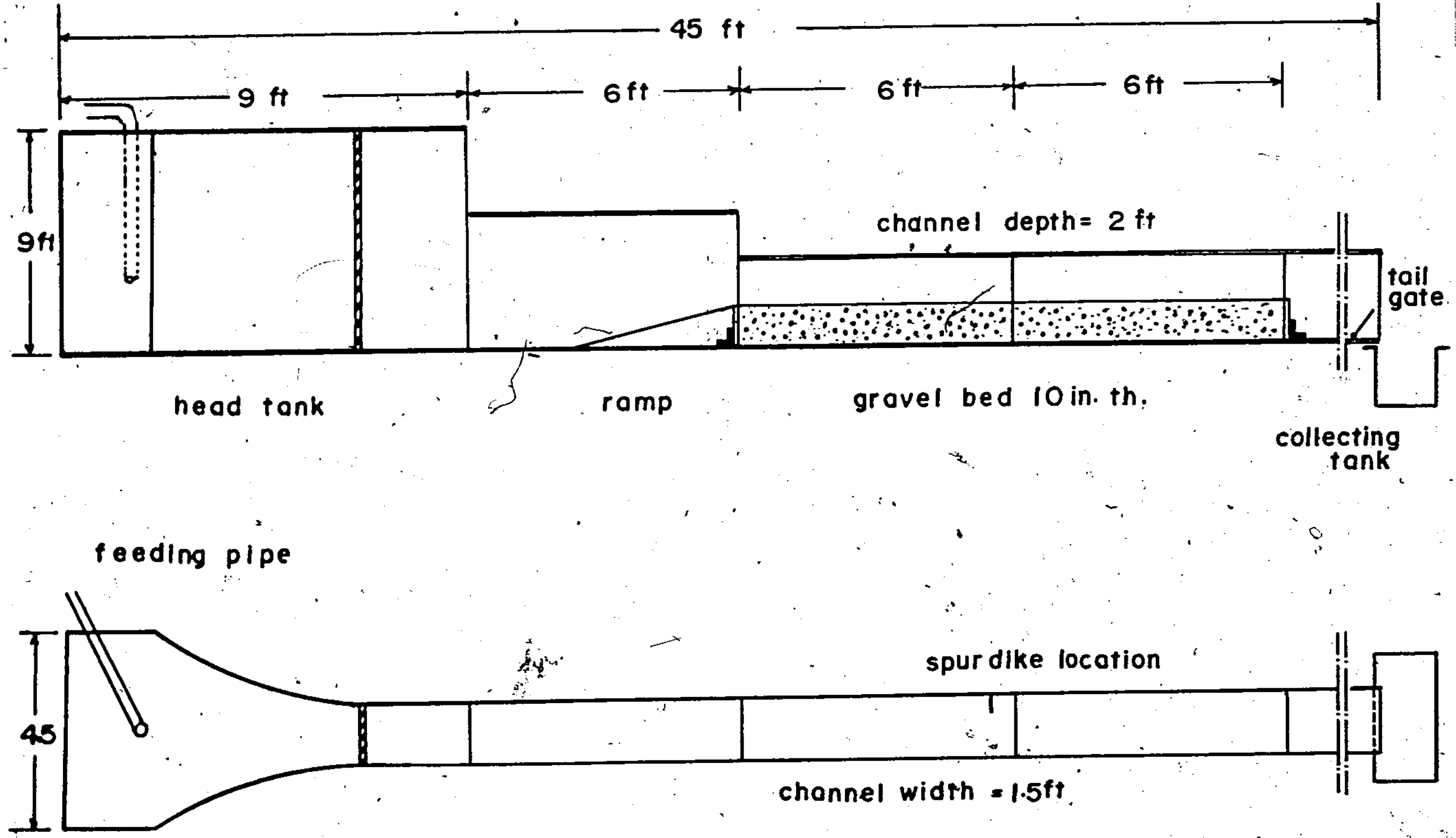

Figure 4.1. Experimental Set Up.

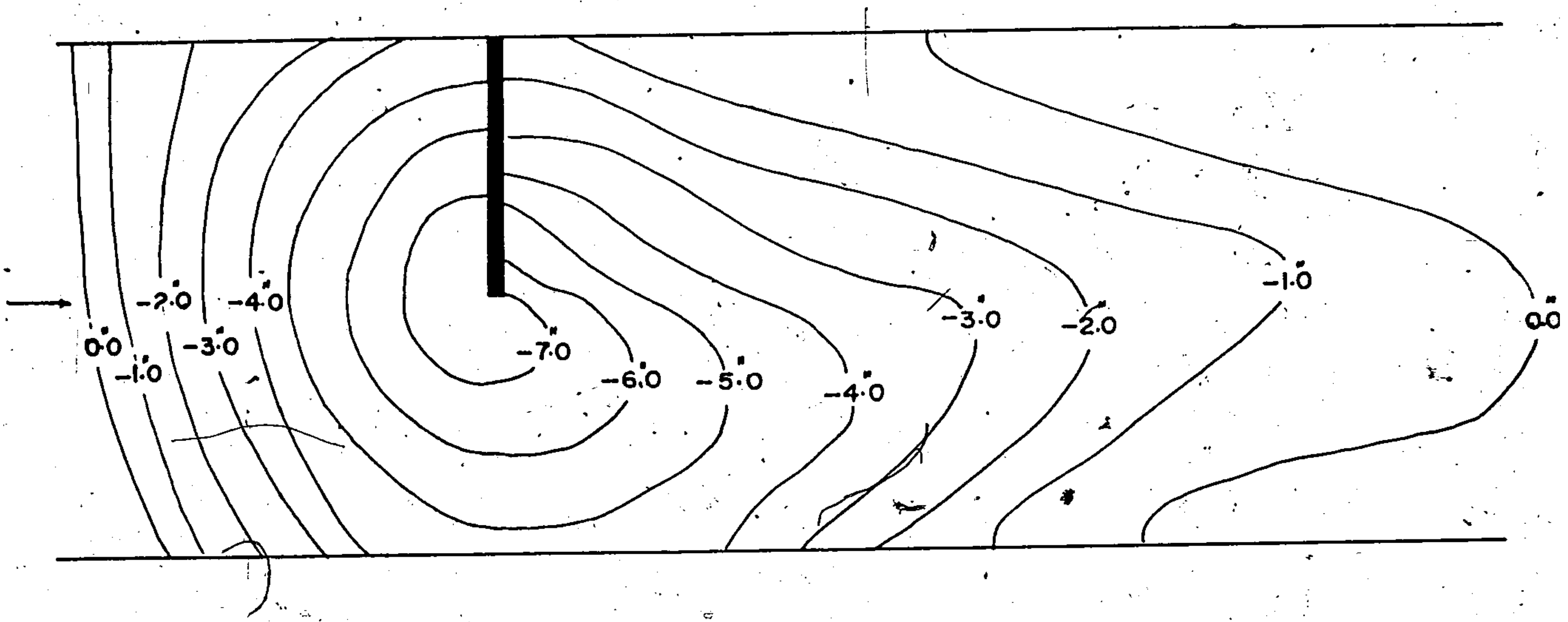

Figure 4.2. Experimental Contour Map for Test No. 2, Table 4.1.

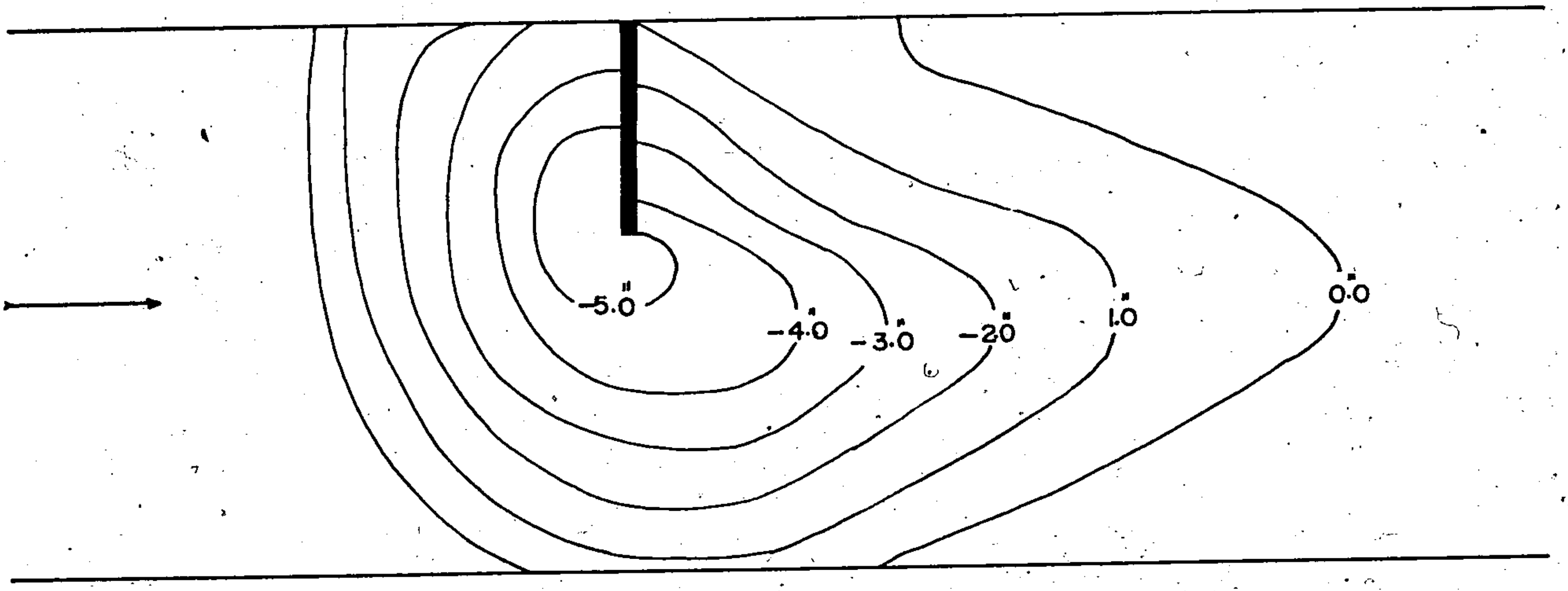

Figure 4.3. Experimental Contour Map for Test No. 3, Table 4.1.

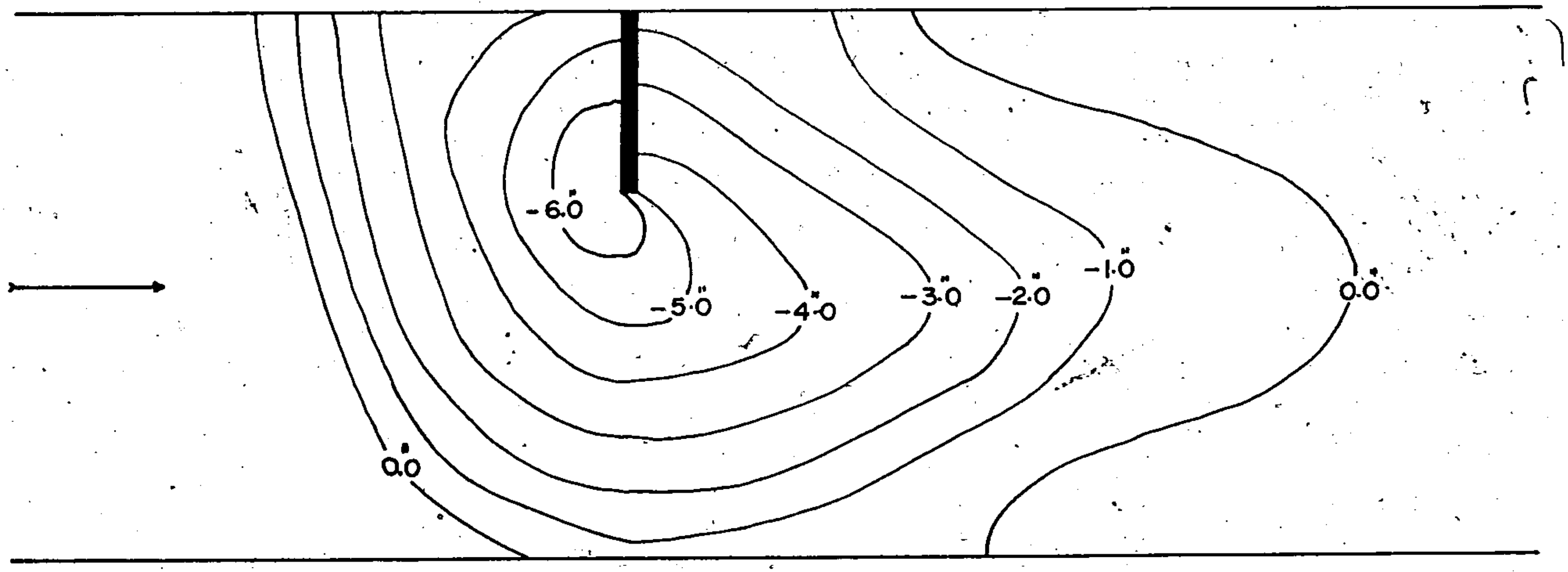

Figure 4.4. Experimental Contour Map for Test No. 13, Table 4.1.

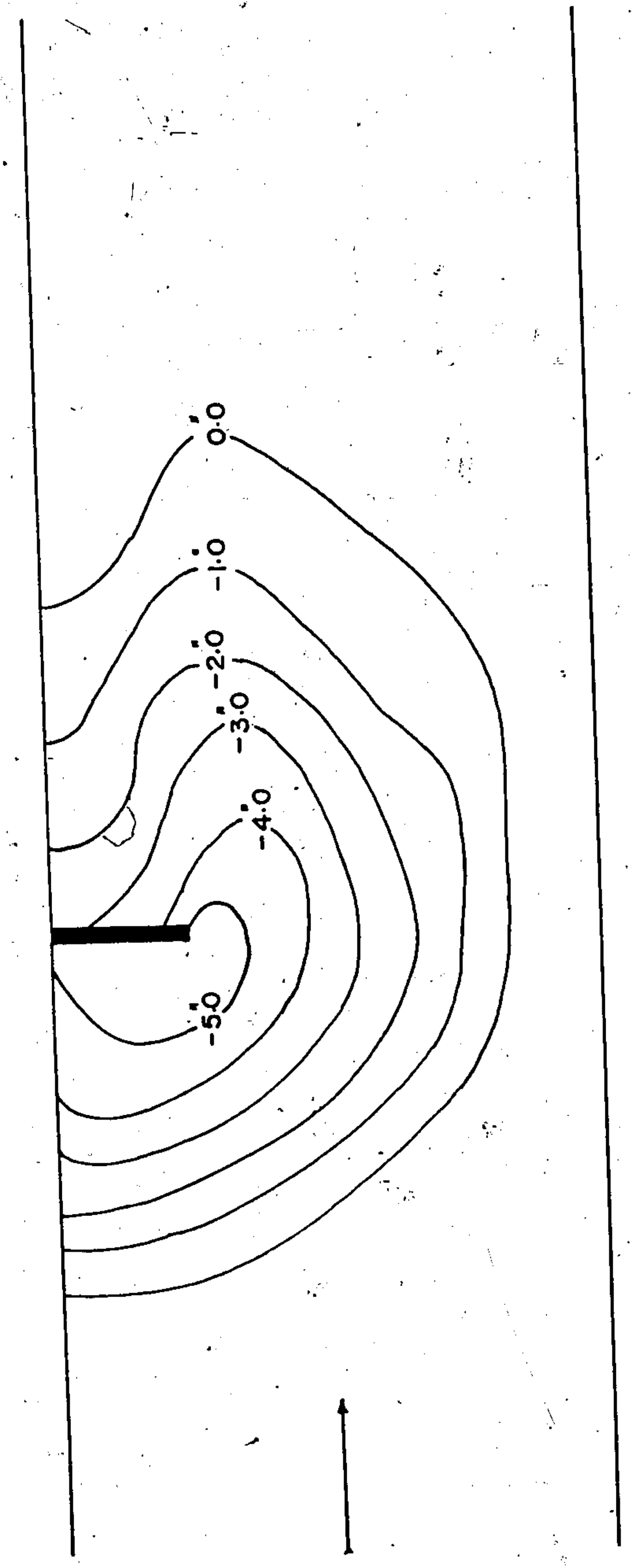

Figure 4.5. Experimental Contour Map for Test No. 17, Table 4.1.

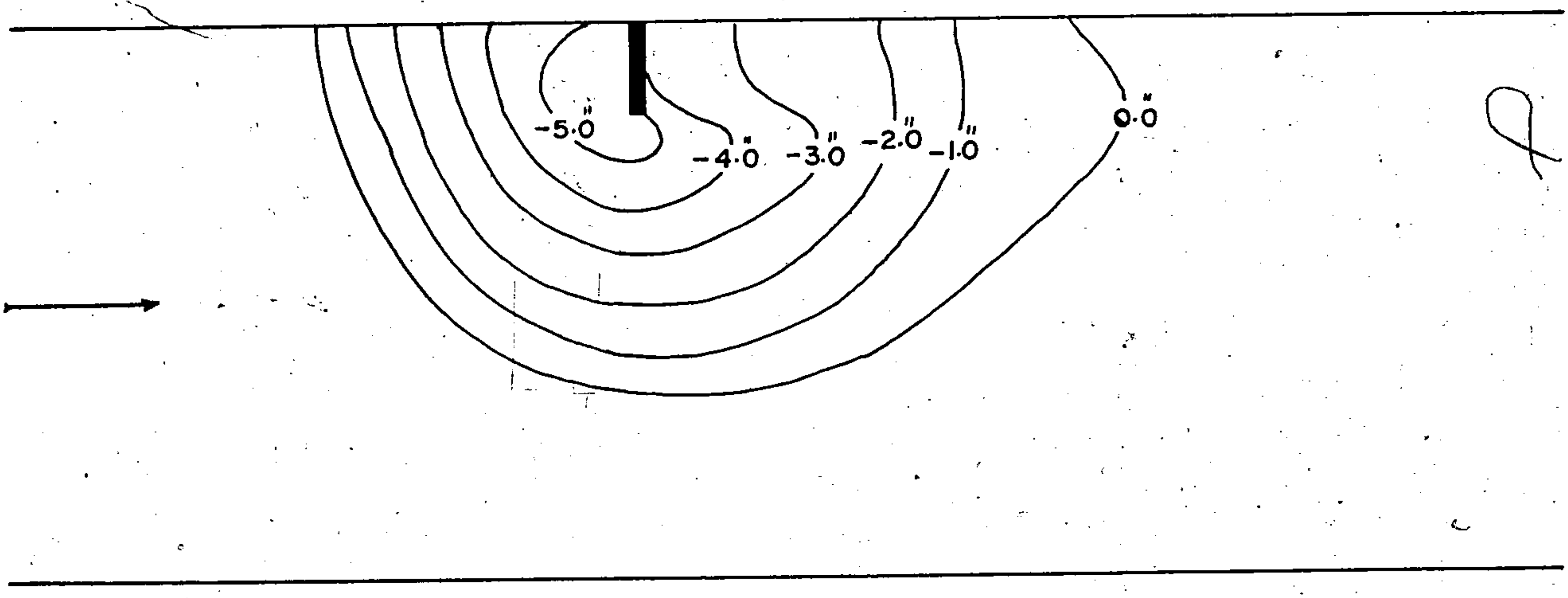

Figure 4.6. Experimental Contour Map for Test No. 22, Table 4.1.

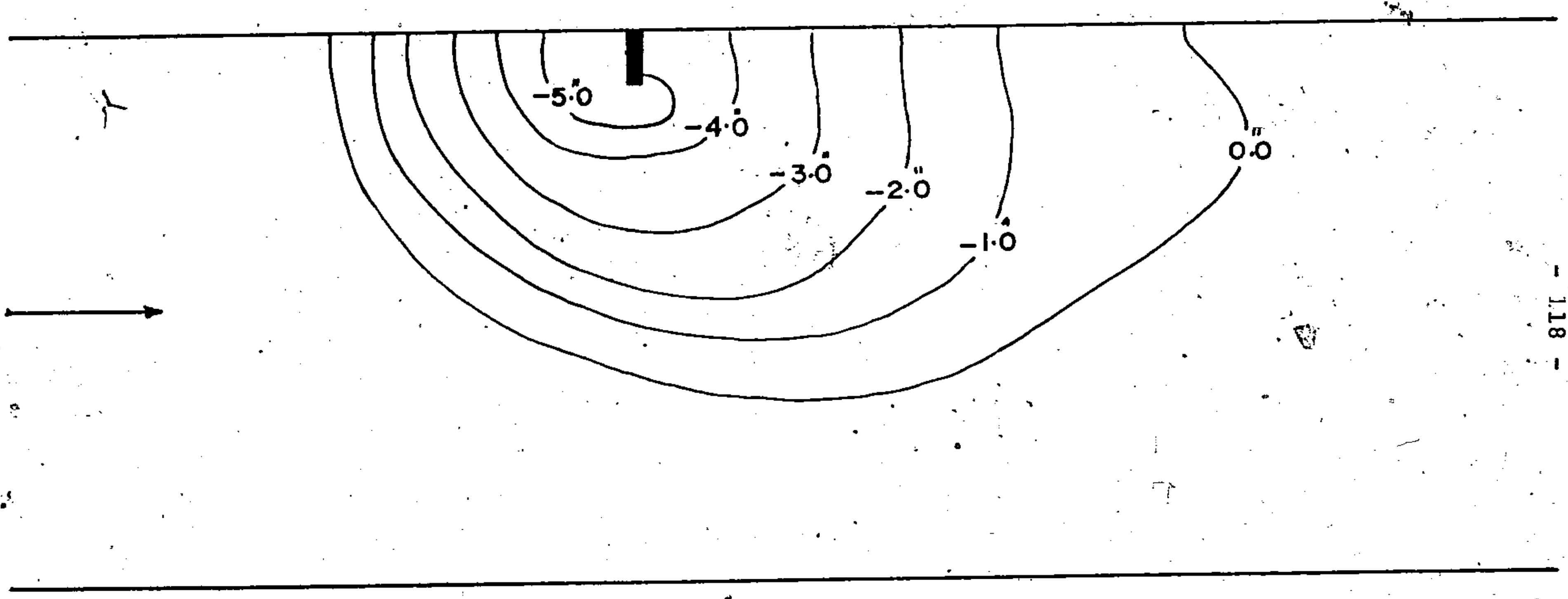

Figure 4.7. Experimental Contour Map for Test No. 25, Table 4.1.

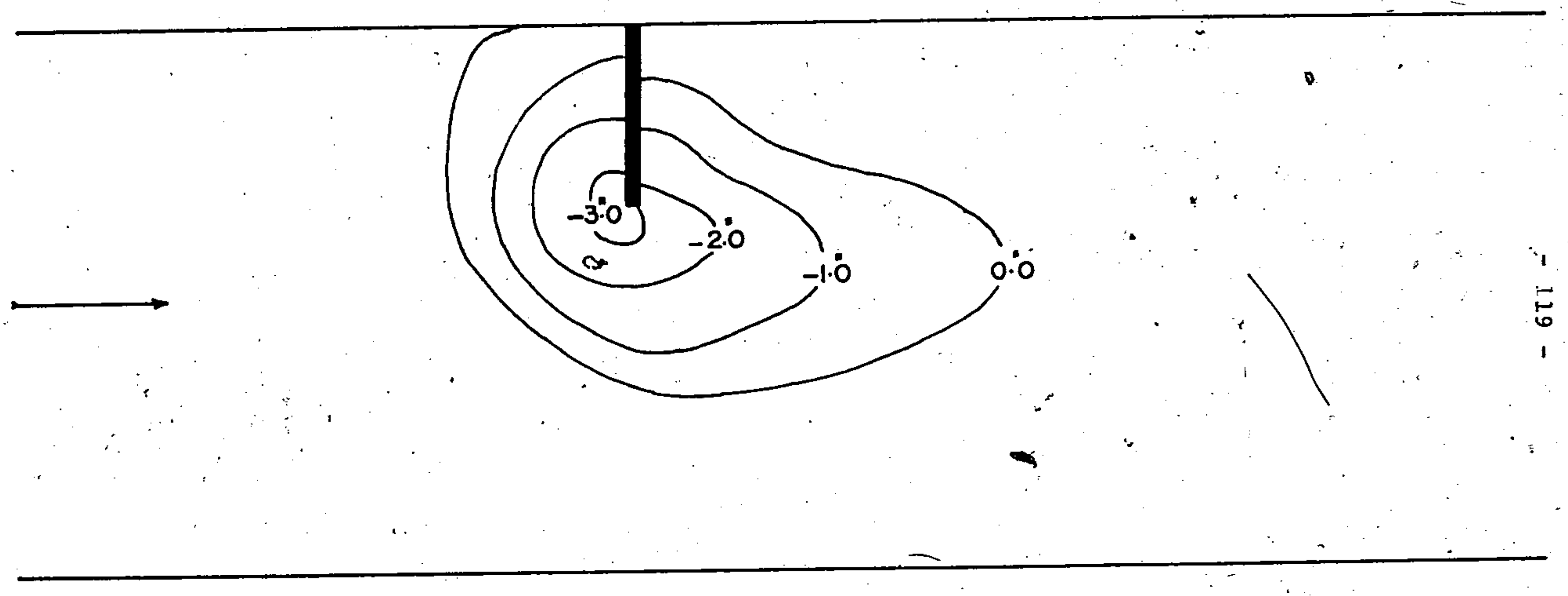

Figure 4.8. Experimental Contour Map for Test No. 4, Table 4.2.

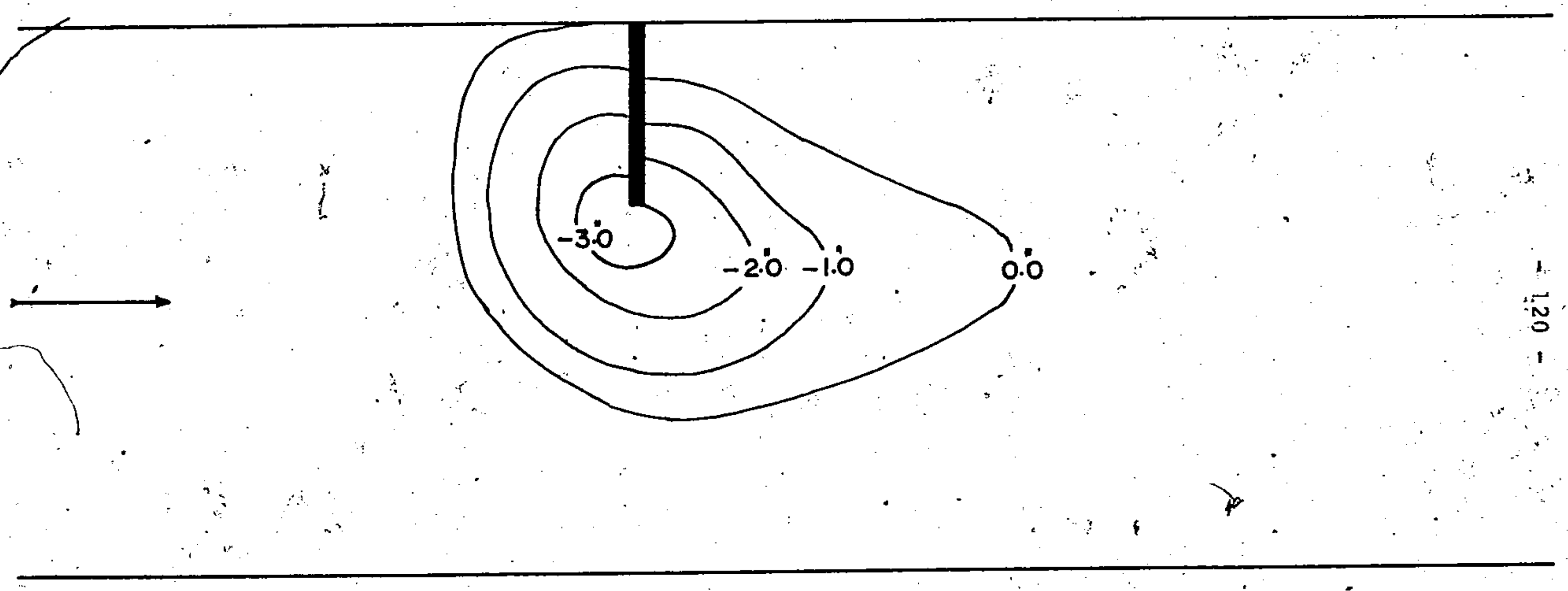

Figure 4.9. Experimental Contour Map for Test No. 6, Table 4.2.

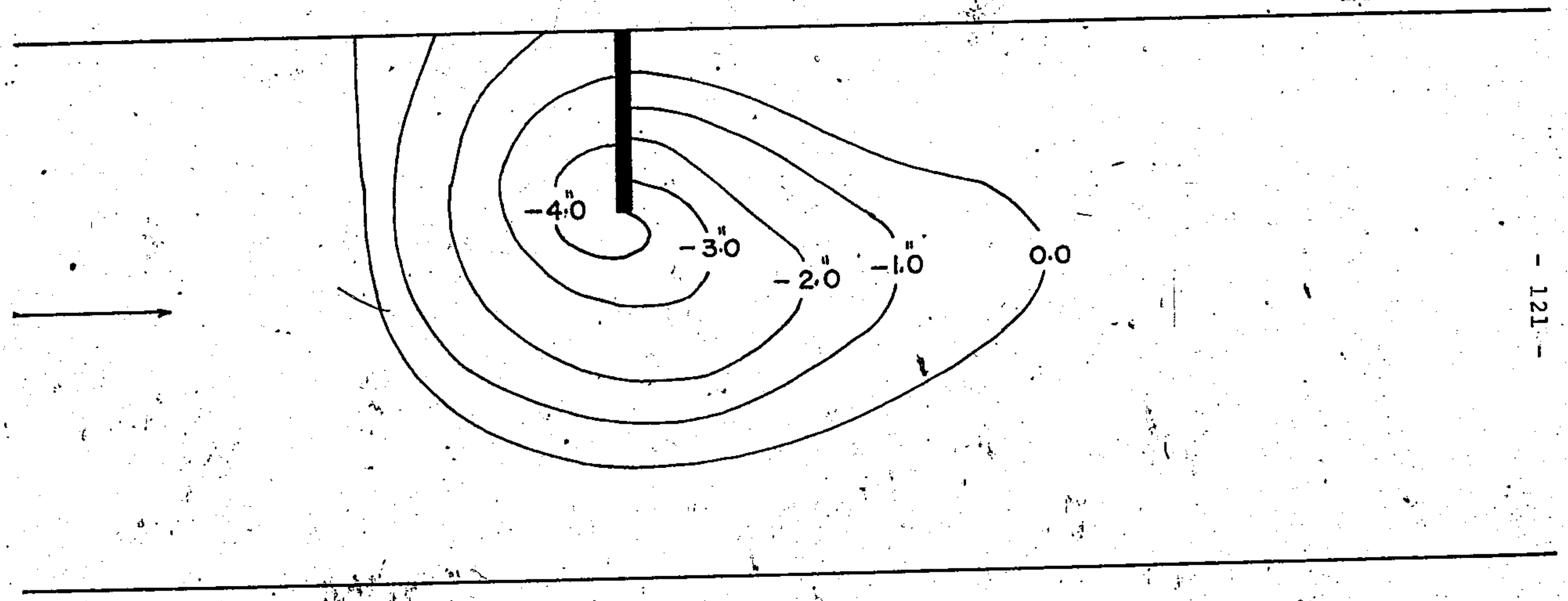

Figure 4.10. Experimental Contour Map for Test No. 7, Table 4.2.

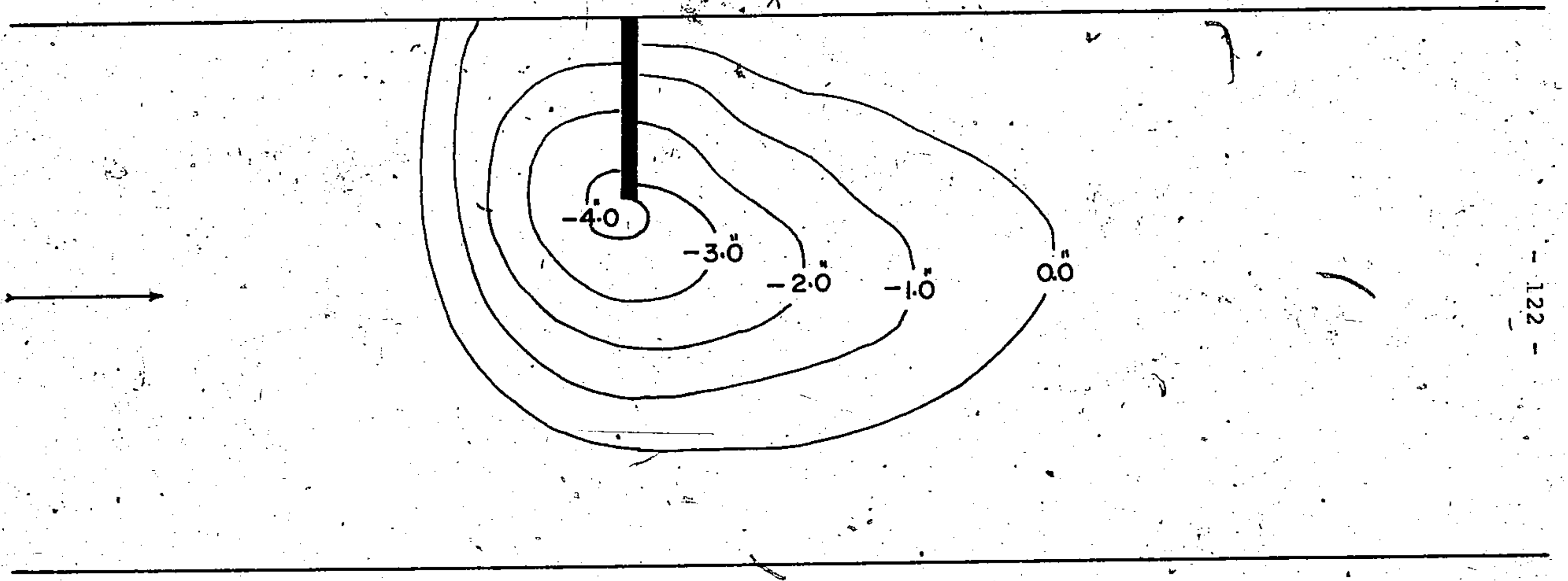

Figure 4.11. Experimental Contour Map for Test No. 9, Table 4.2.

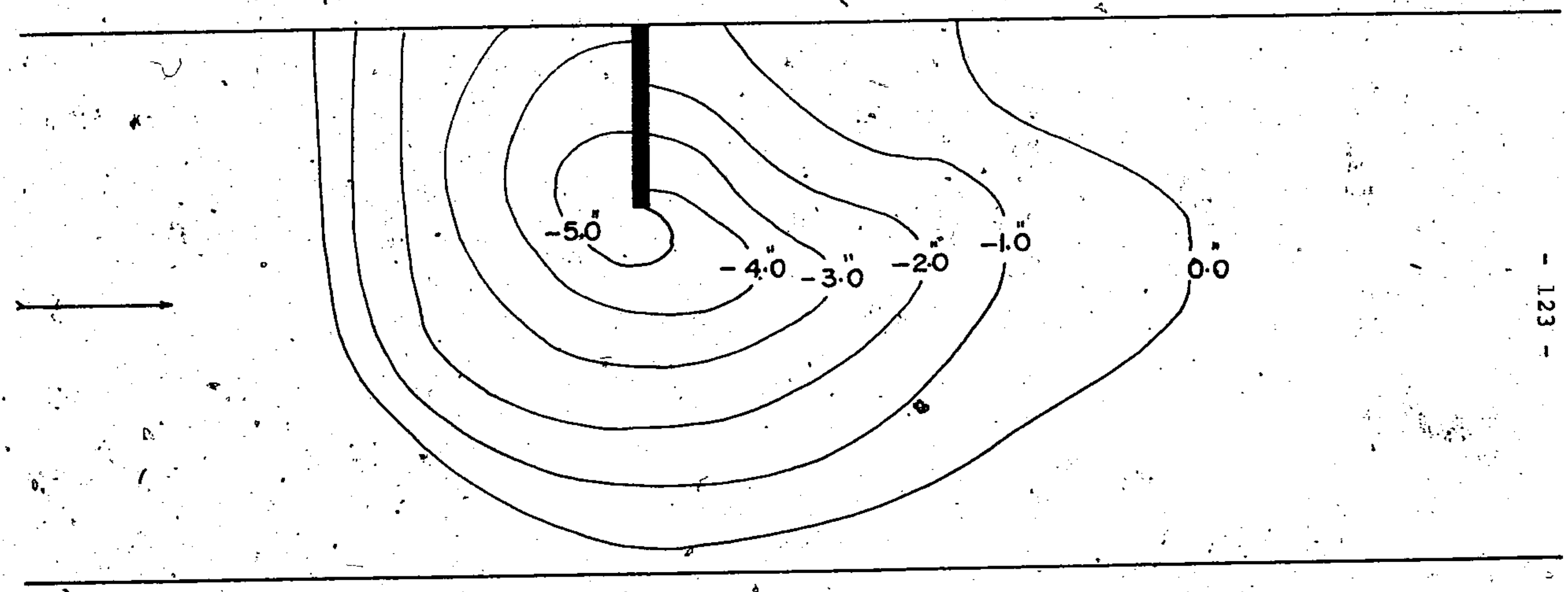

Figure 4.12. Experimental Contour Map for Test No. 10, Table 4.2.

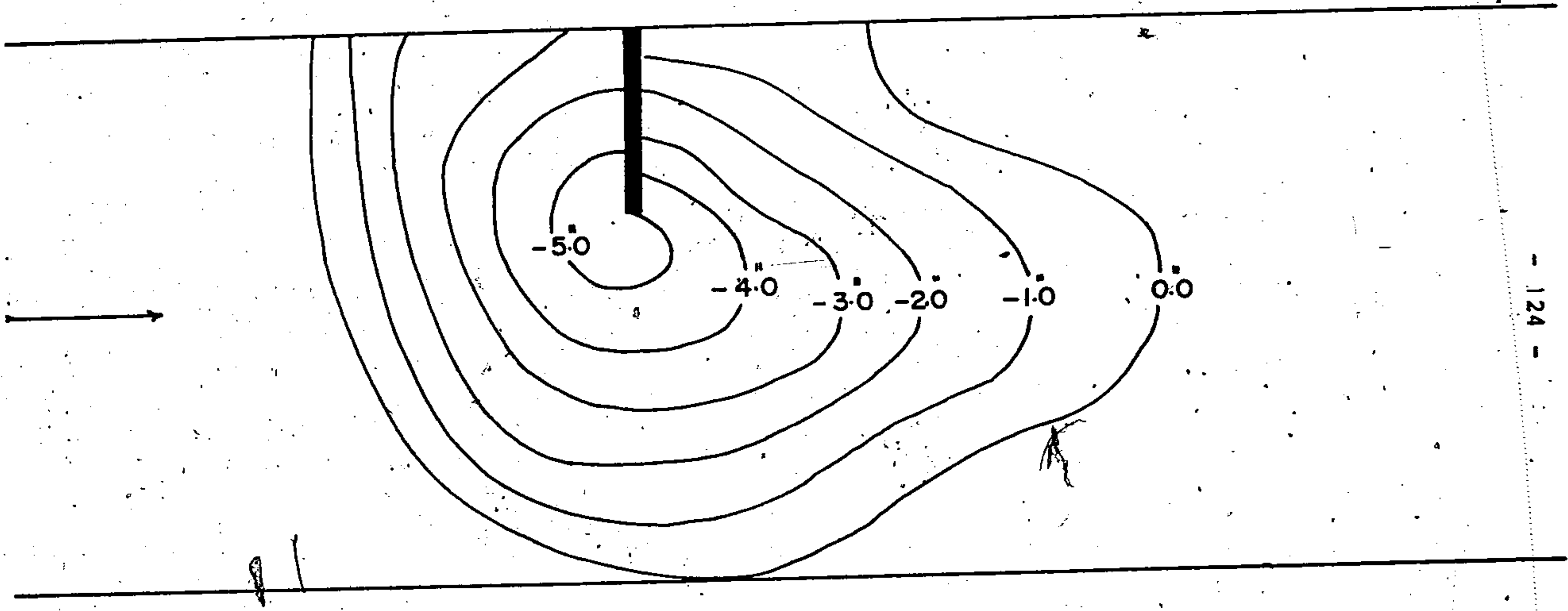

Figure 4.13. Experimental Contour Map for Test No. 12, Table 4.2.

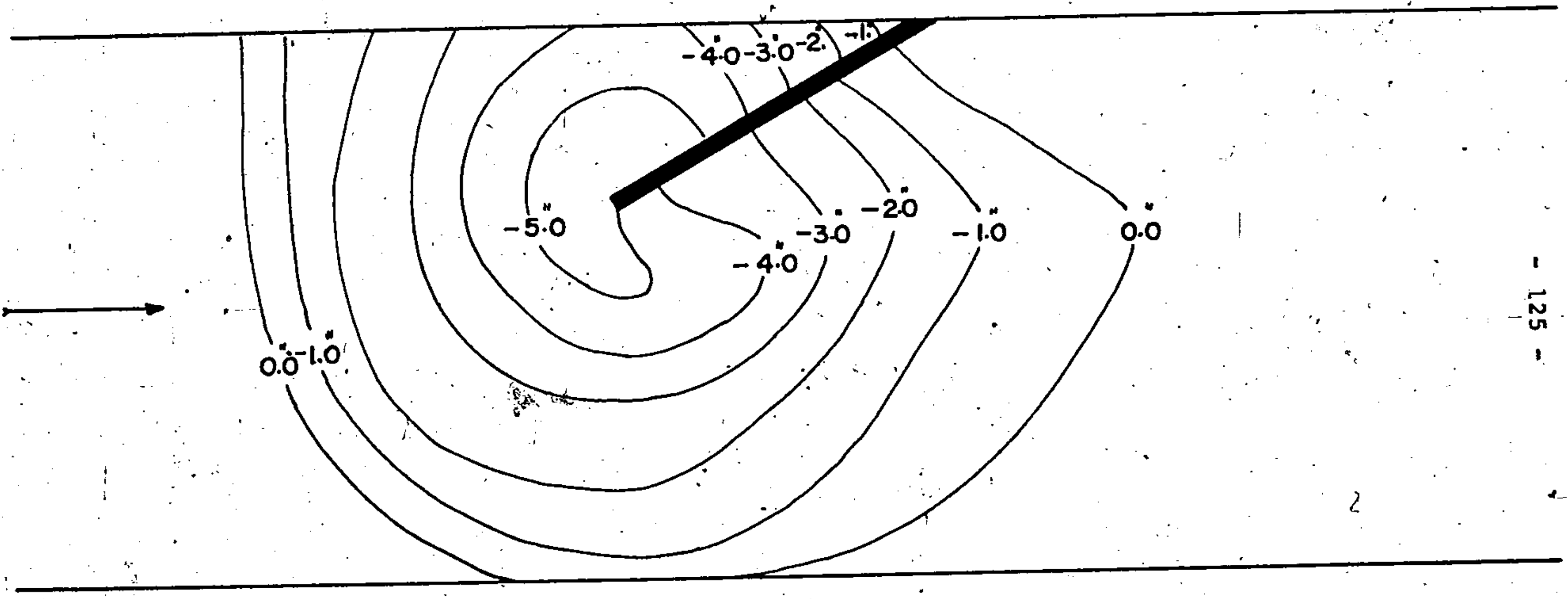

Figure 4.14. Experimental Contour Map for Test No. 1, Table 4.4.

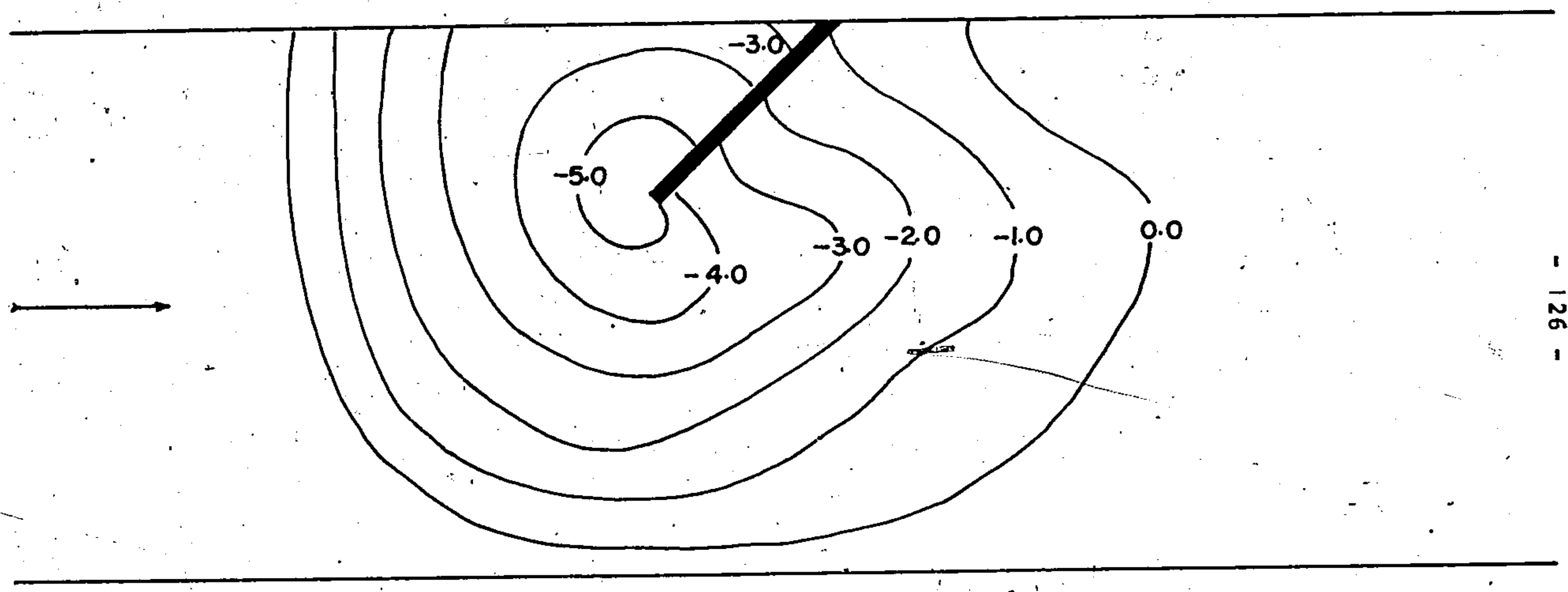

Figure 4.15. Experimental Contour Map for Test No. 2, Table 4.4.

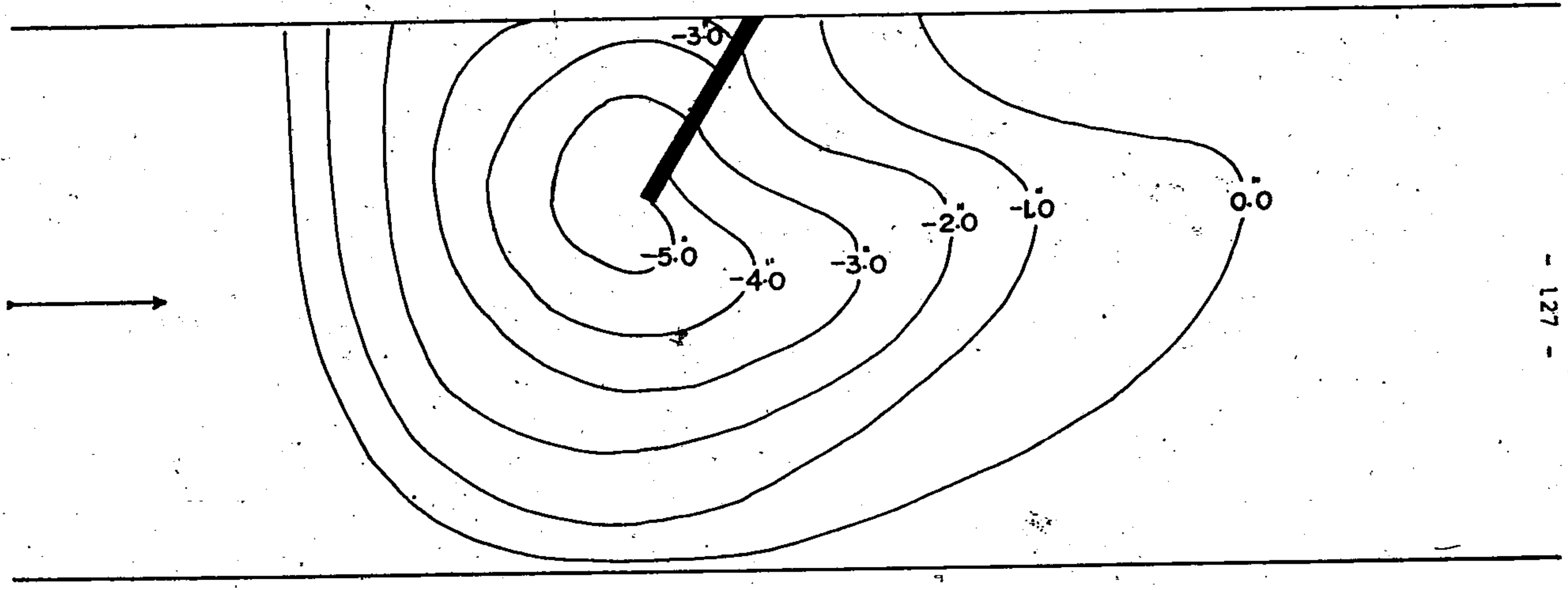

Figure 4.16. Experimental Contour Map for Test No. 3, Table 4.4.

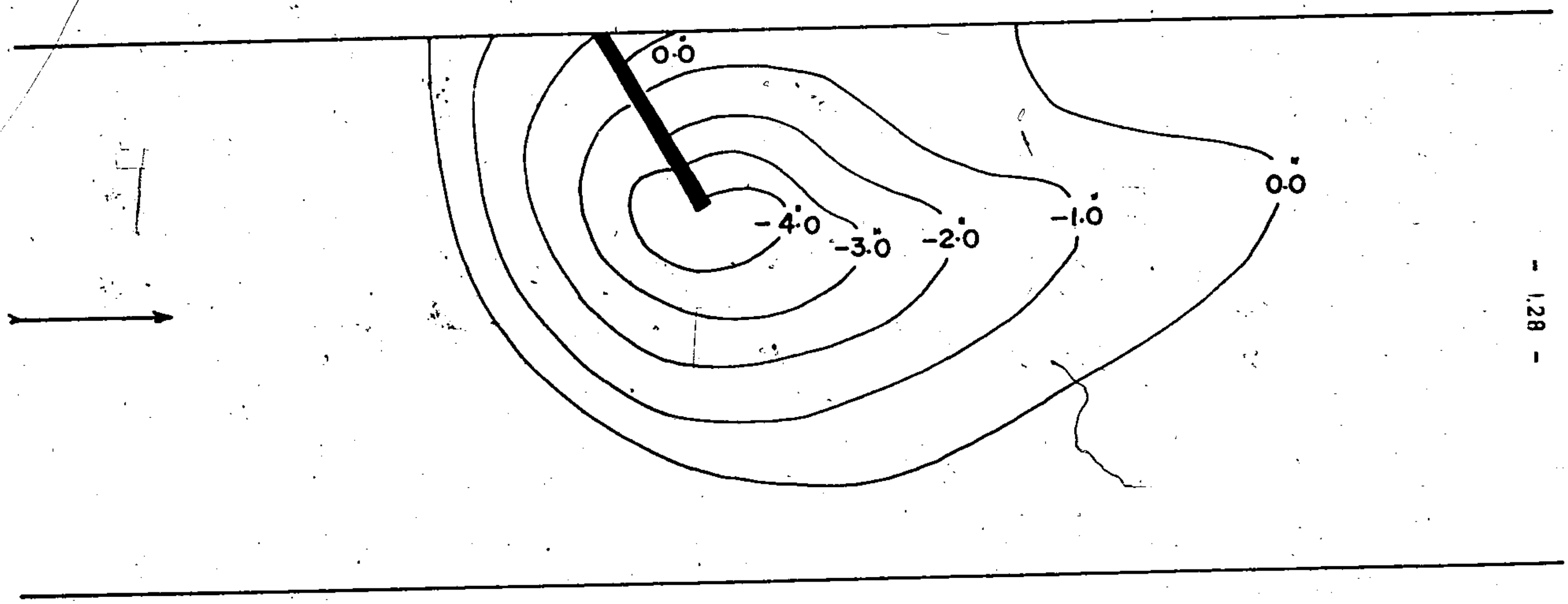

Figure 4.17. Experimental Contour Map for Test No. 5, Table 4.4.

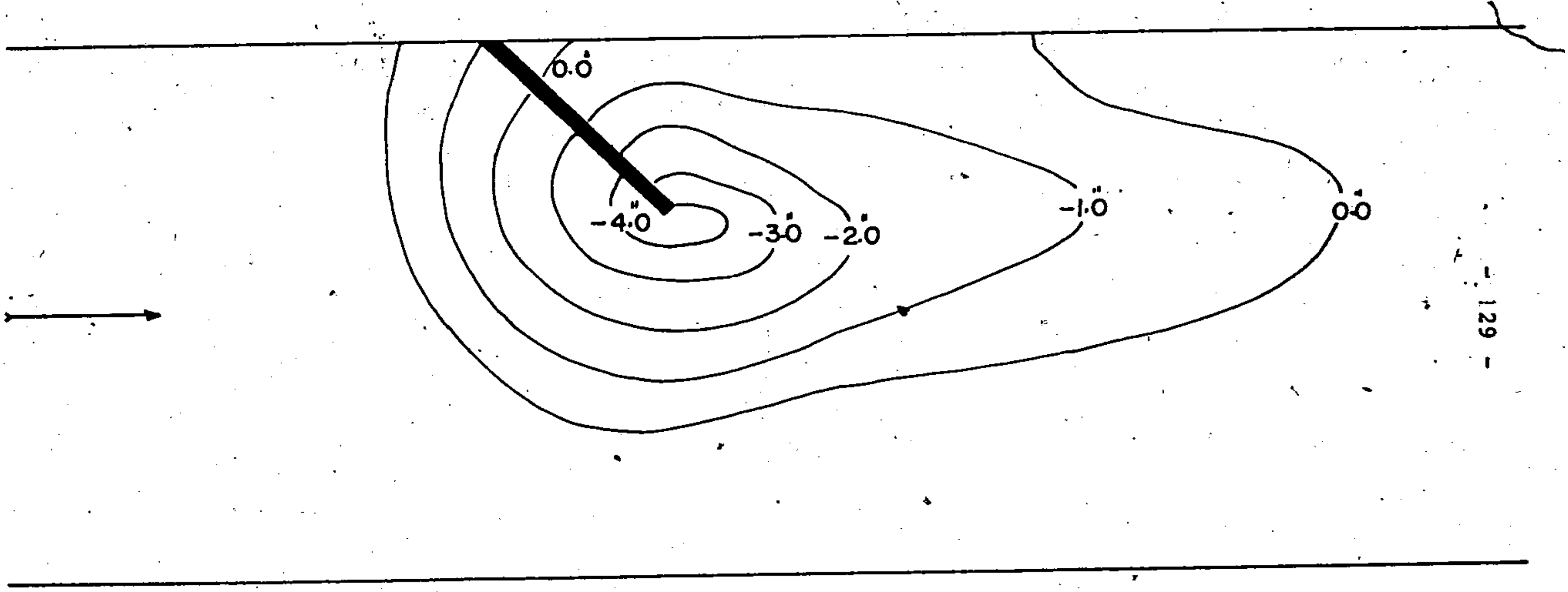

Figure 4.18. Experimental Contour Map for Test No. 6, Table 4.4.

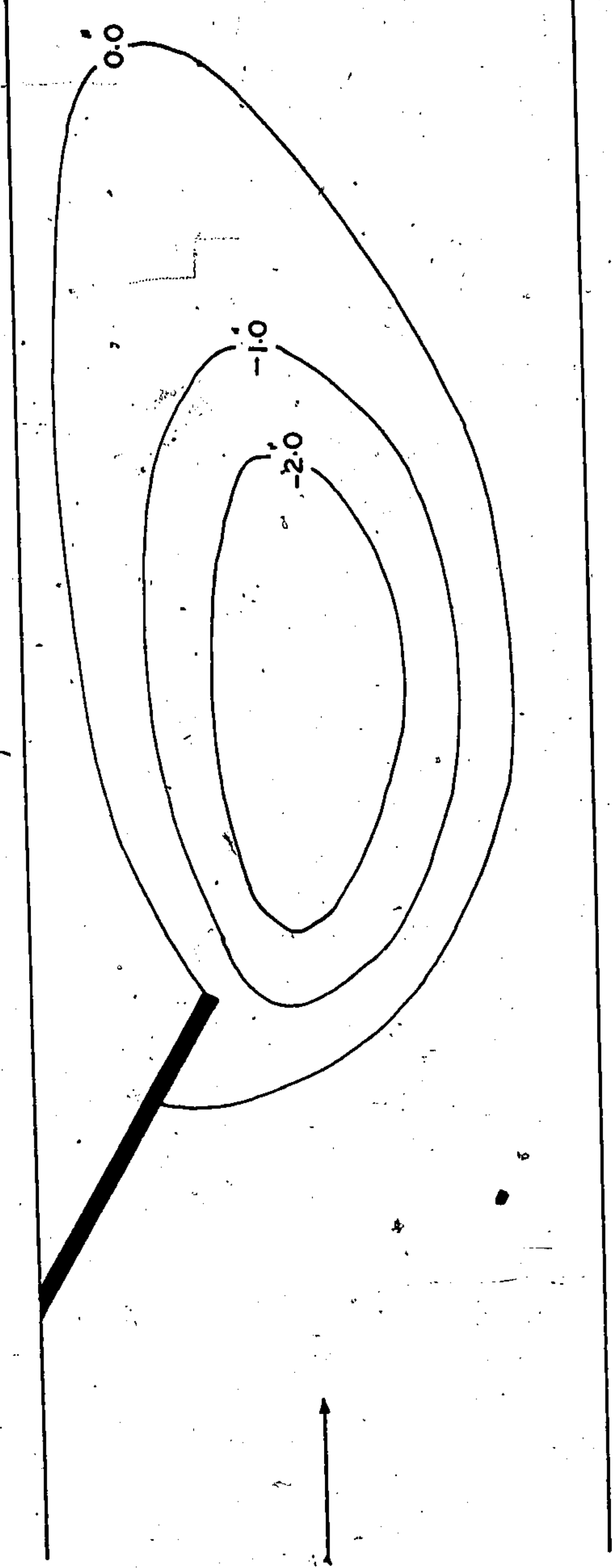

Figure 4.19. Experimental Contour Map for Test No. 7, Table 4.4.

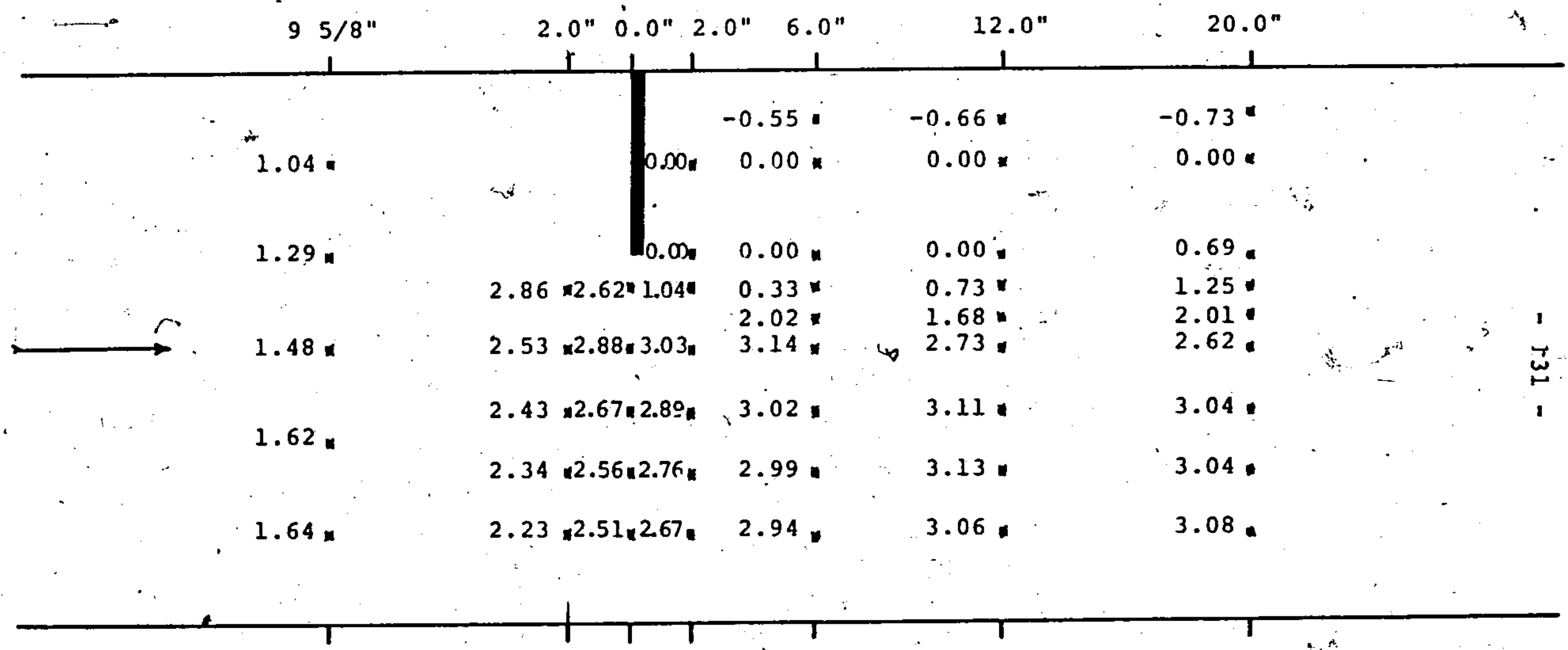

Figure 4.20. Pitot-Tube Velocity Values (ft/sec).

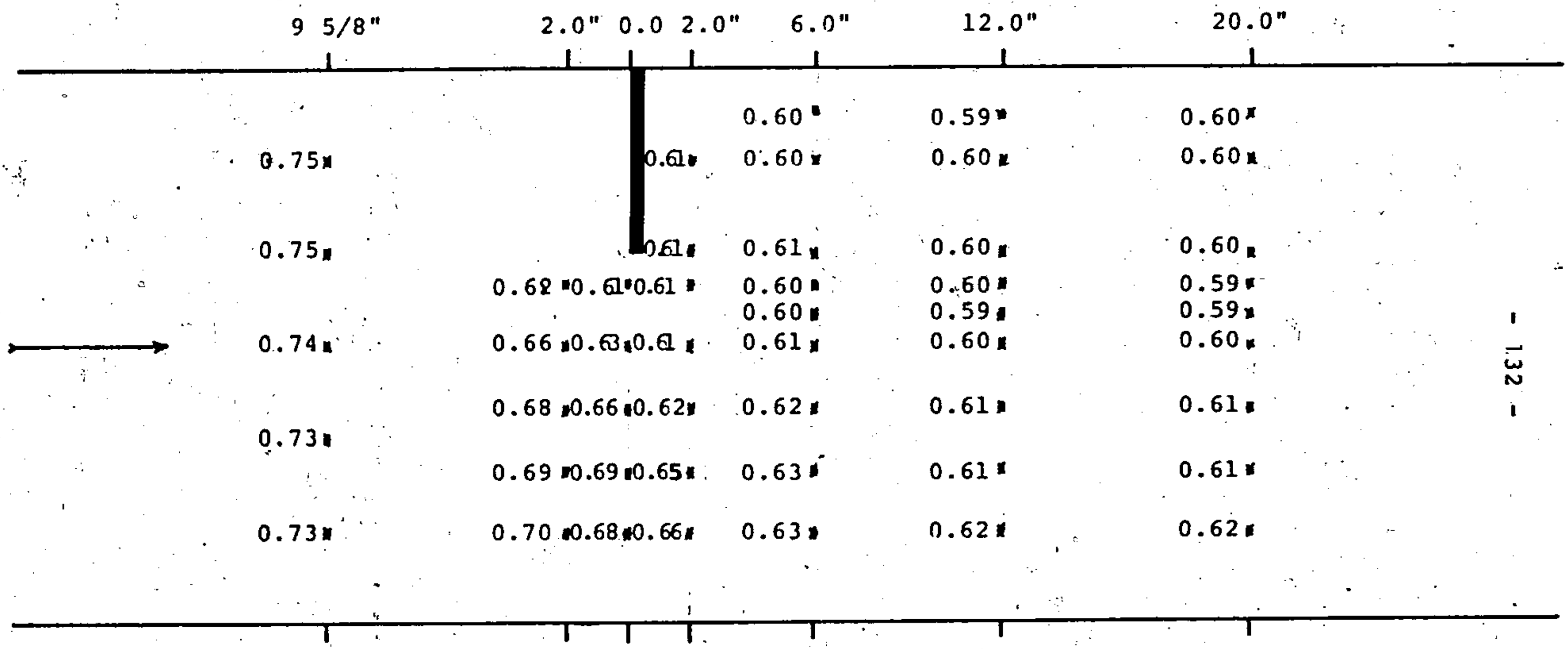

Figure 4.21. Water Depth Values Using Manometer Measurements (Feet).

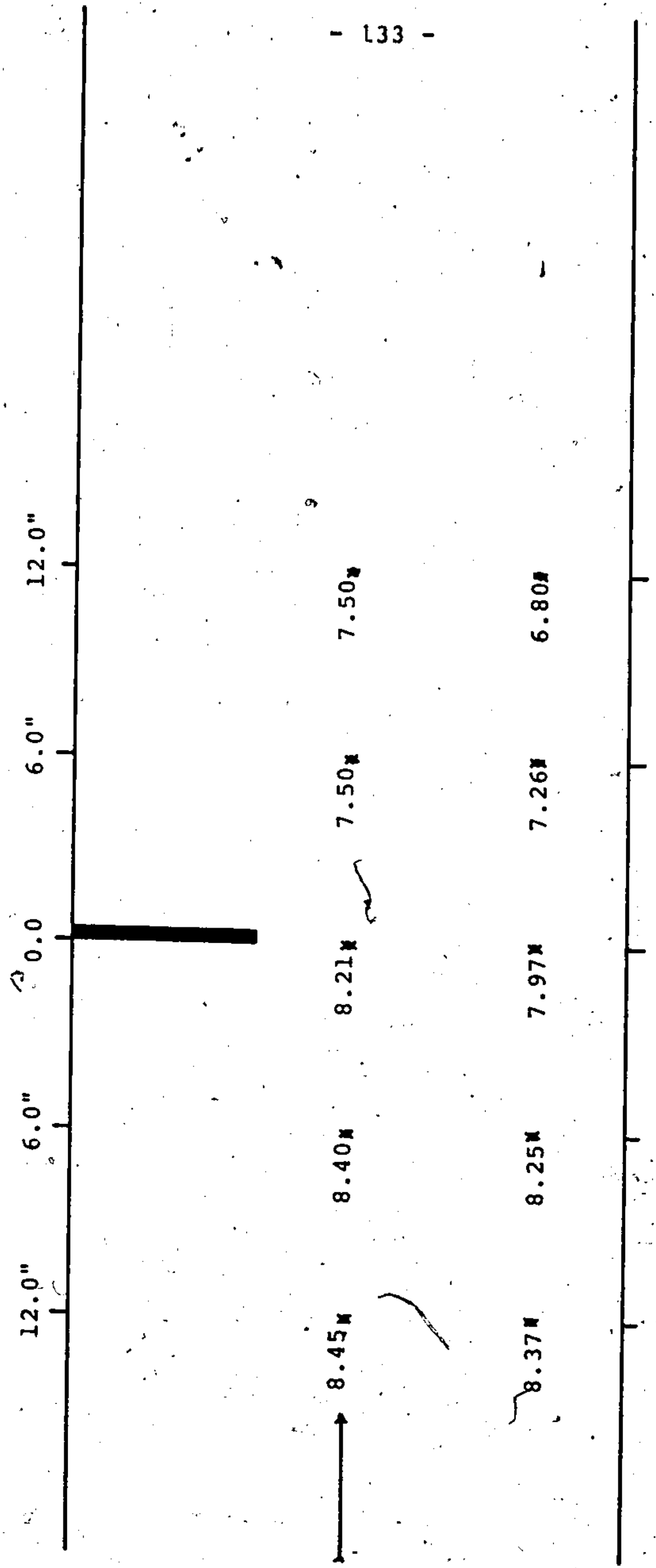

Figure 4.22. Water Depth Values Using Point-Gauge Measurements (inches).

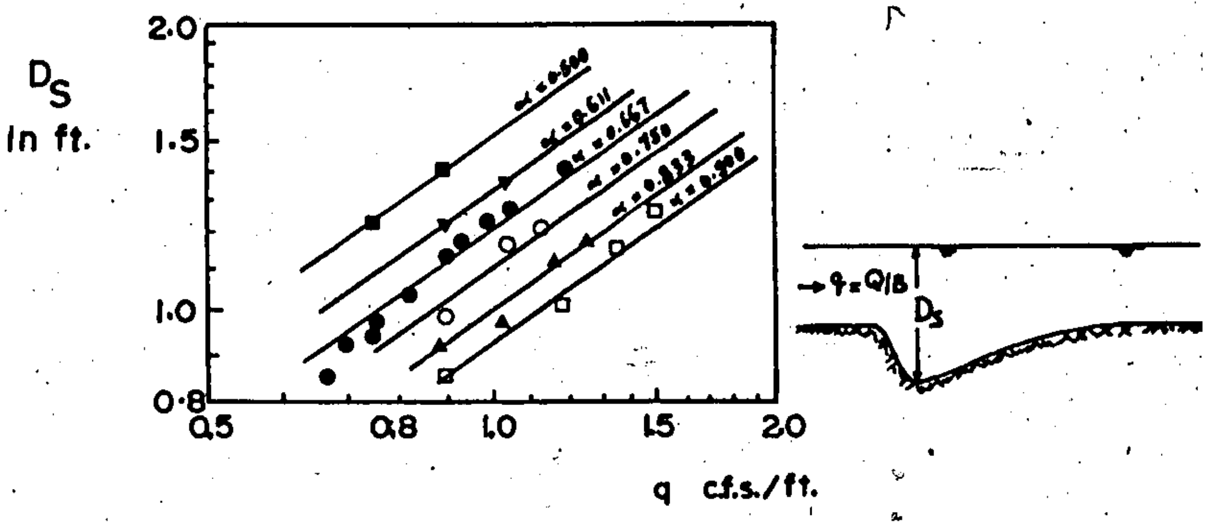

Figure 5.1. Variation of D_s with q and α.

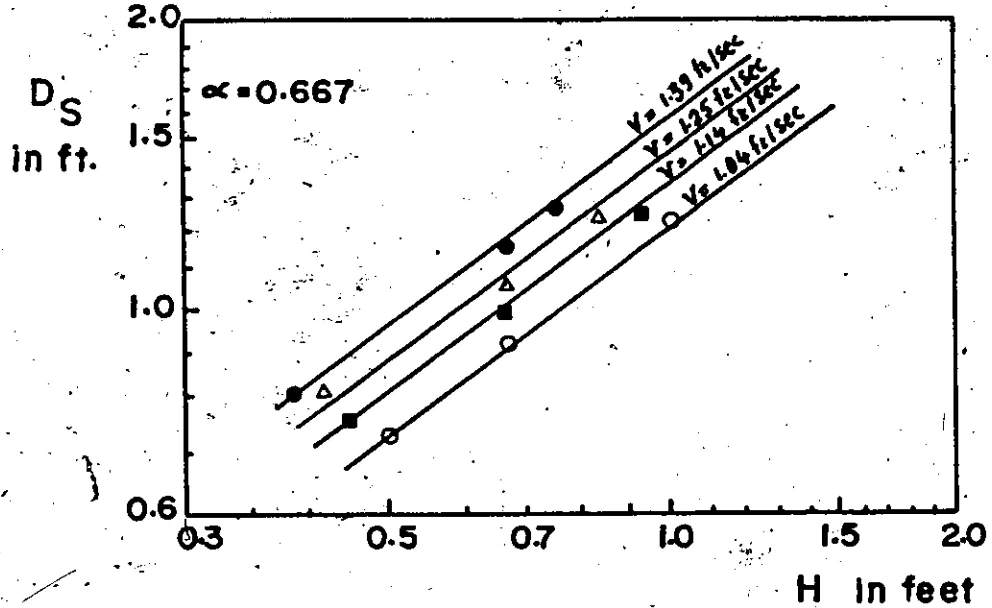

Figure 5.2. Variation of D_s with H and v.

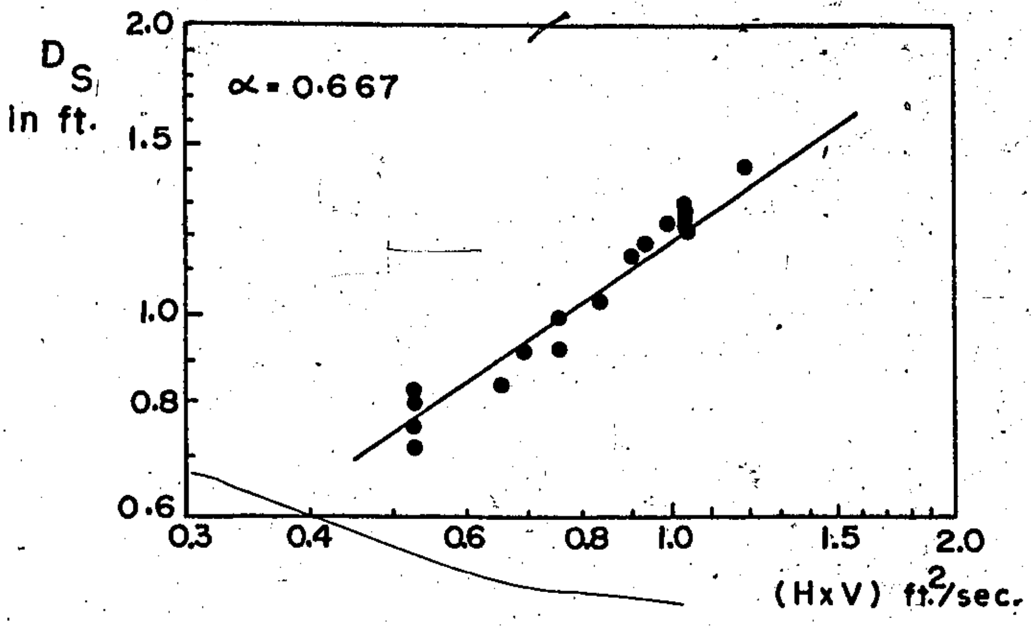

Figure 5.3. Variation of D_s with (Hxv).

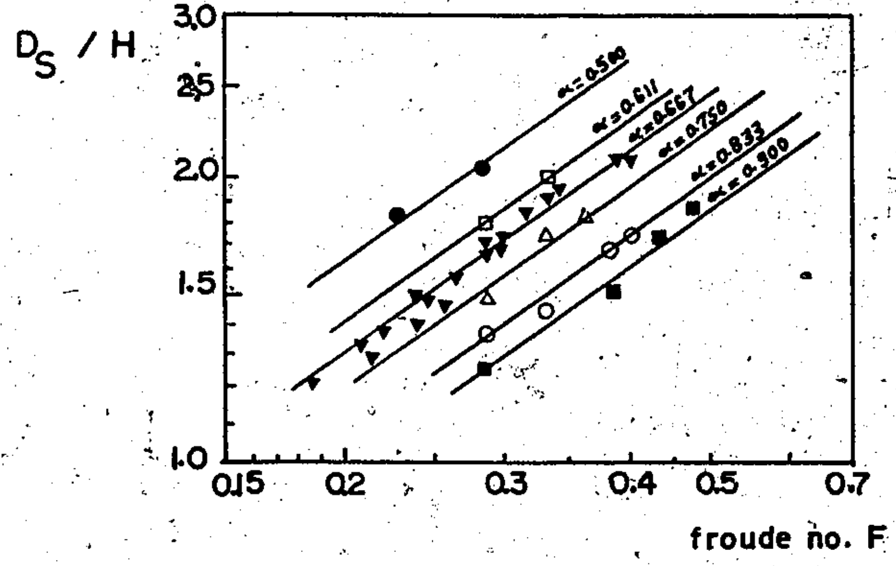

Figure 5.4. Variation of D_s/H with F and α.

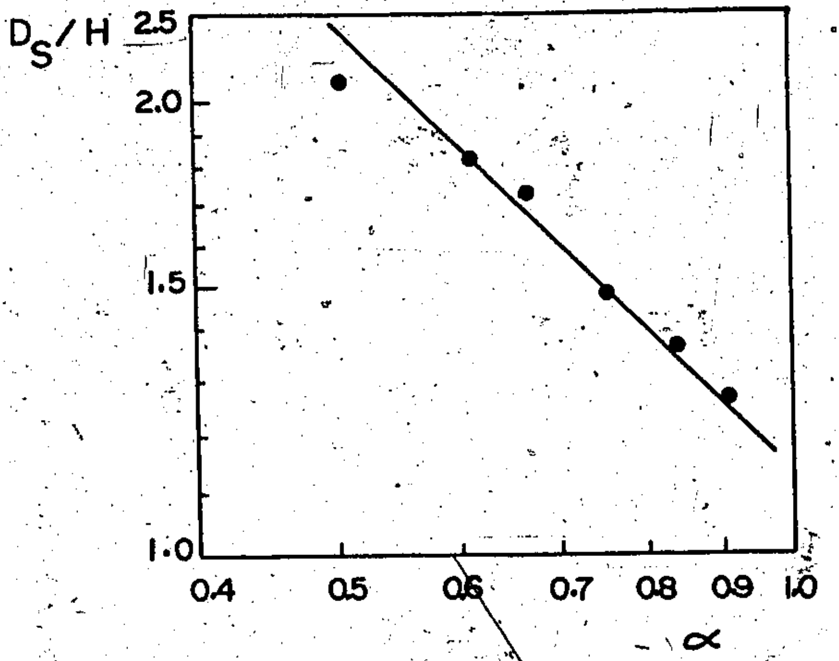

Figure 5.5. Variation of D_s/H with α.

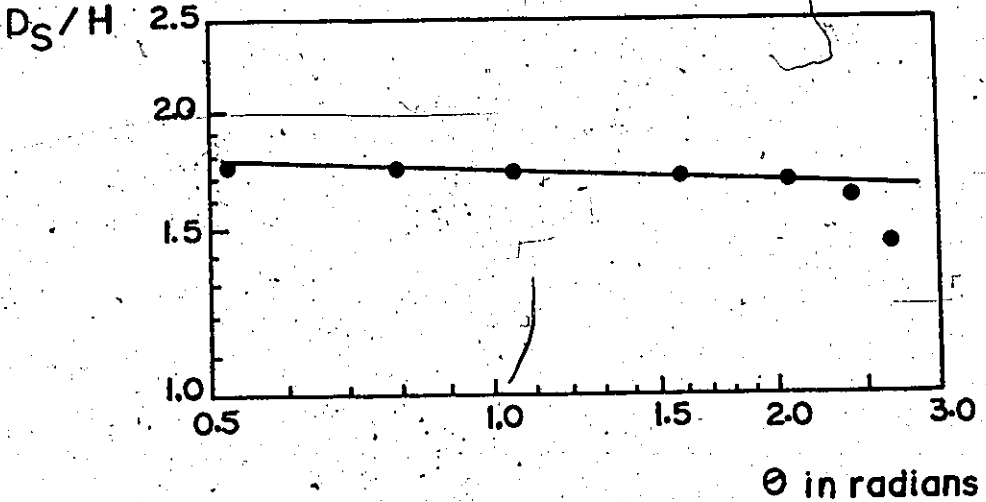

Figure 5.6. Variation of D_s/H with θ.

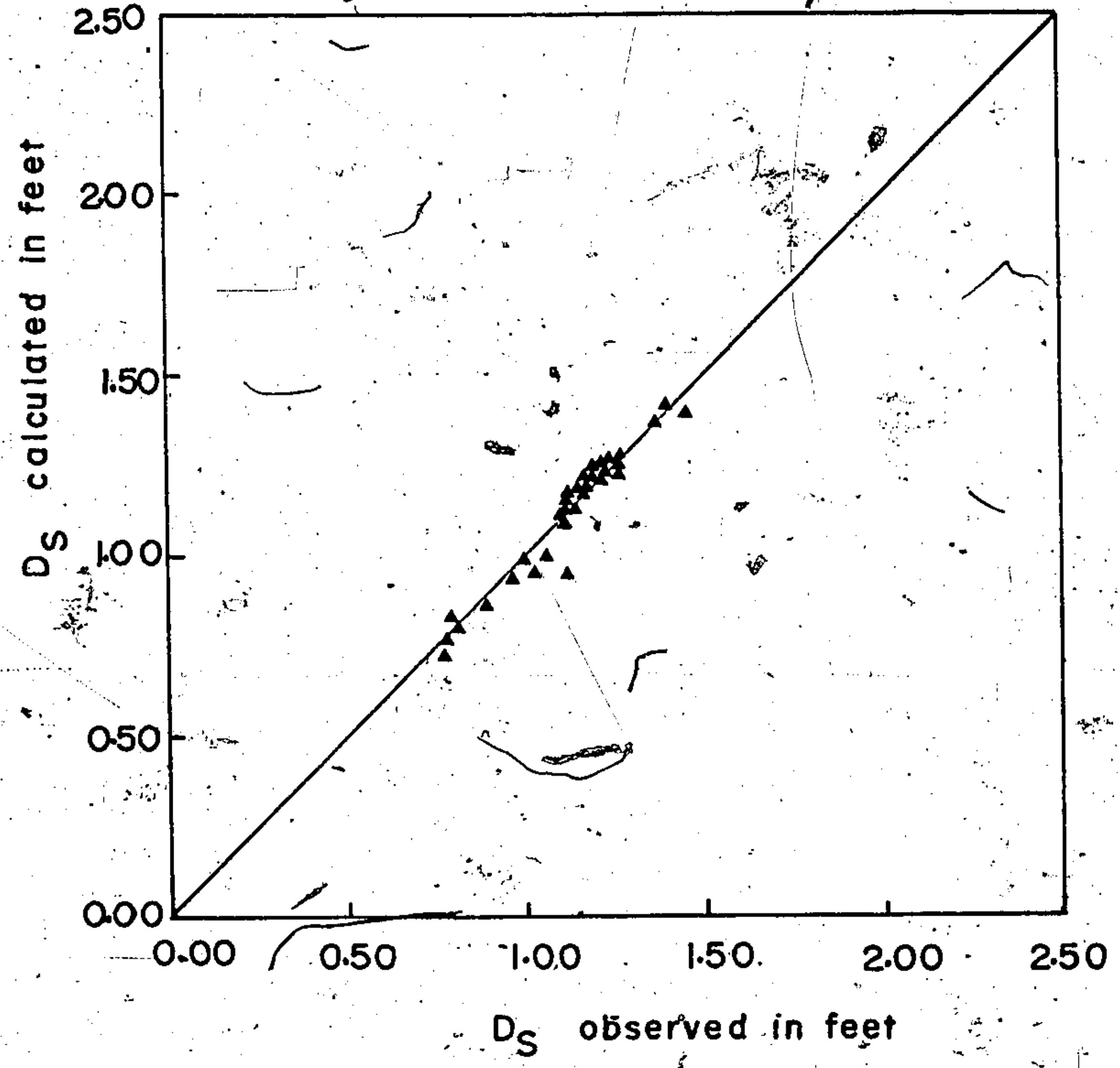

Figure 5.7. Calculated D_s (Eqn. 5.16) Versus Observed D_s.

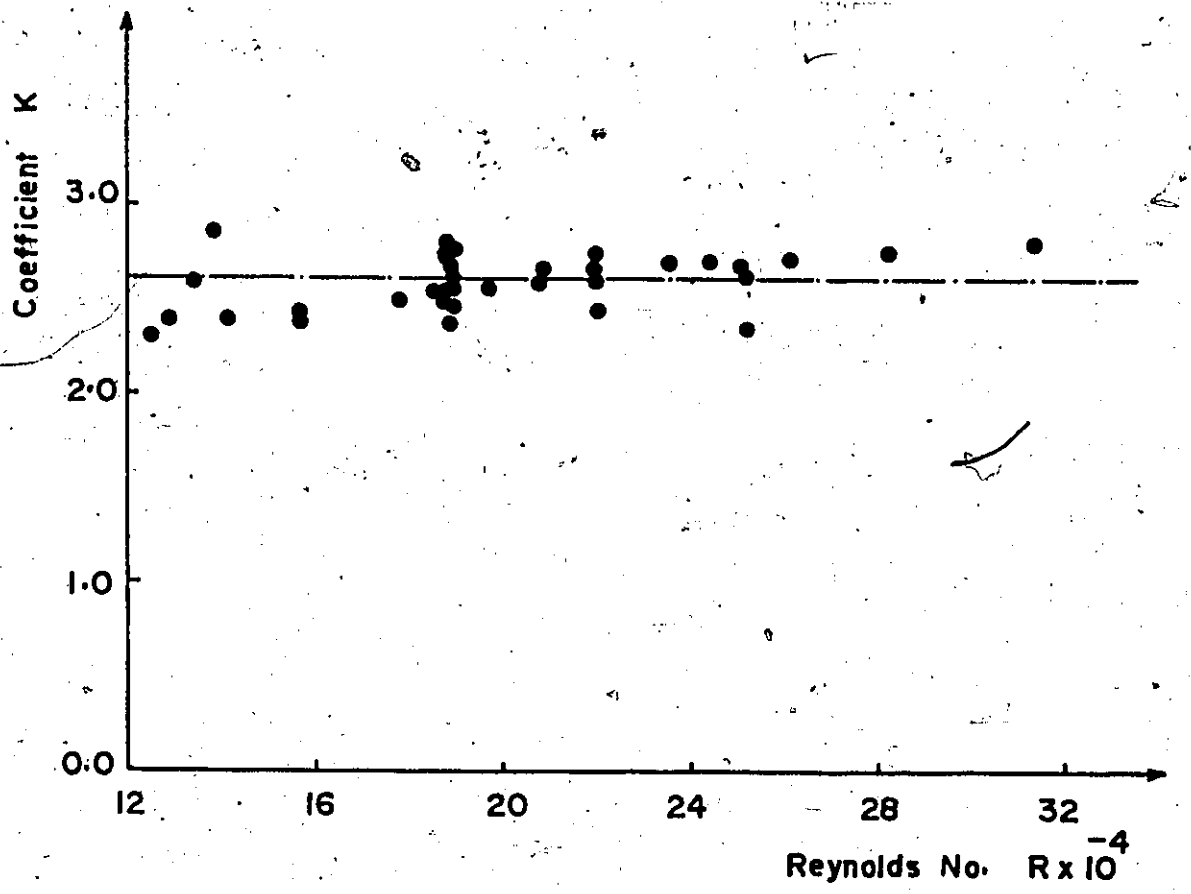

Figure 5.8. Variation of k with R_N.

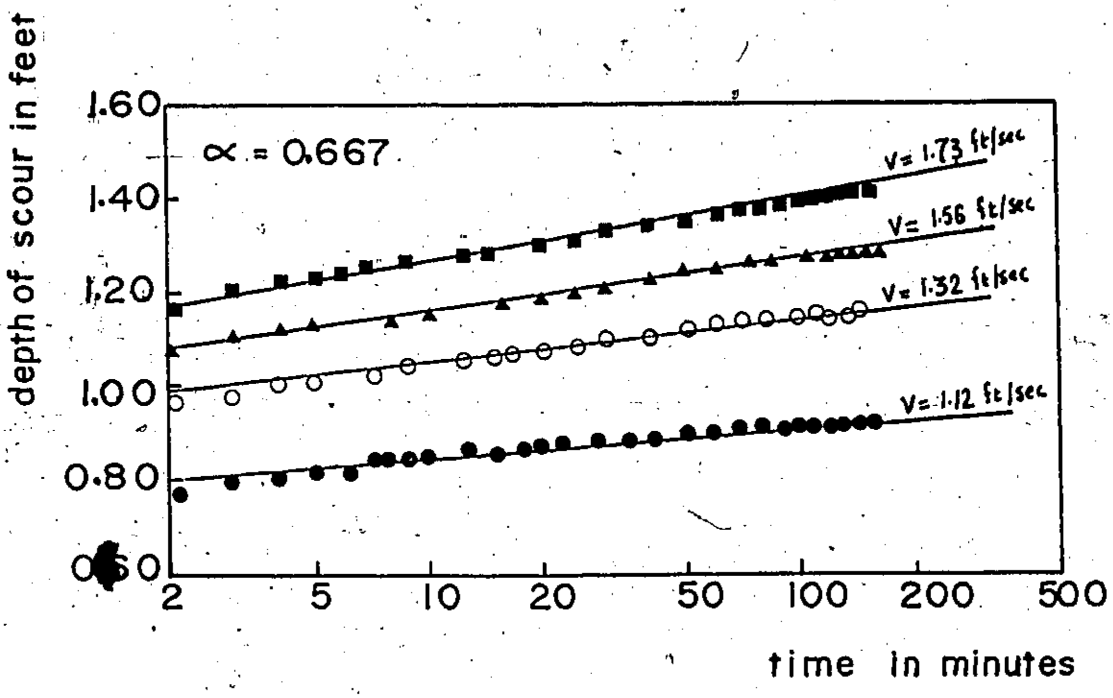

Figure 5.9 Variation of Scour Depth with t and v.

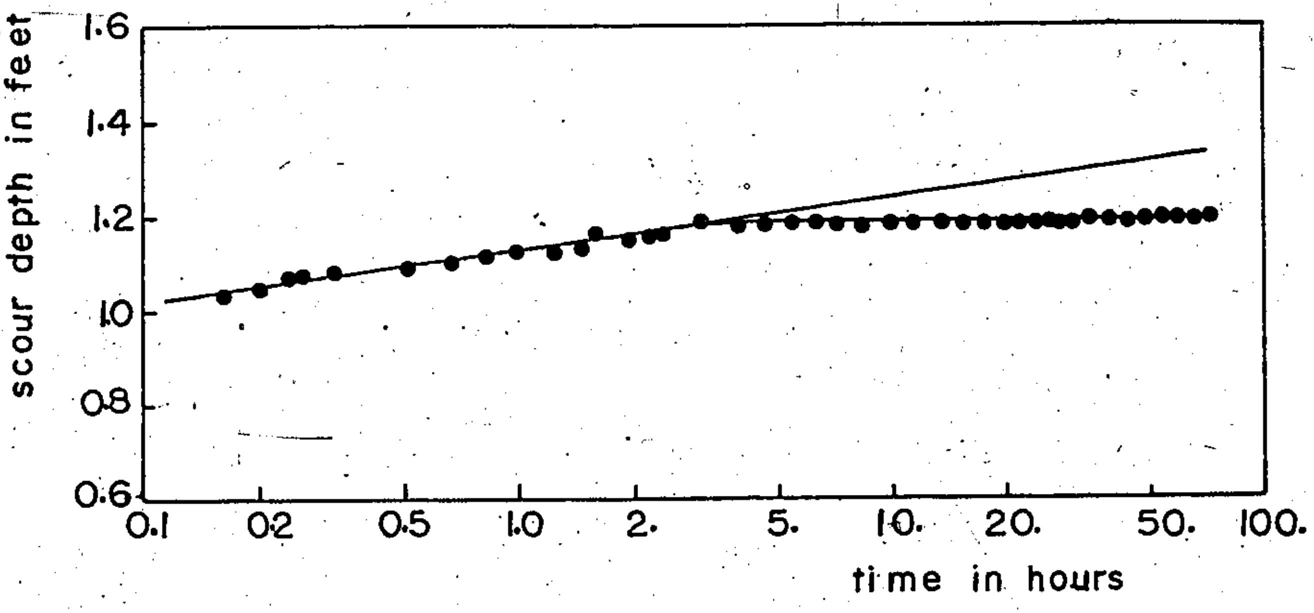

Figure 5.10 Development of Scour Depth.

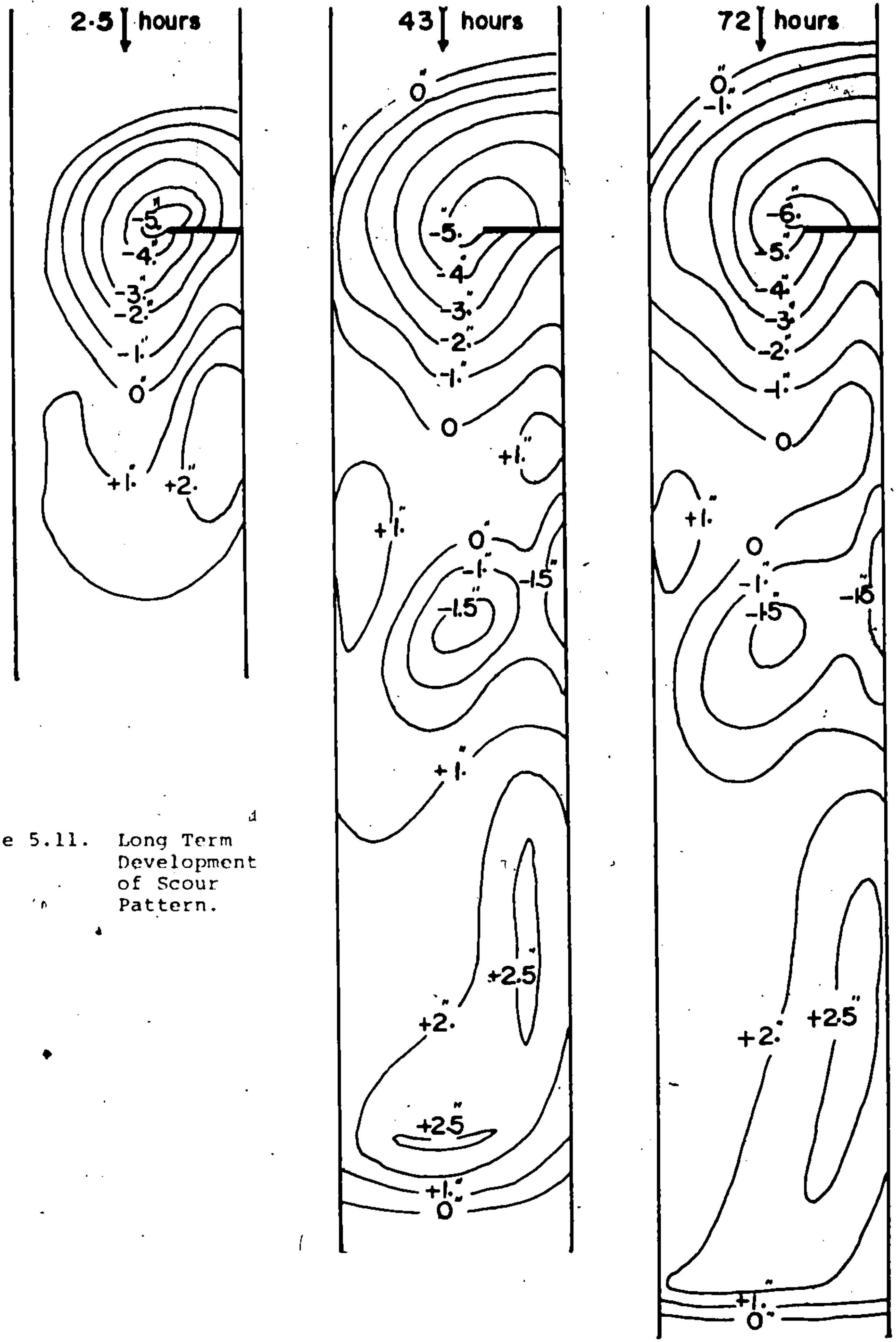

Figure 5.11. Long Term Development of Scour Pattern.

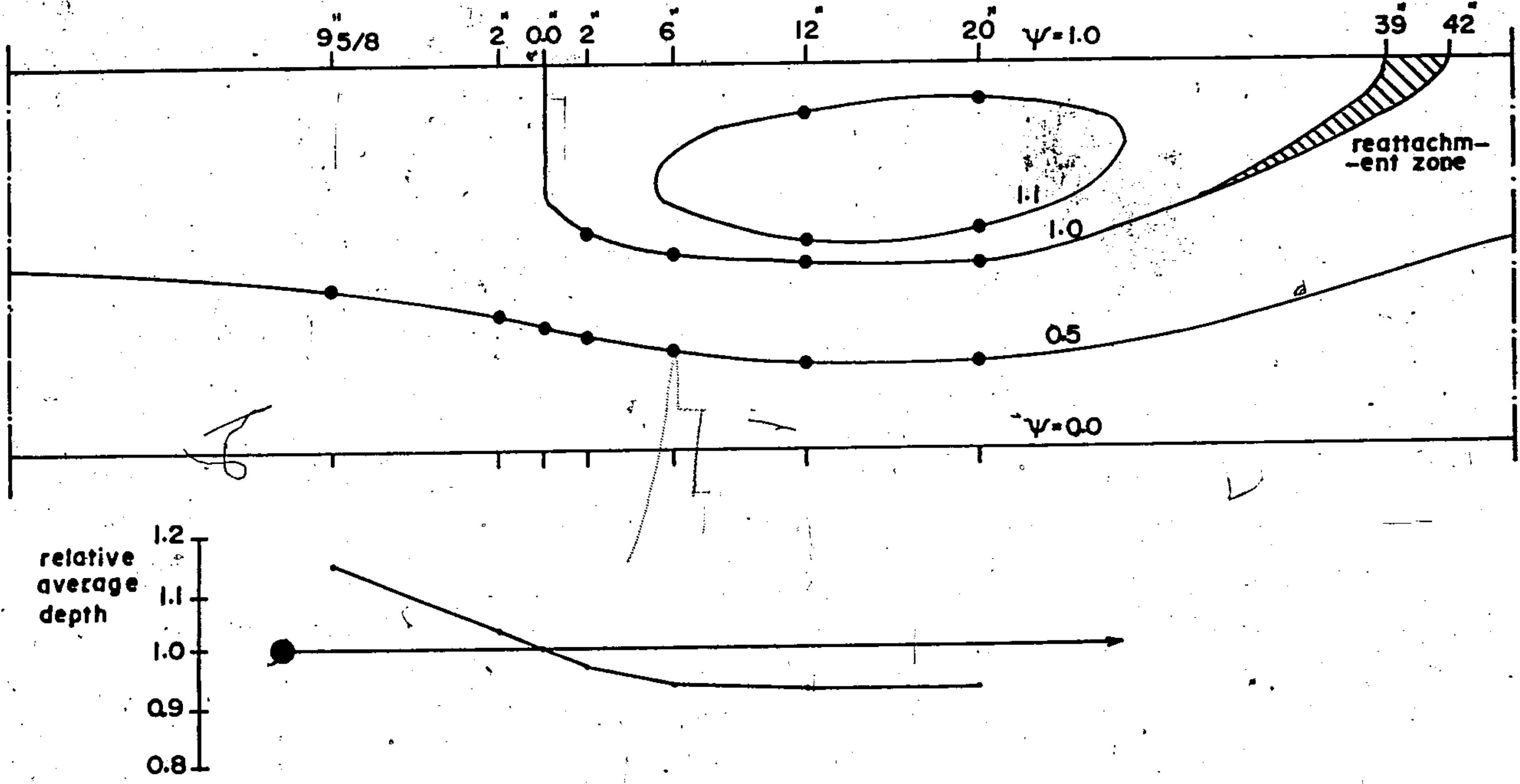

Figure 5.12. Dimensionless Experimental Stream Function Distribution.

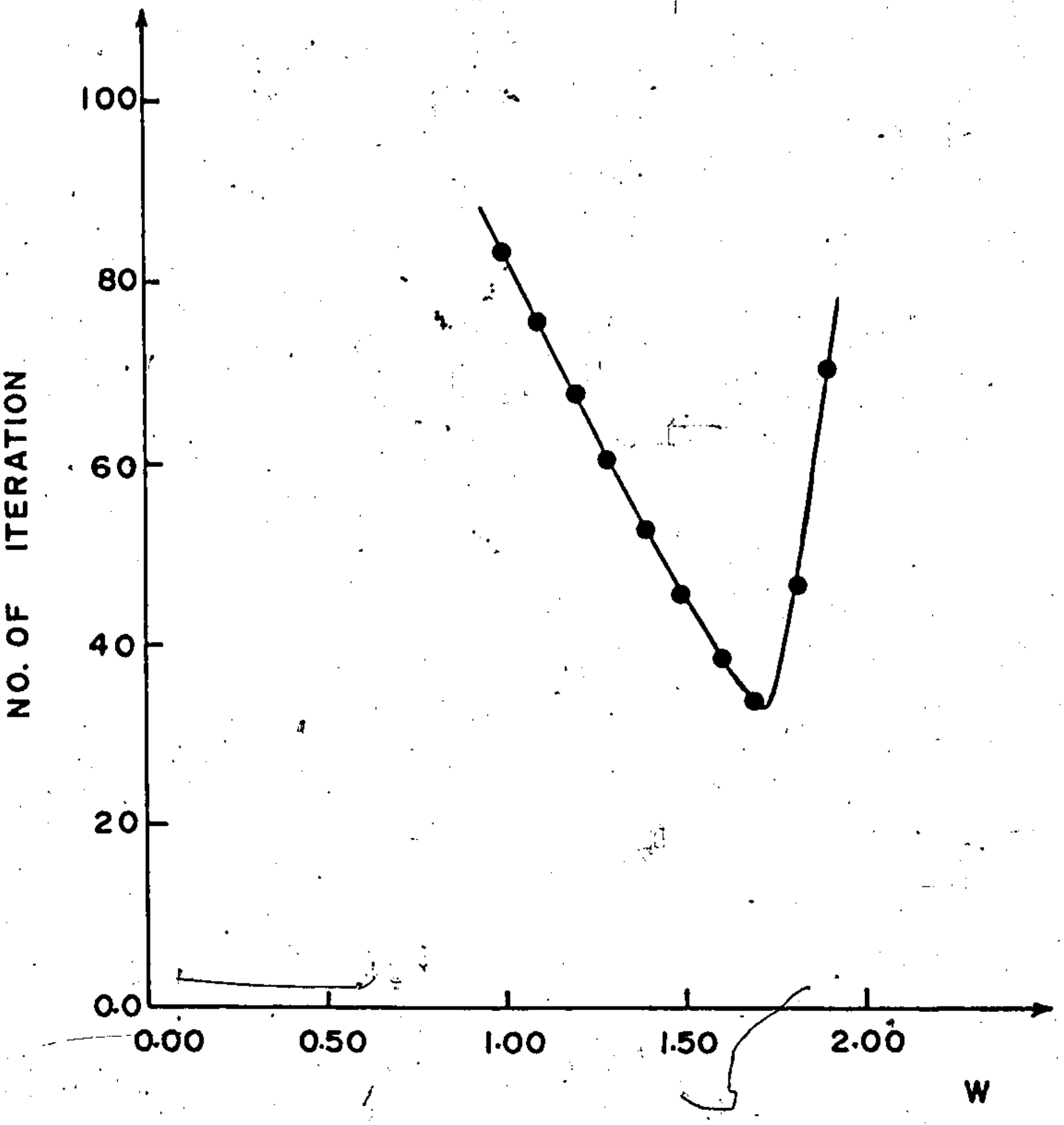

Figure 6.1. The Optimization of the Over-Relaxation Factor.

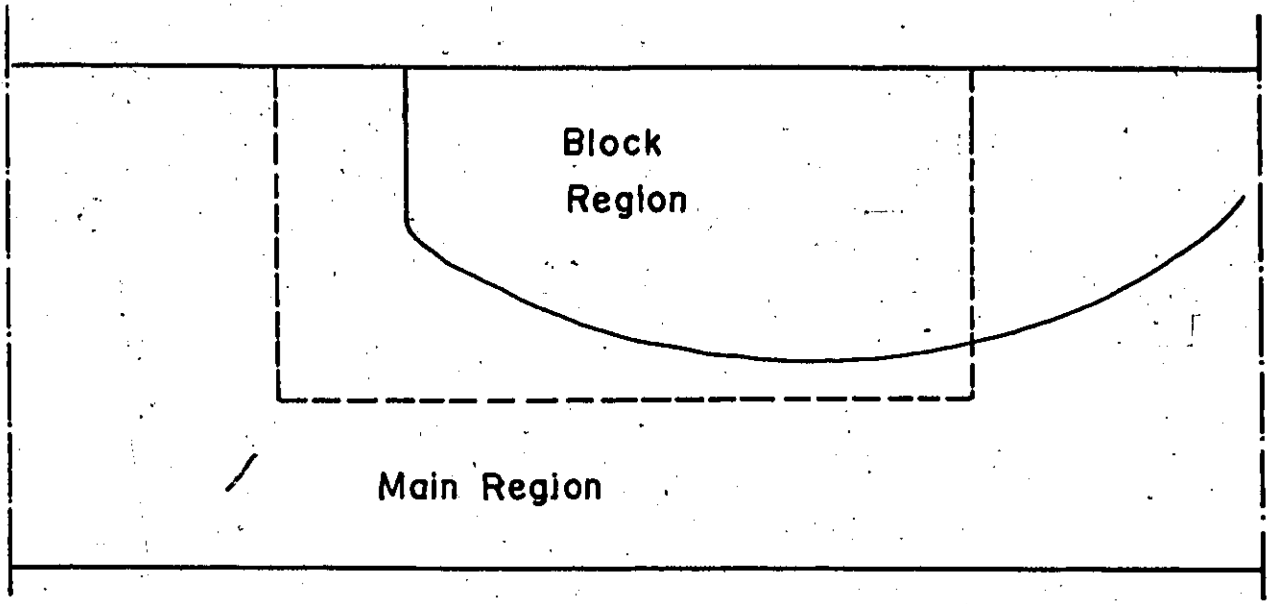

Figure 6.2. Block Iterative Scheme.

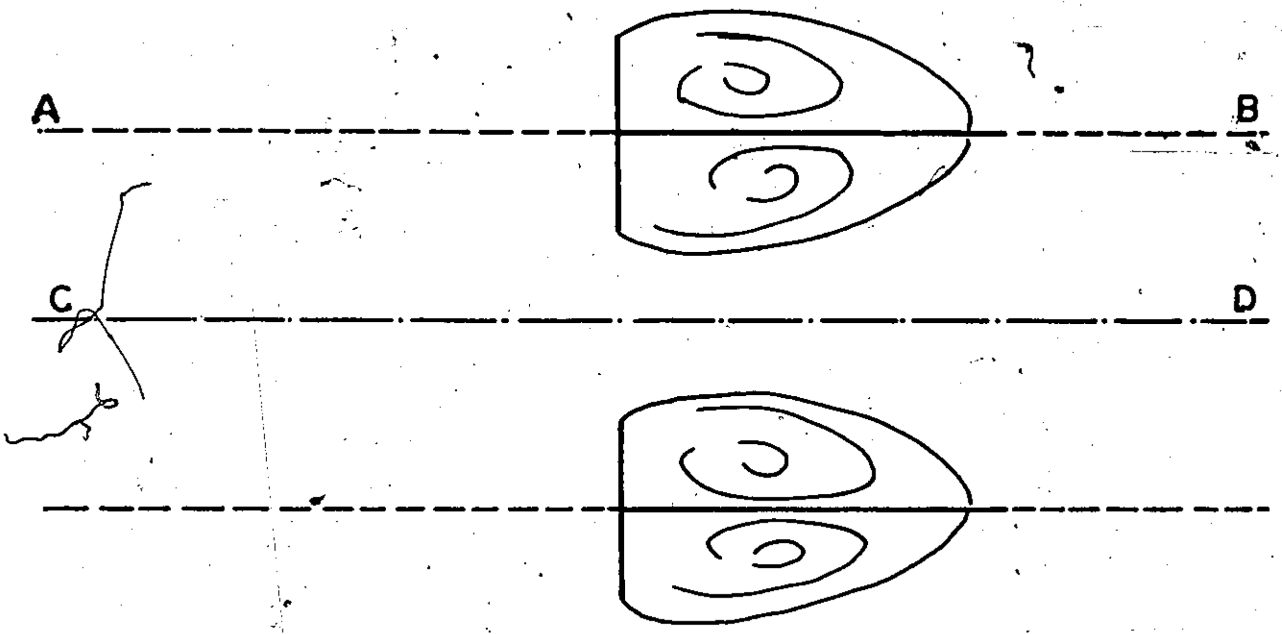

Figure 6.3. Flow Around Two Symmetrical Plates.

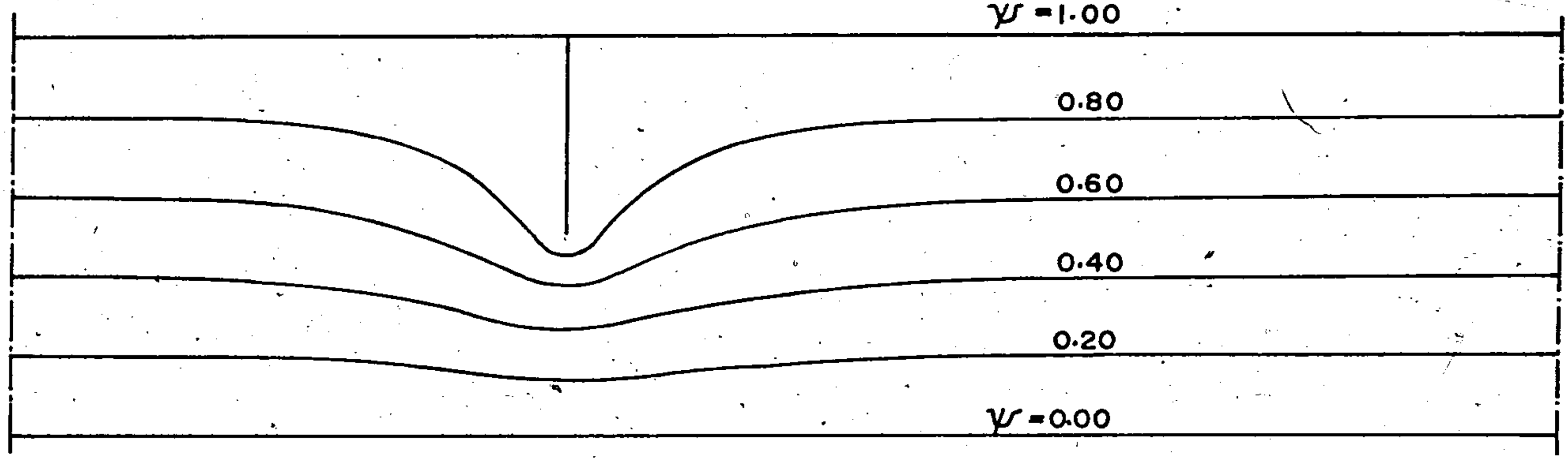

Figure 6.4a. Stream Function Distribution (initial Laplace solution) for α = 0.50.

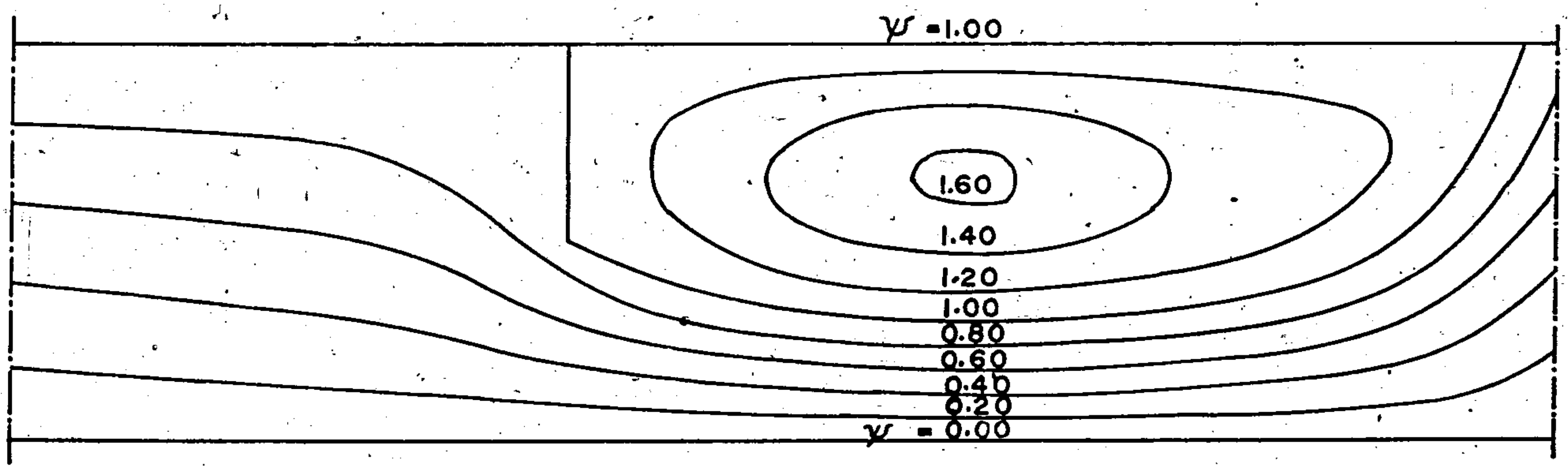

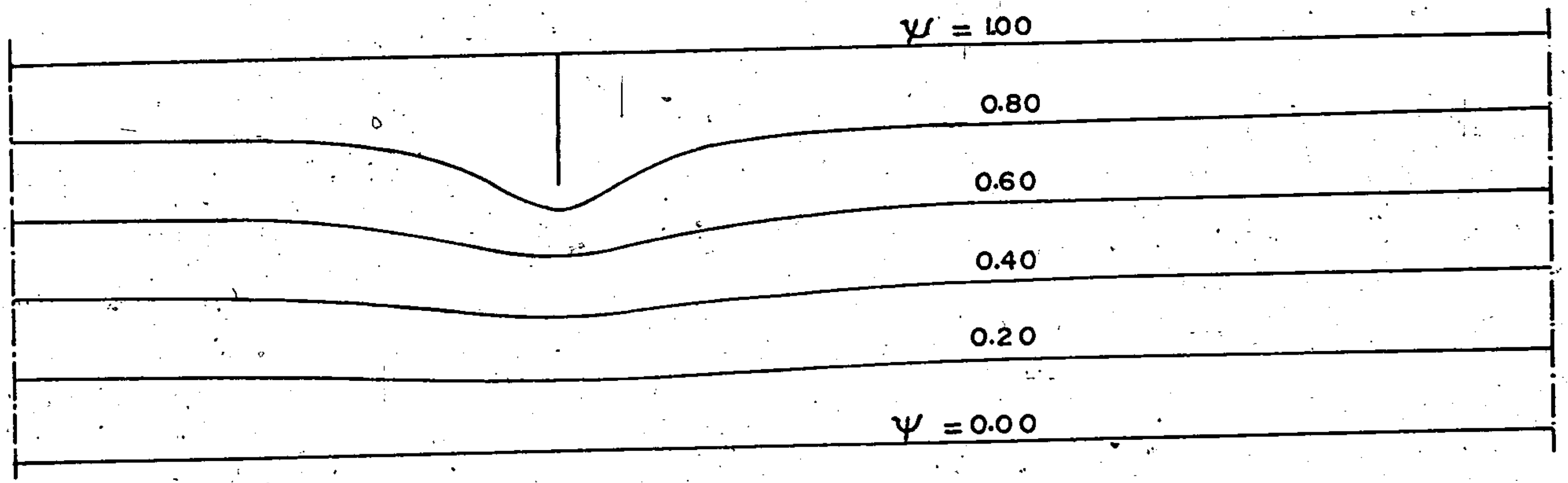

Figure 6.5a. Stream Function Distribution (Initial Laplace Solution) for α = 0.667.

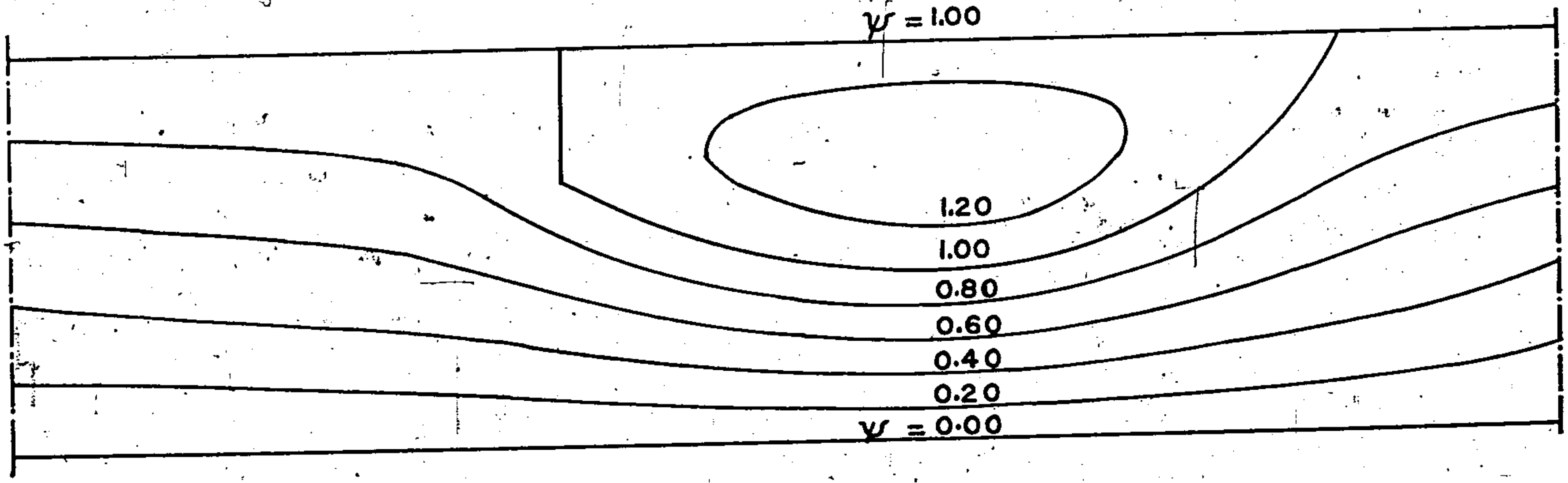

Figure 6.5b. Stream Function Distribution (Final Poisson Solution).

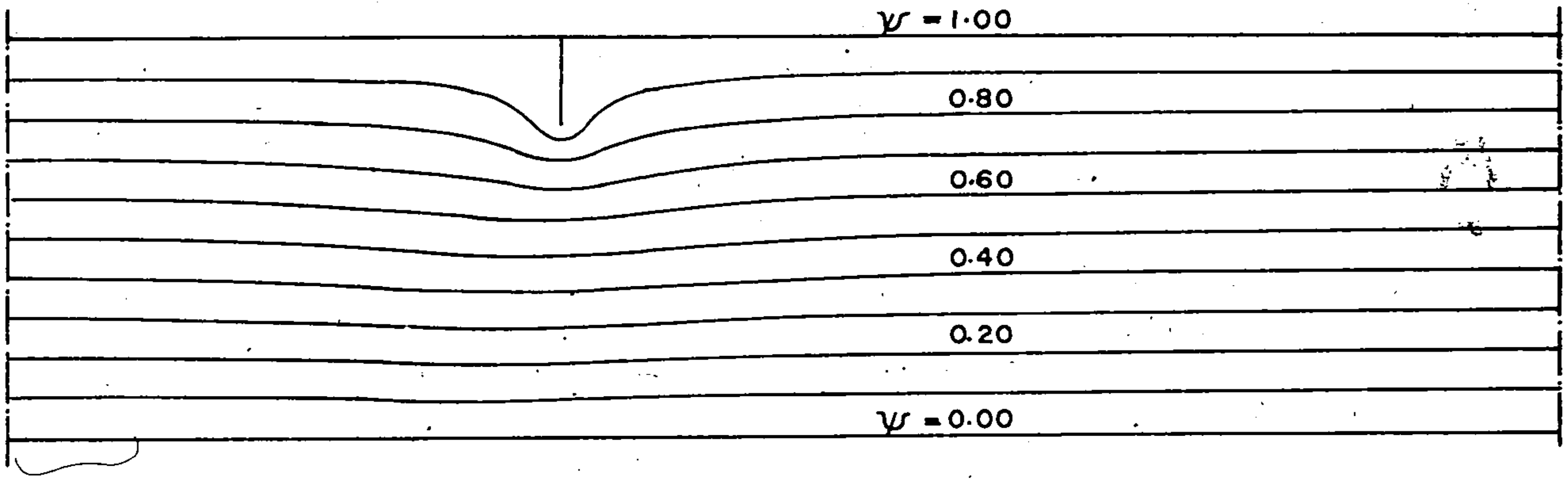

Figure 6.6a. Stream Function Distribution (Initial Laplace Solution) for $\alpha = 0.778$.

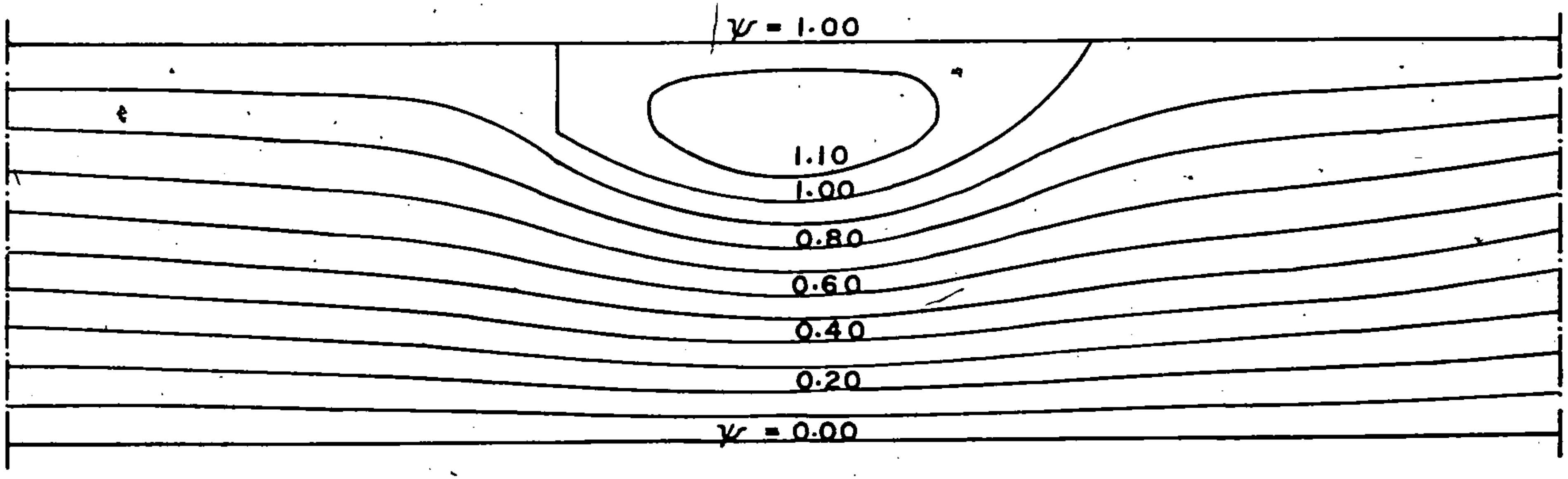

Figure 6.6b. Stream Function Distribution (Final Poisson Solution).

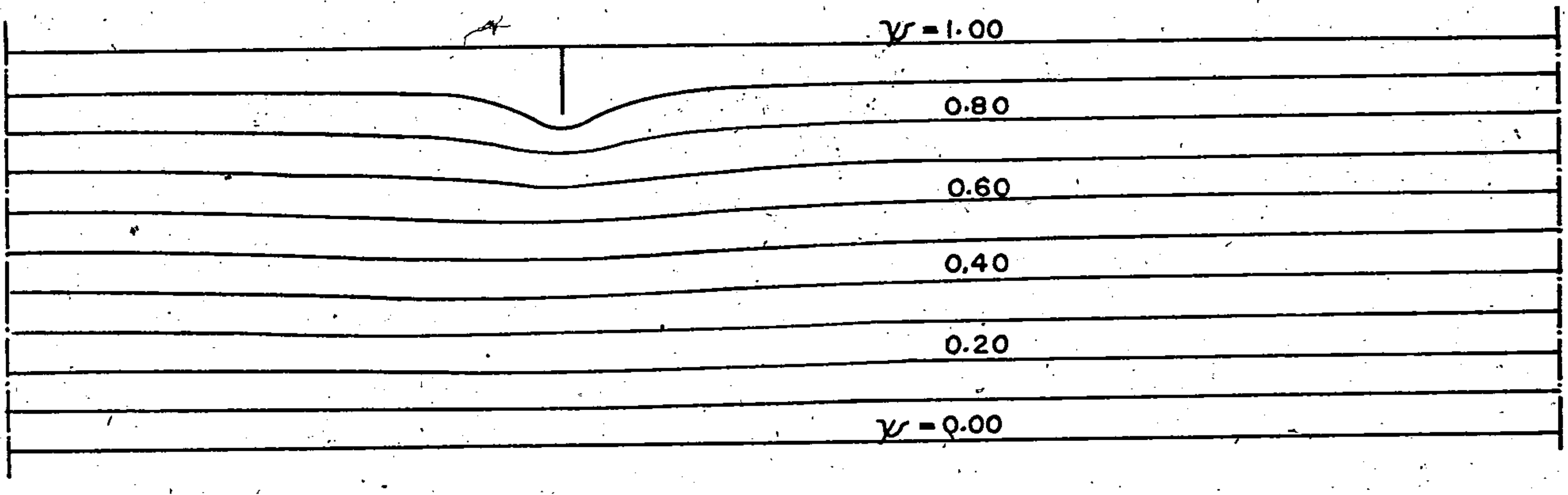

Figure 6.7a. Stream Function Distribution (Initial Laplace Solution) for $\alpha = 0.833$.

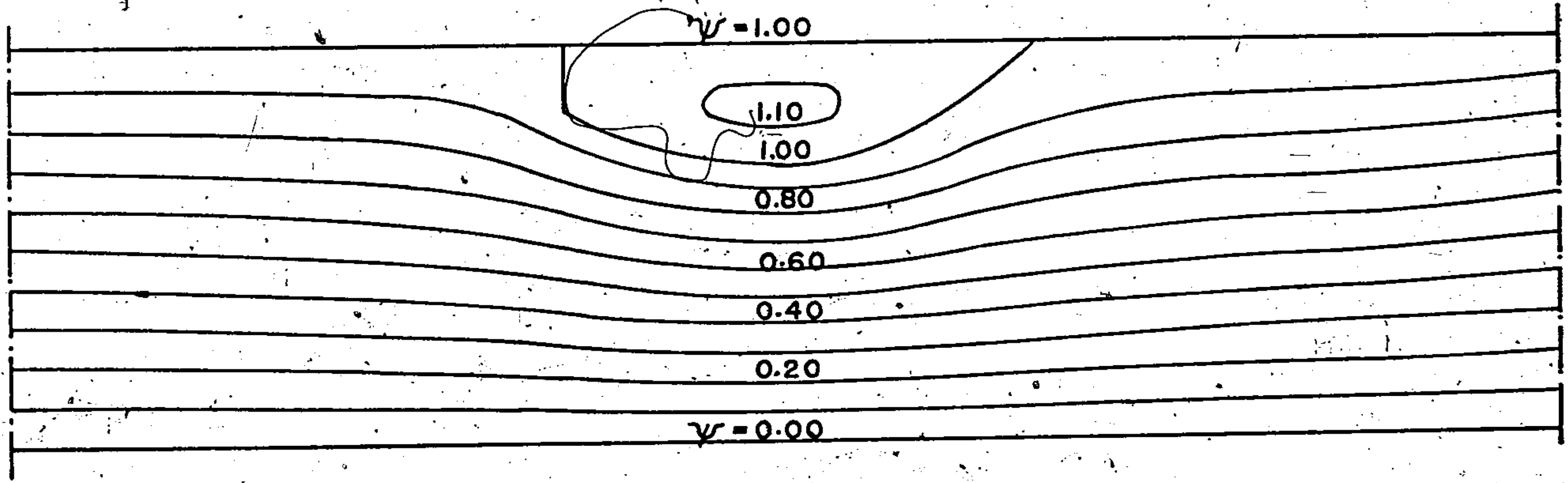

Figure 6.7b. Stream Function Distribution (Final Poisson Solution).

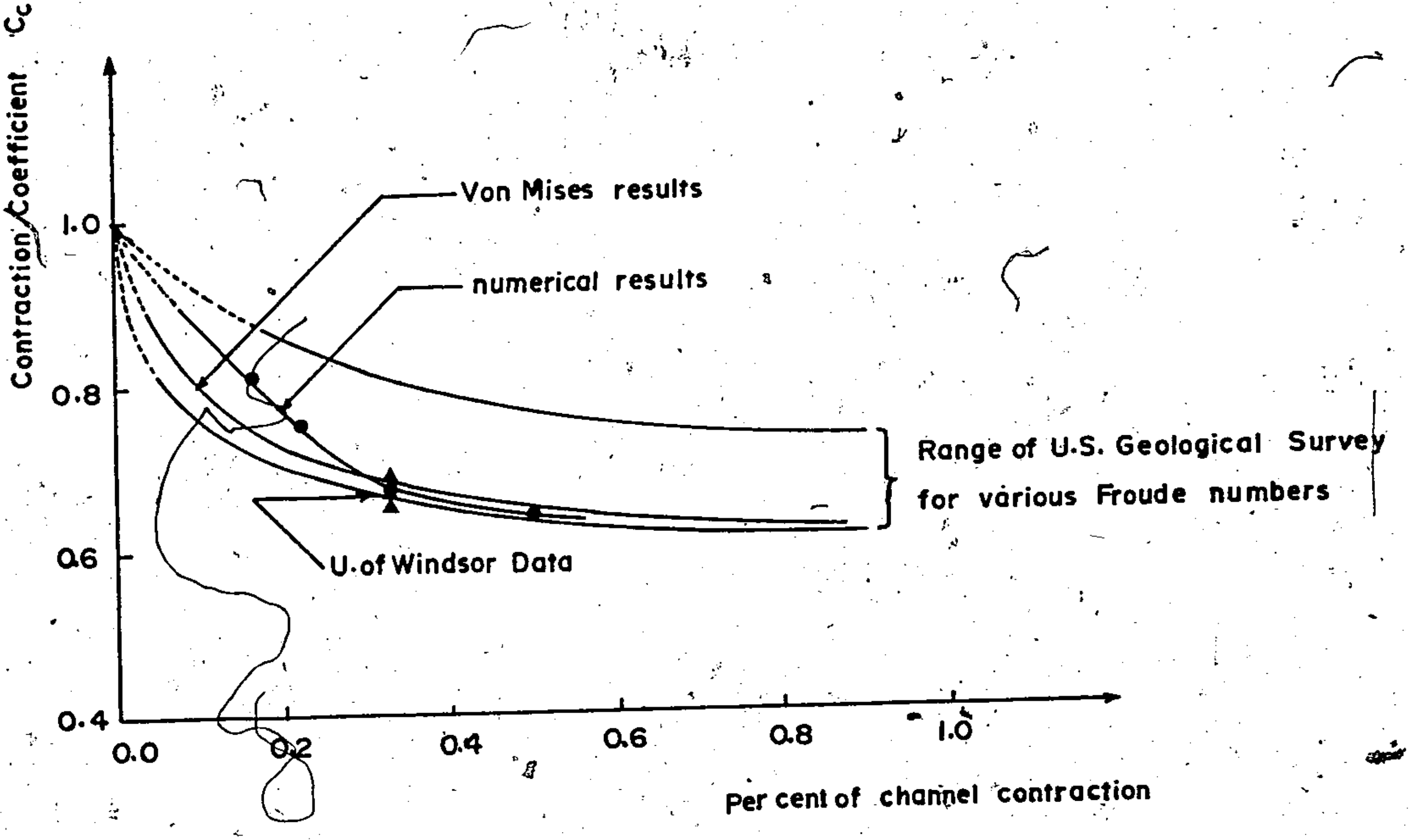

Figure 6.8. Coefficient of Contraction Curves.

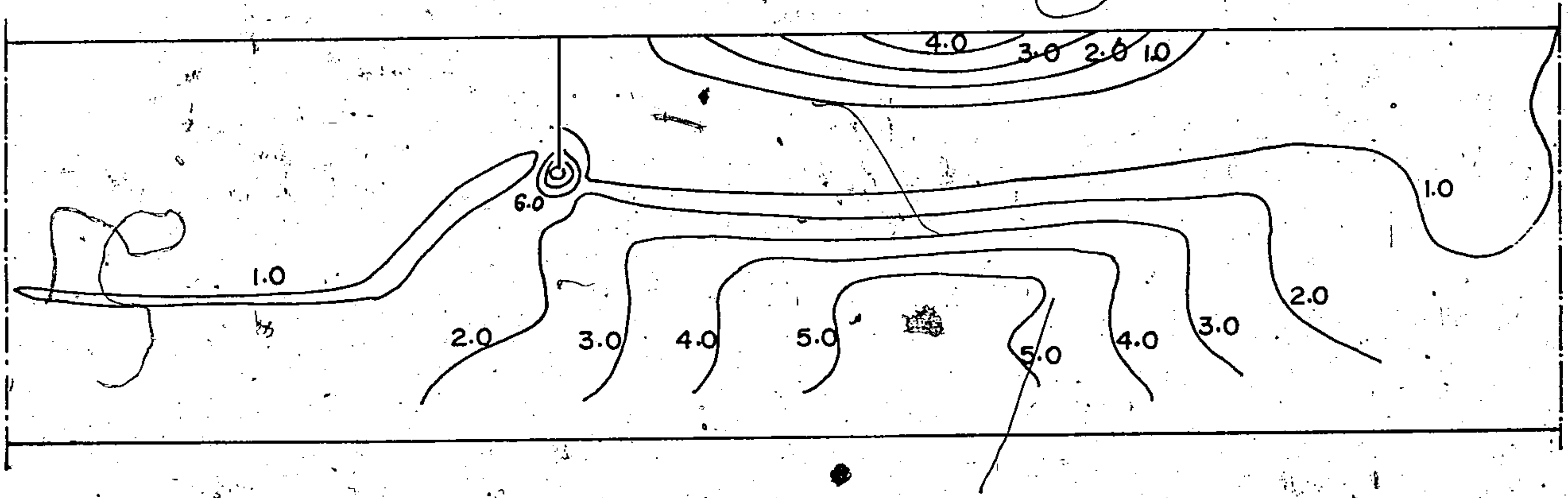

Figure 6.9. Dimensionless Iso-Velocity Squared.

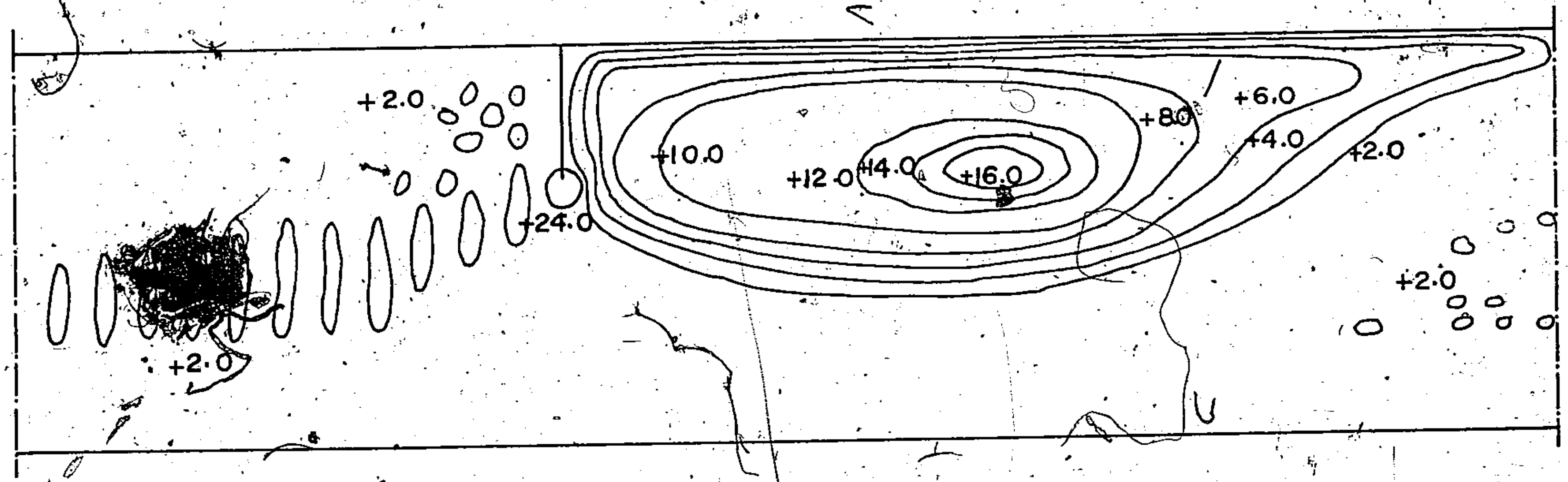

Figure 6.10. Dimensionless Iso-Vorticity

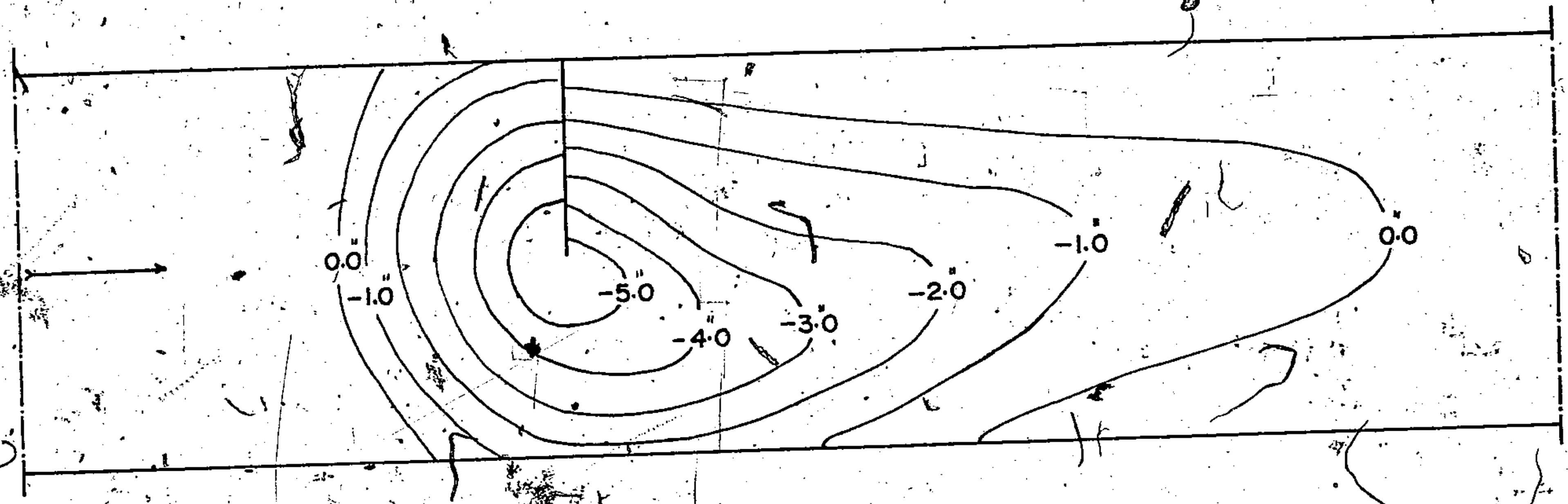

Figure 6.11a. Experimental Scour Pattern for Test No. 1, Table 4.1.

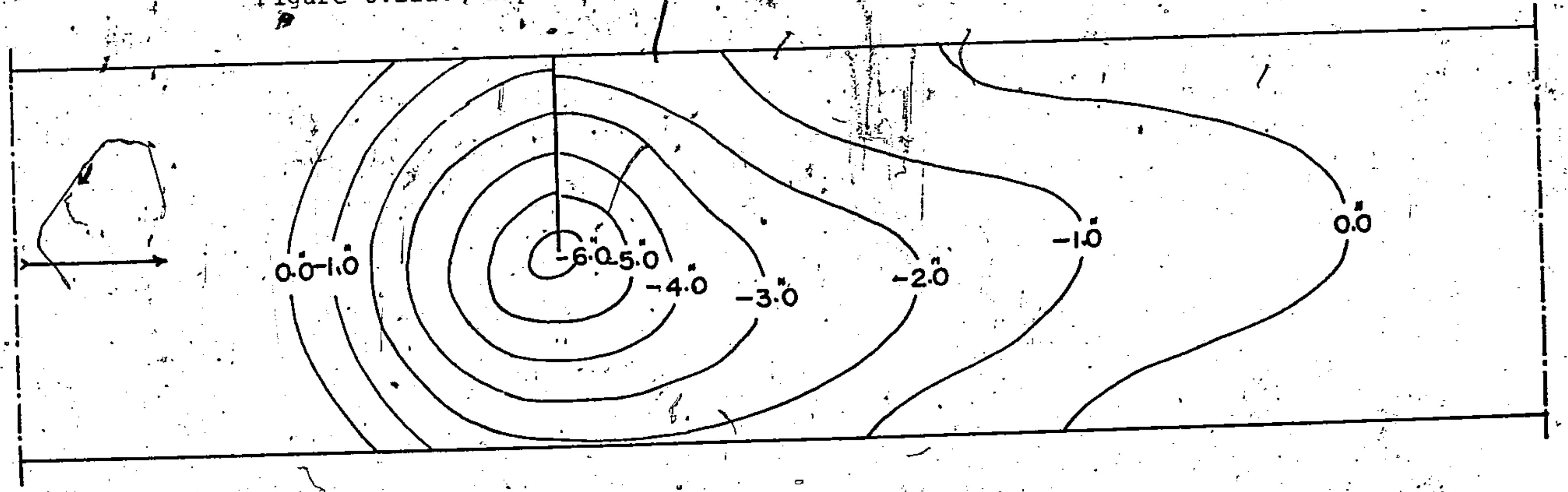

Figure 6.11b. Computed Scour Pattern.

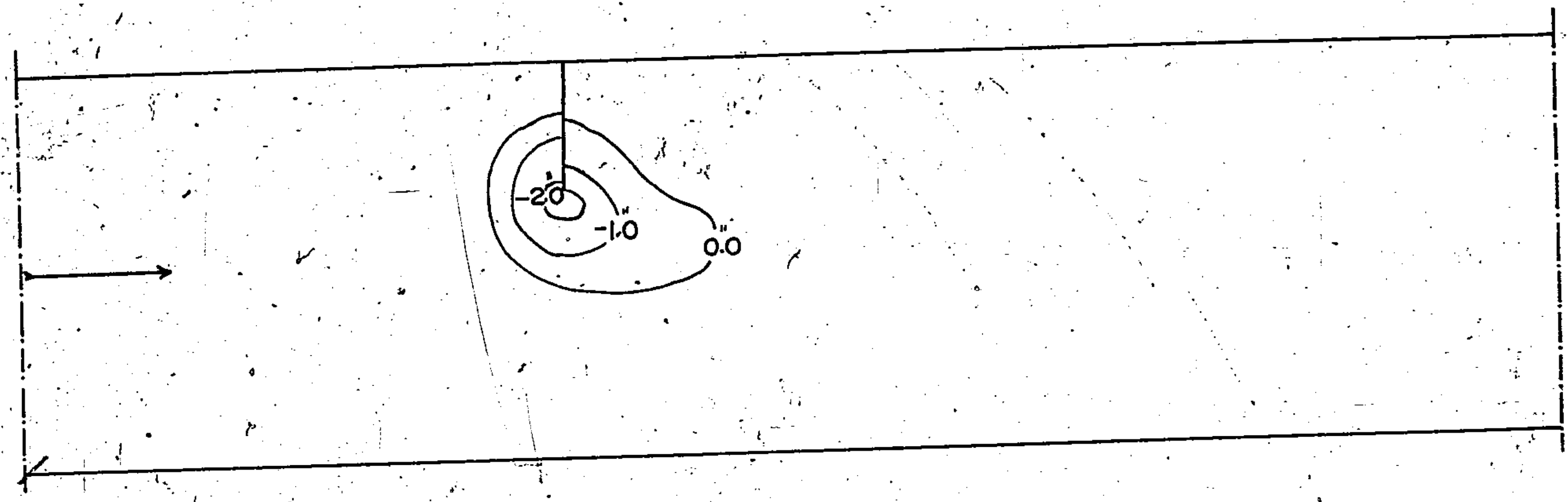

Figure 6.12a. Experimental Scour Pattern for Test No. 3, Table 4.2.

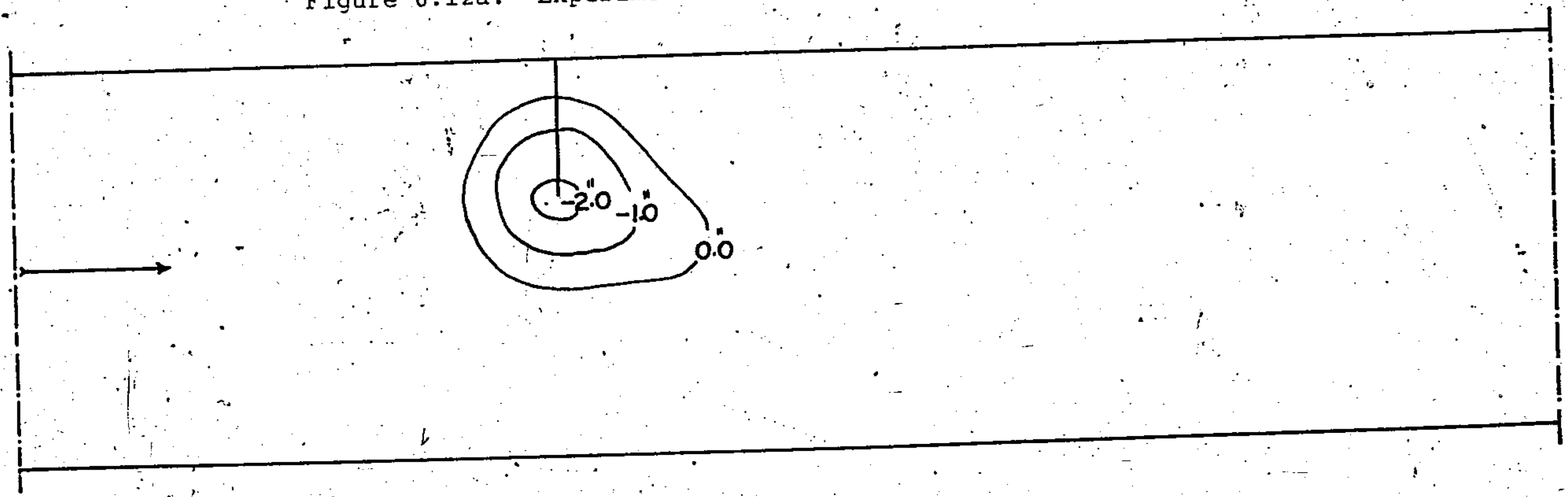

Figure 6.12b. Computed Scour Pattern.

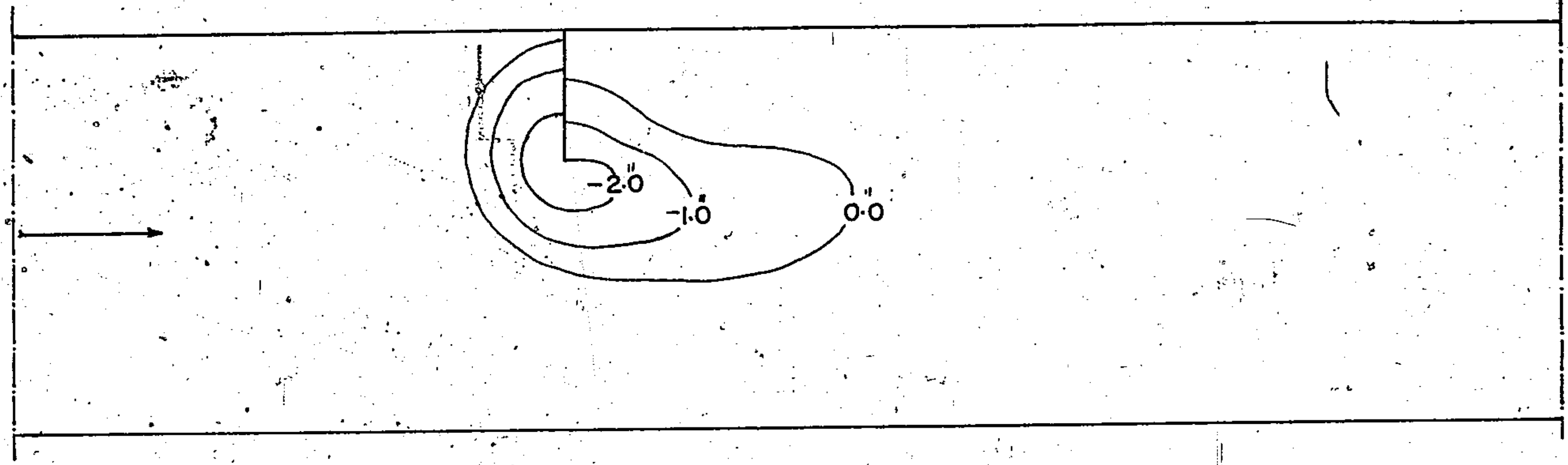

Figure 6.13a. Experimental Scour Pattern for Test No. 7, Table 4.1.

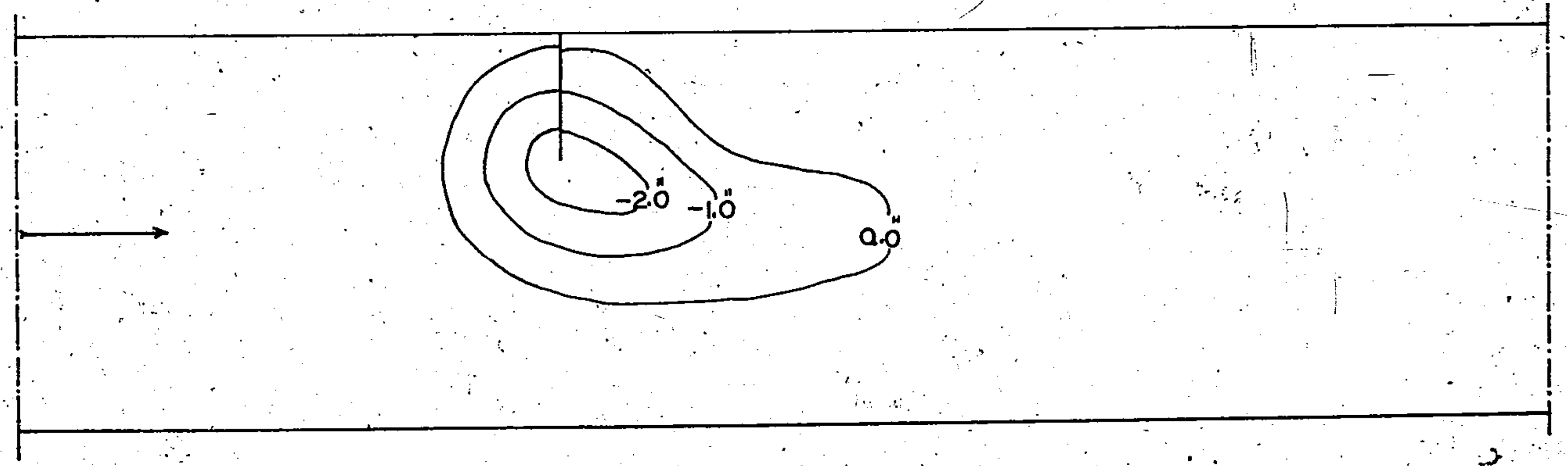

Figure 6.13b. Computed Scour Pattern.

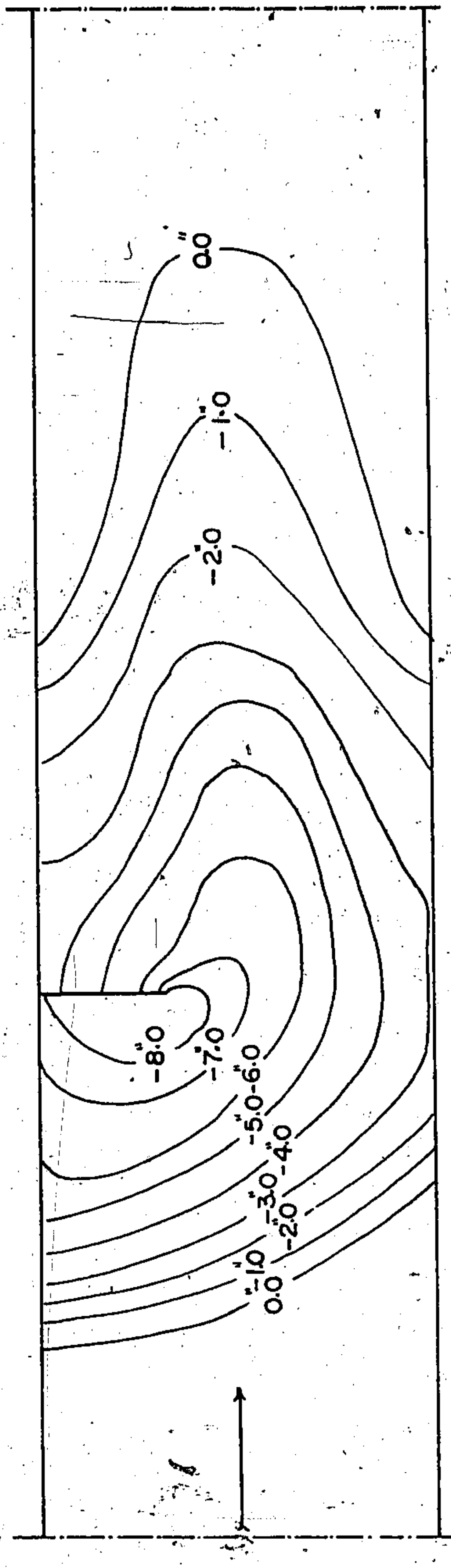

Figure 6.14a. Experimental Scour Pattern for Test No. 14, Table 4.1.

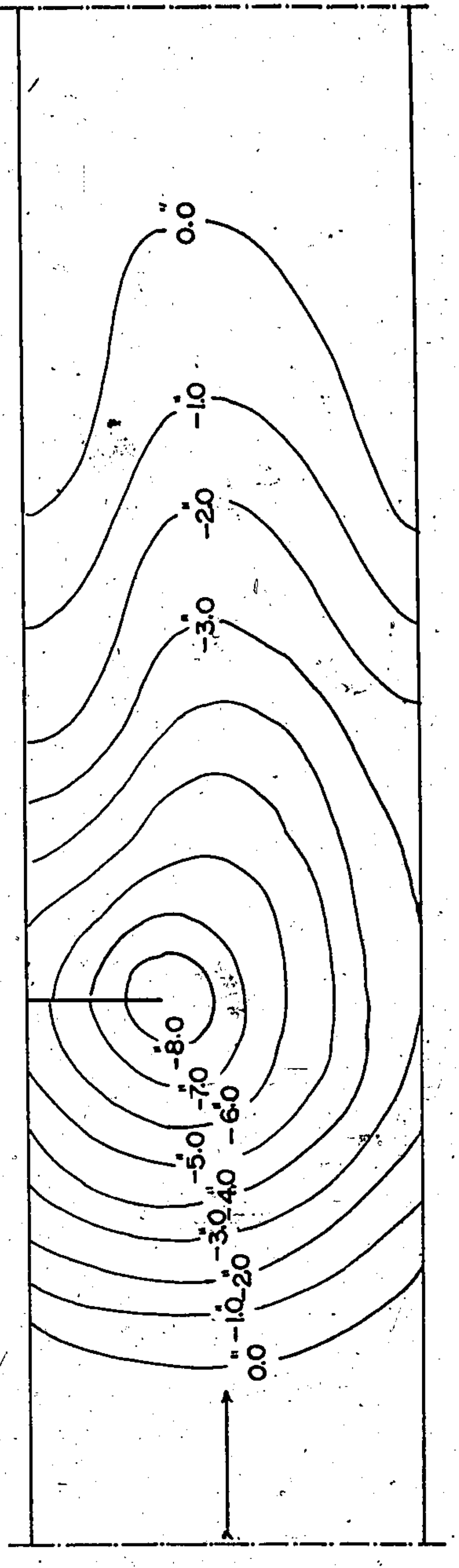

Figure 6.14b. Computed Scour Pattern.

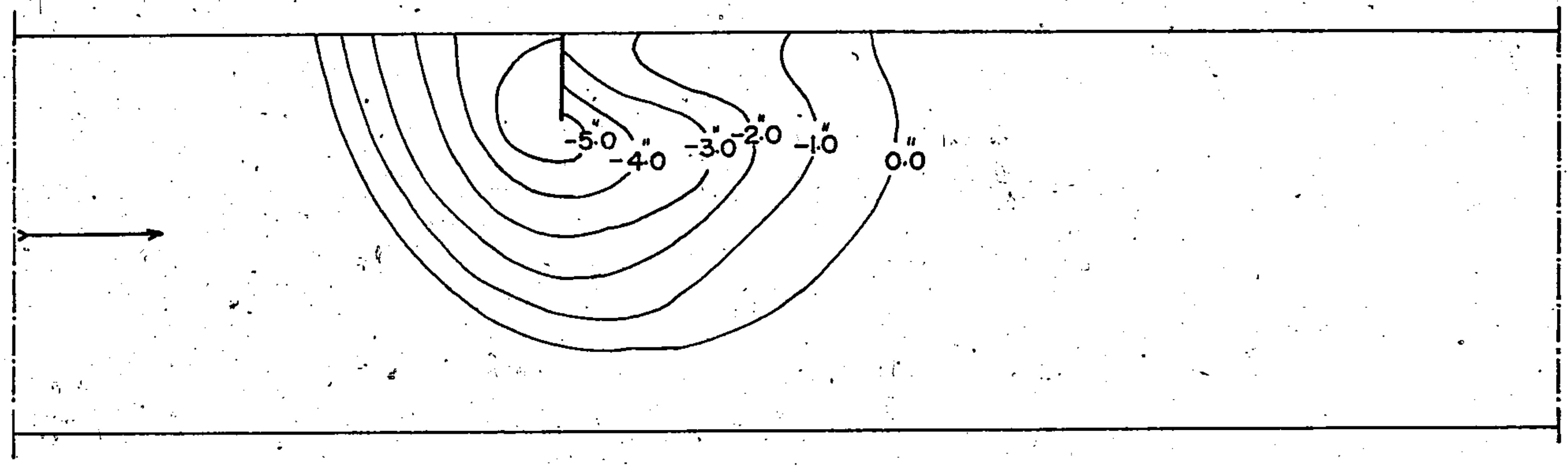

Figure 6.15a. Experimental Scour Pattern for Test No. 18, Table 4.1.

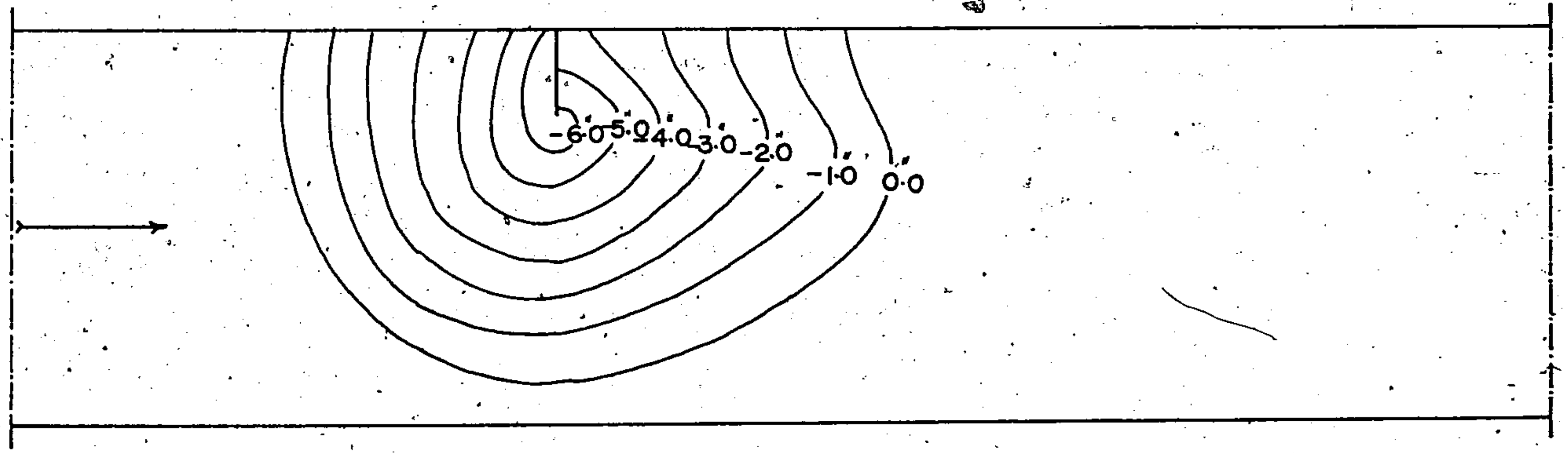

Figure 6.15b. Computed Scour Pattern.

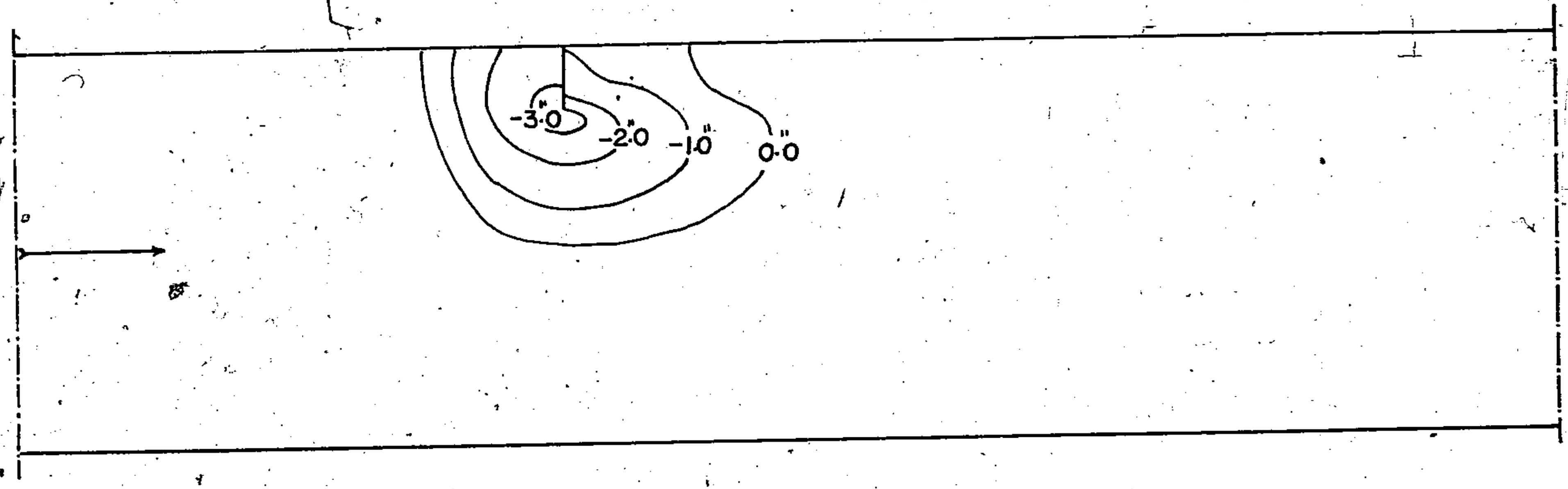

Figure 6.16a. Experimental Scour Pattern for Test No. 20, Table 4.4.

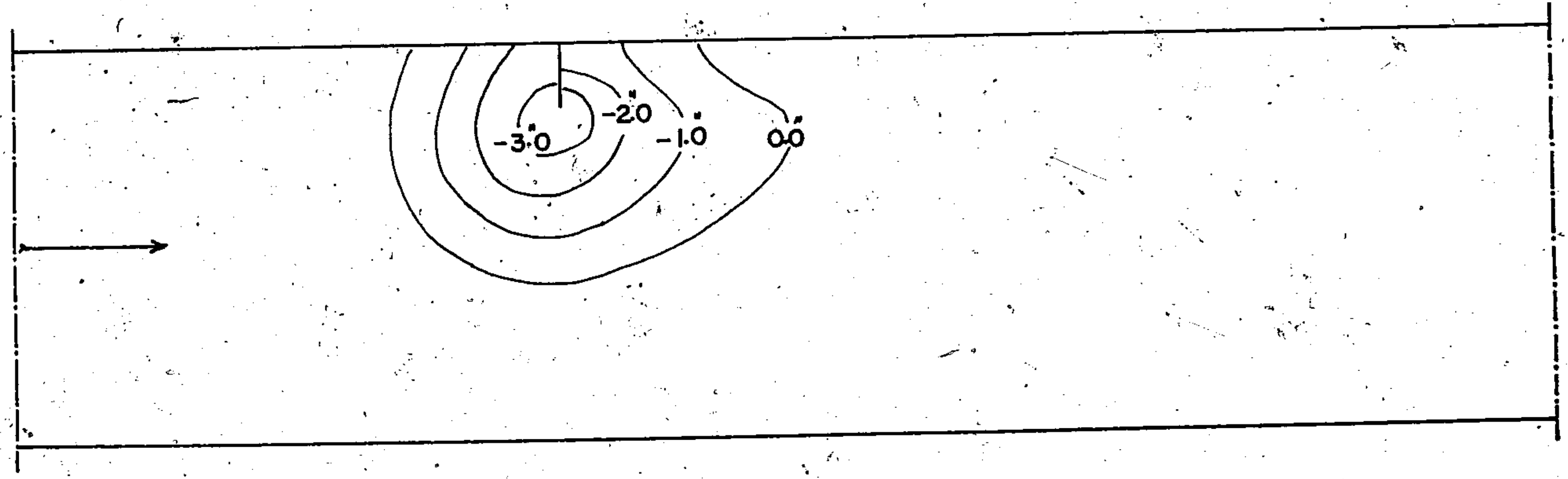

Figure 6.16b. Computed Scour Pattern.

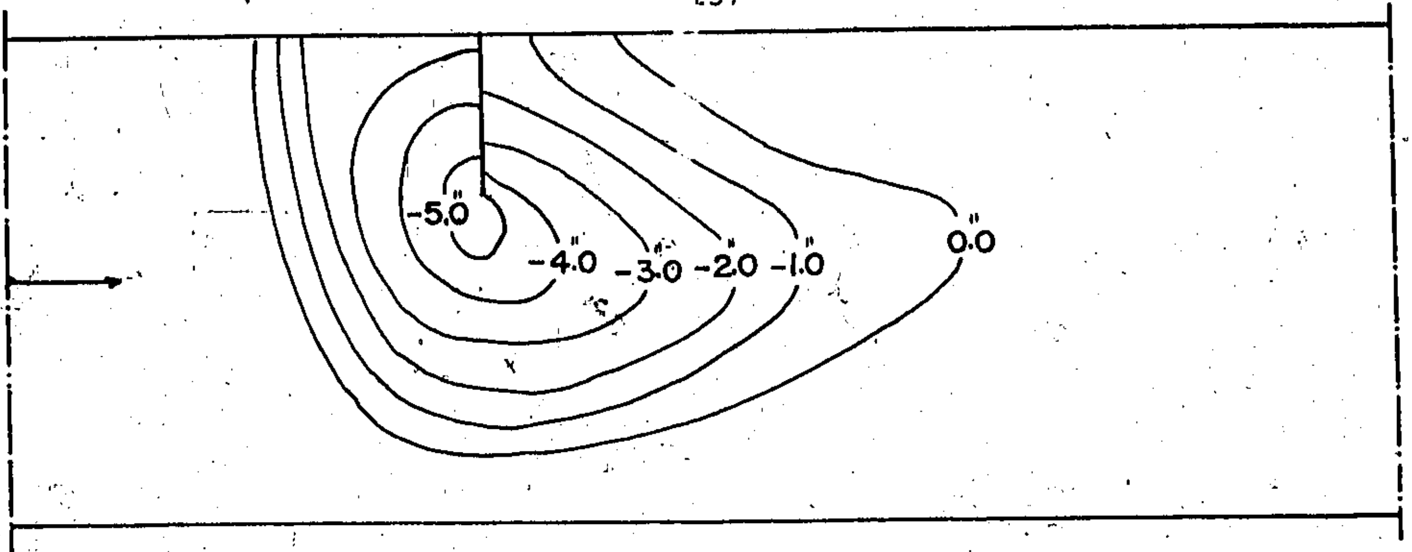

Figure 6.17a. Experimental Scour Pattern for Test No. 10, Table 4.1 developed after 2½ hours.

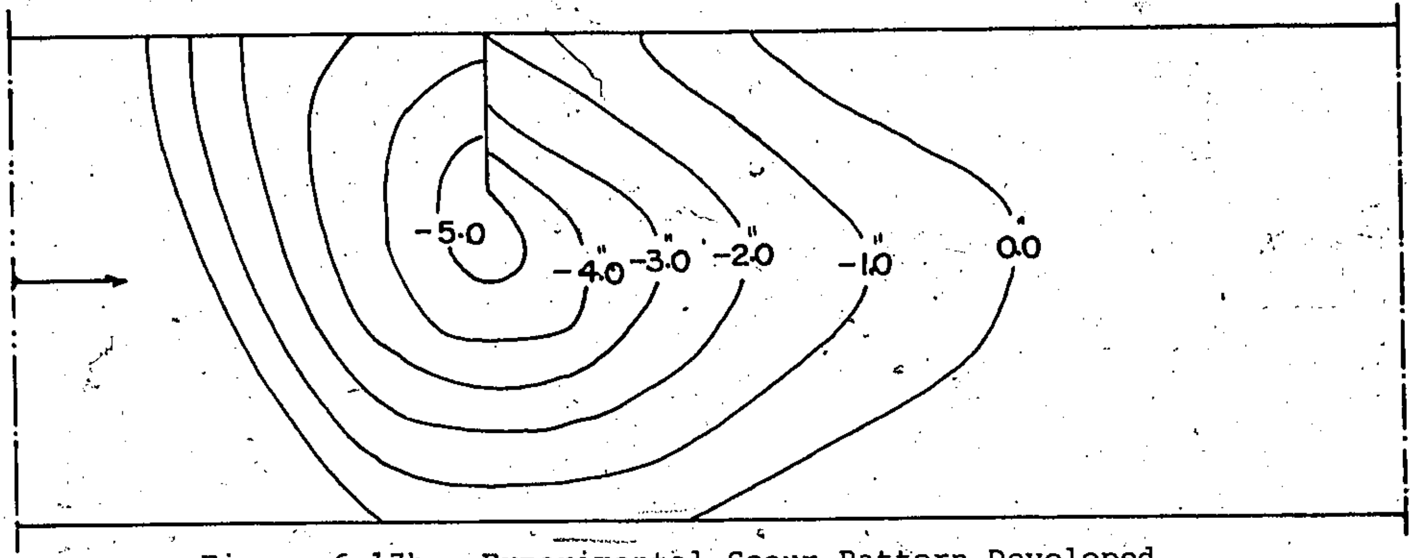

Figure 6.17b. Experimental Scour Pattern Developed After 24 hours.

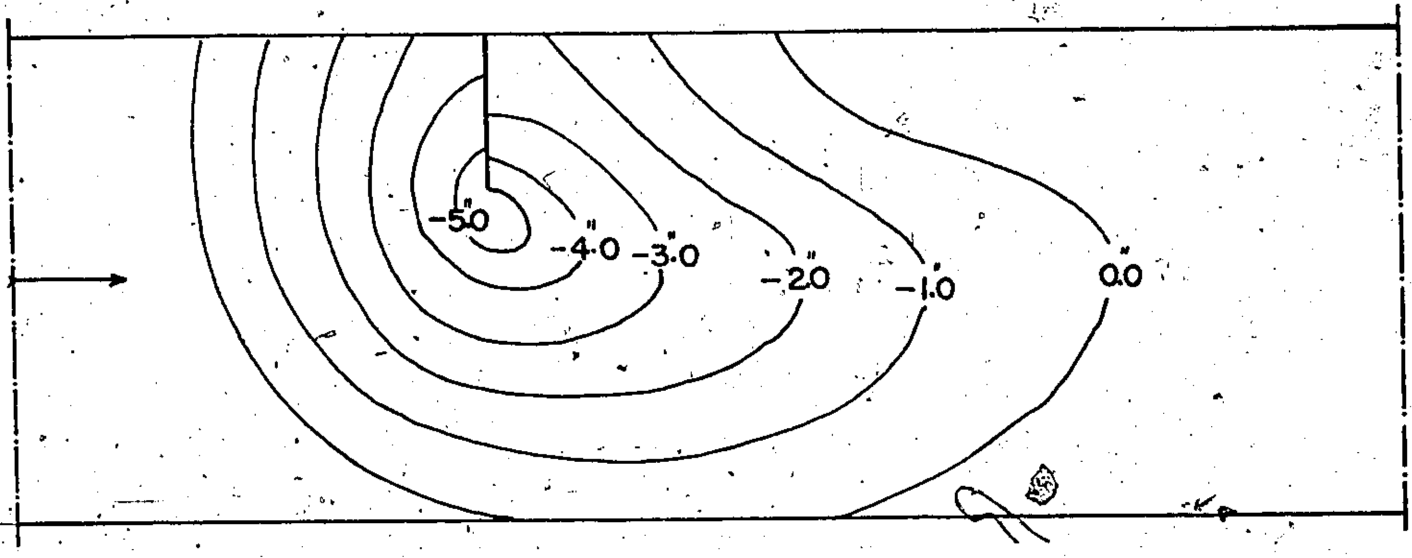

Figure 6.17c. Computed Scour Pattern.

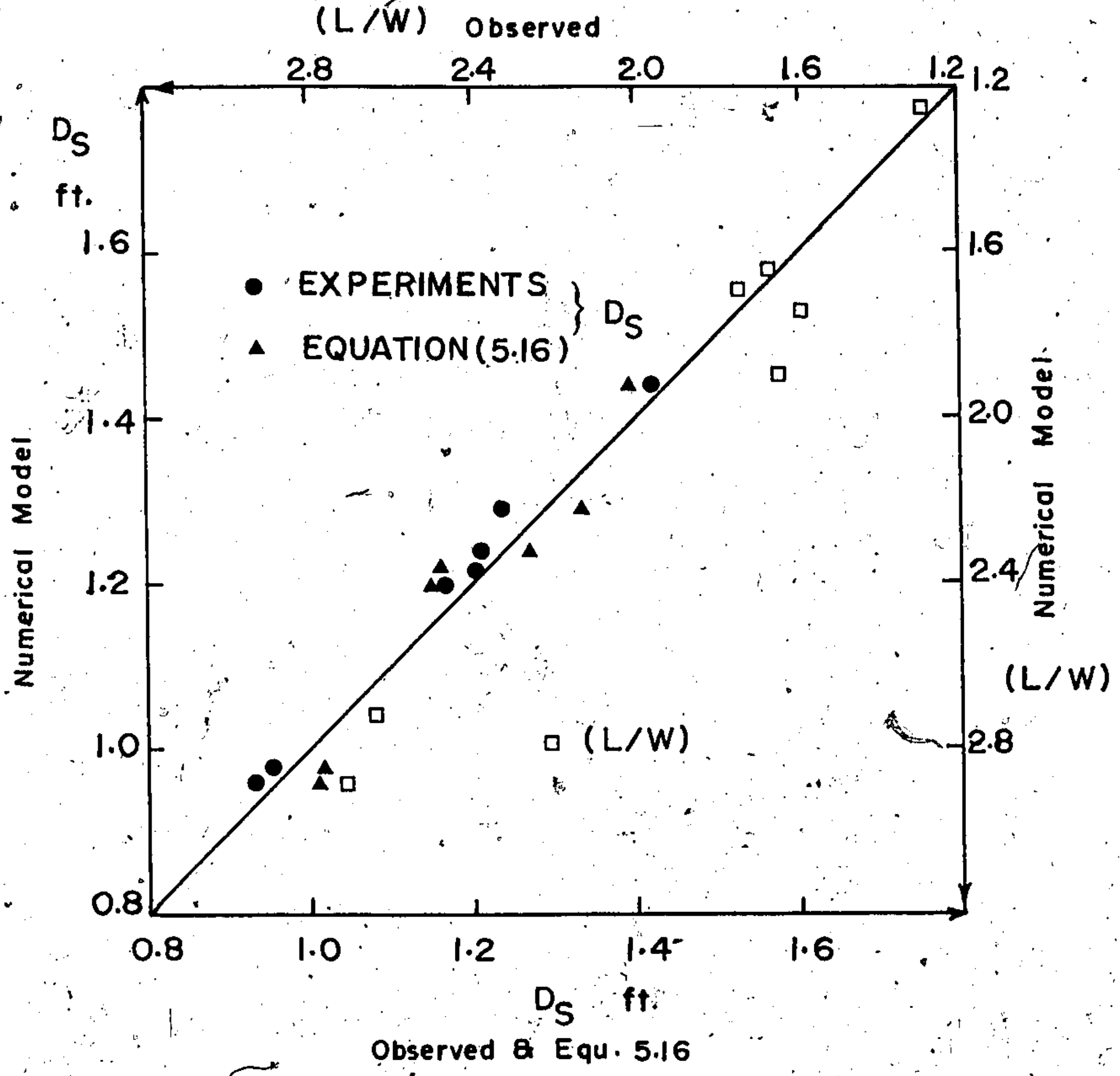

Figure 6.18. Comparison of Computed and Experimental Data.

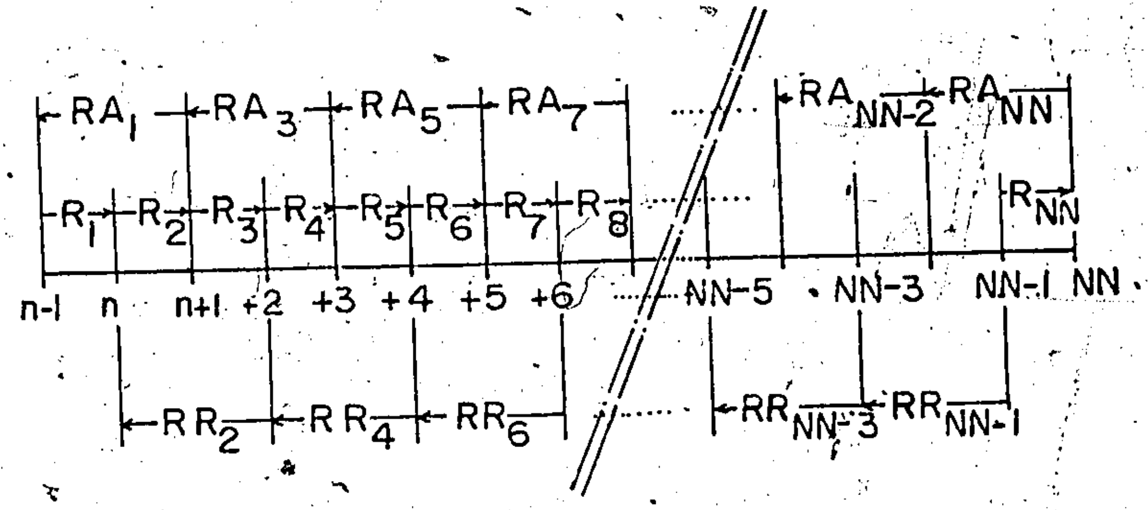

Figure 6.19. Error Advancement Ratios.

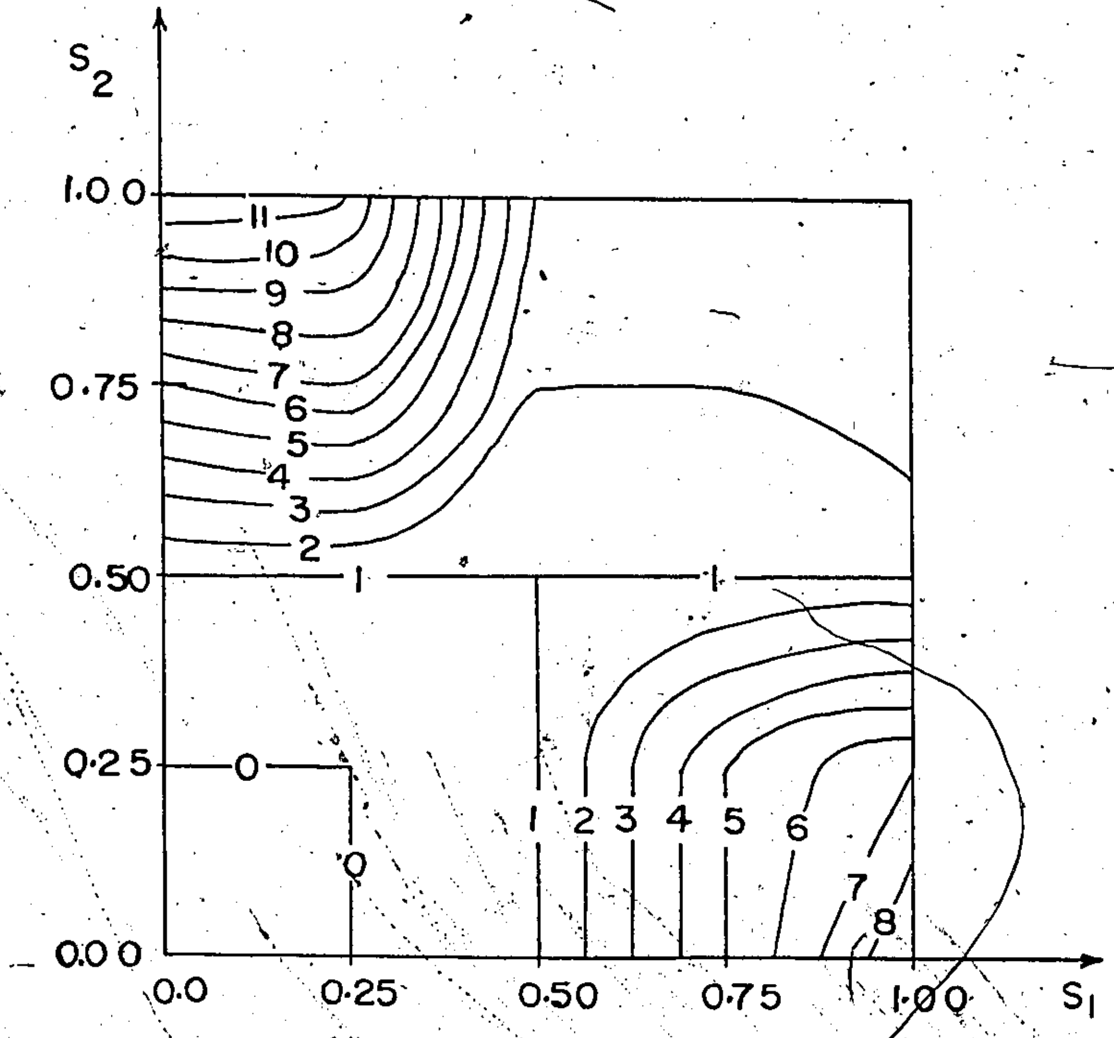

Figure 6.20. Stability Contours (ρ) for $C_1 = 0$ and $C_2 = 0$.

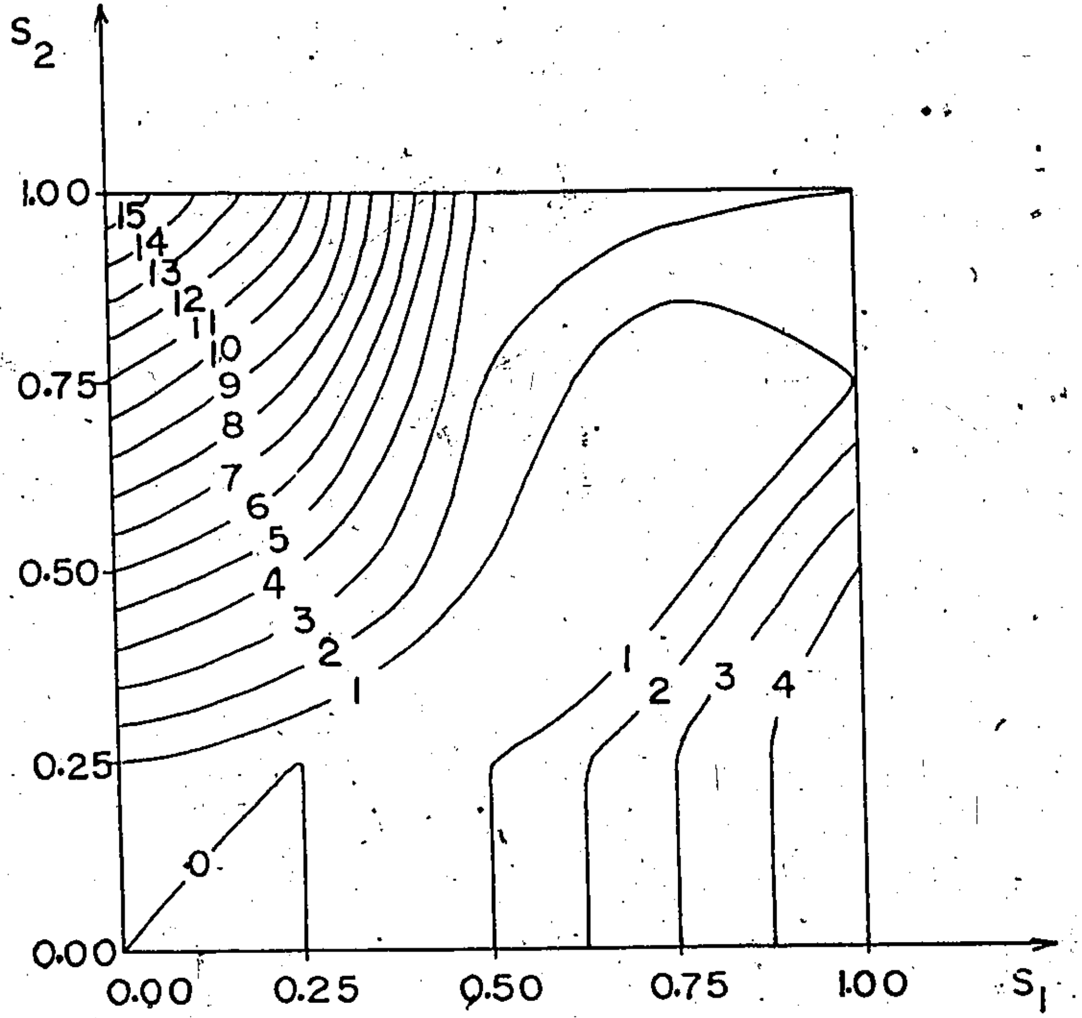

Figure 6.21. Stability Contours (ρ) for $C_1 = 0$ and $C_2 = 1$.

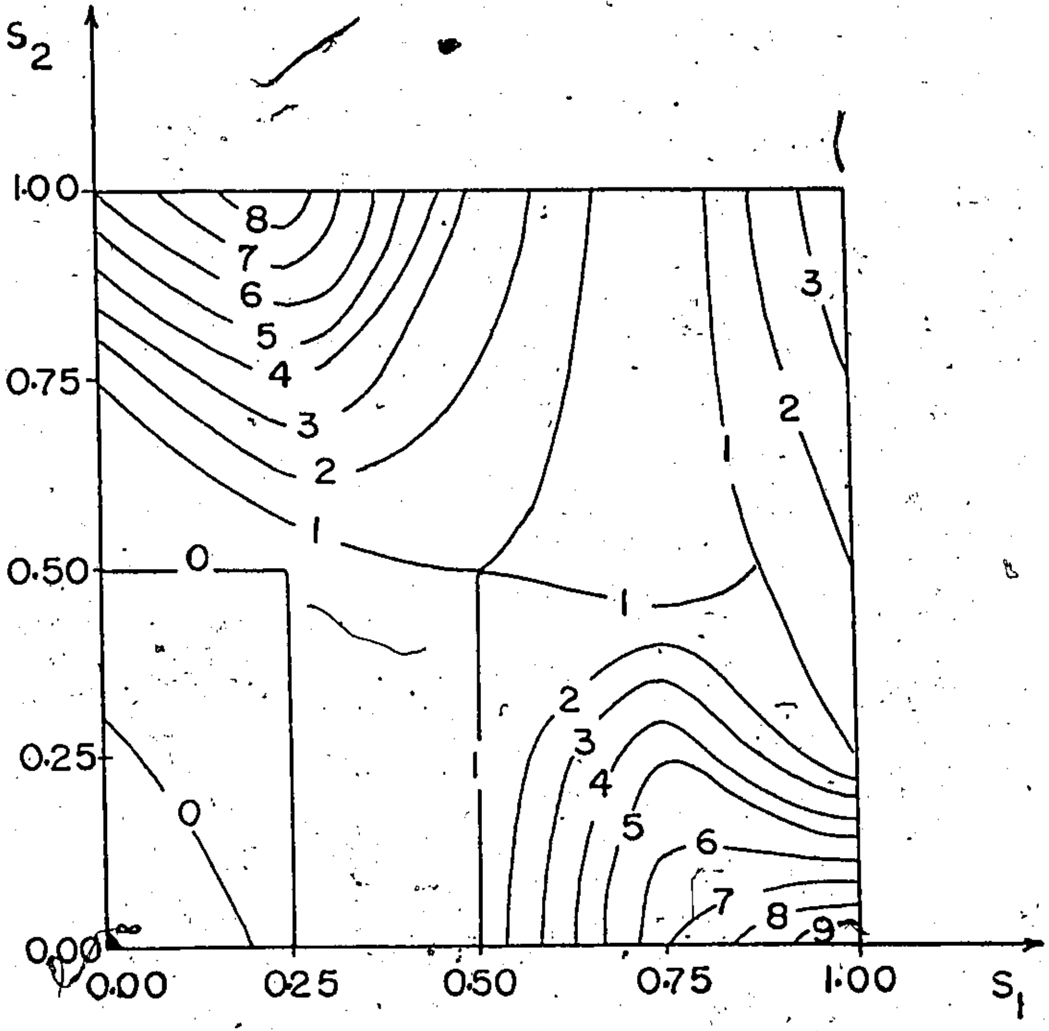

Figure 6.22. Stability Contours (ρ) for $C_1 = 0$ and $C_2 = -1$.

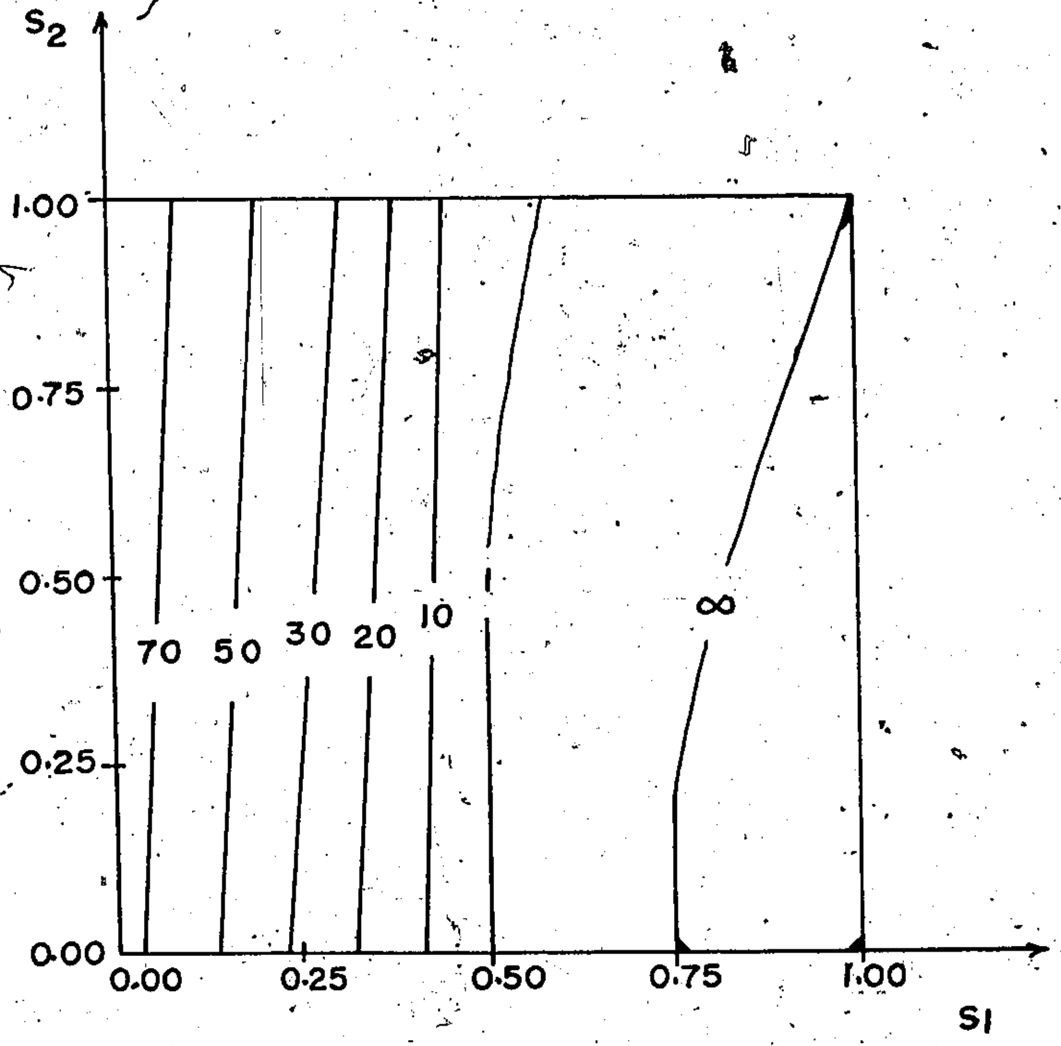

Figure 6.23: Stability Contours (ρ) for $C_1 = 0$ and $C_2 = 10$.

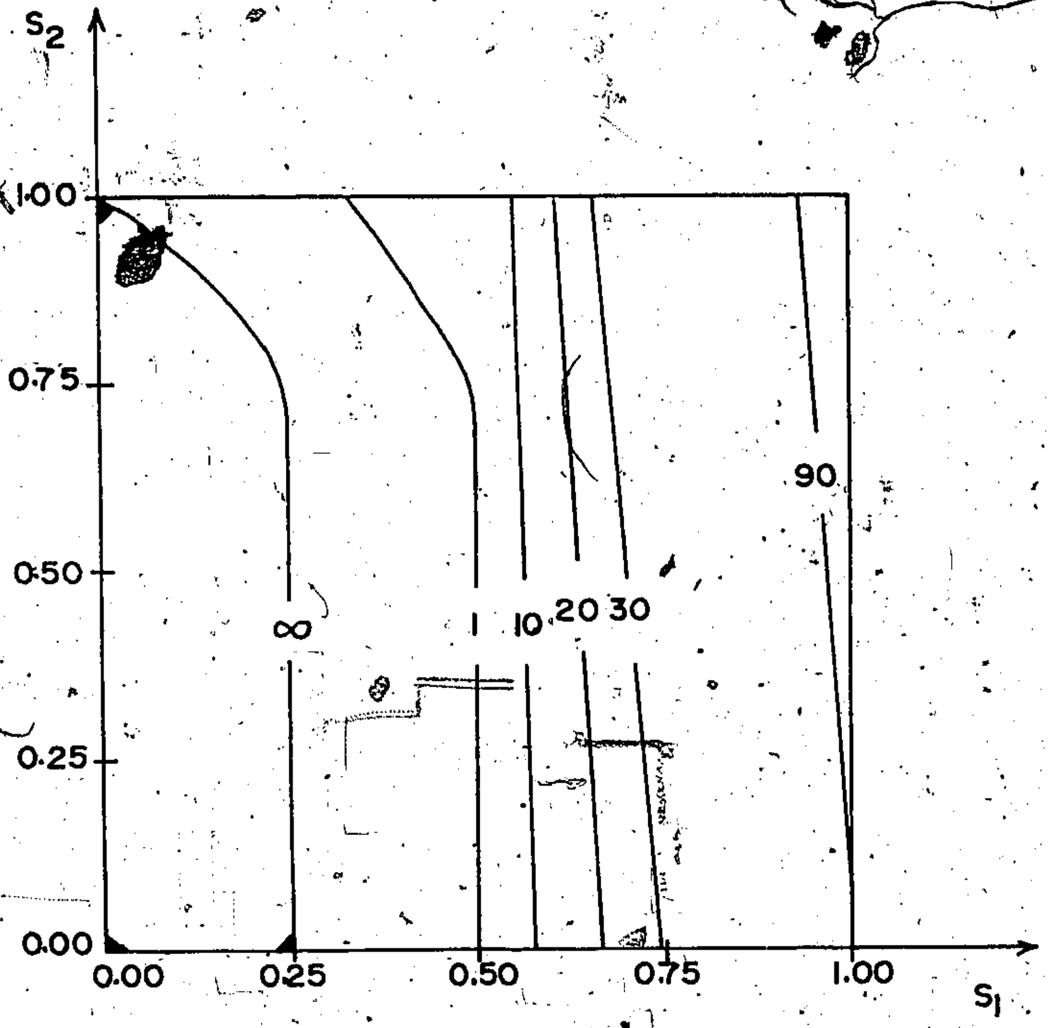

Figure 6.24. Stability Contours (ρ) for $C_1 = 0$ and $C_2 = -10$.

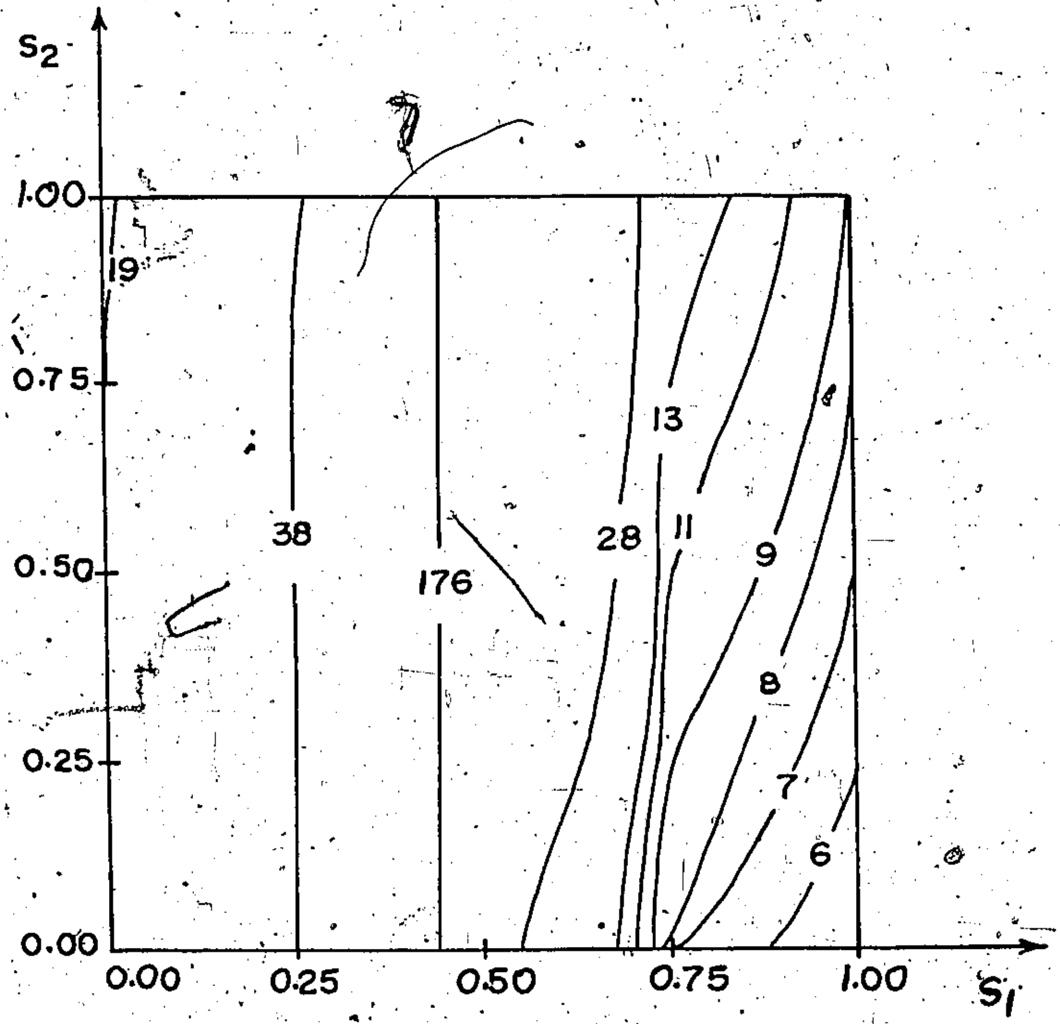

Figure 6.25. Stability Contours ($+C_2$) for $C_1 = 0$ and $\rho = 170$.

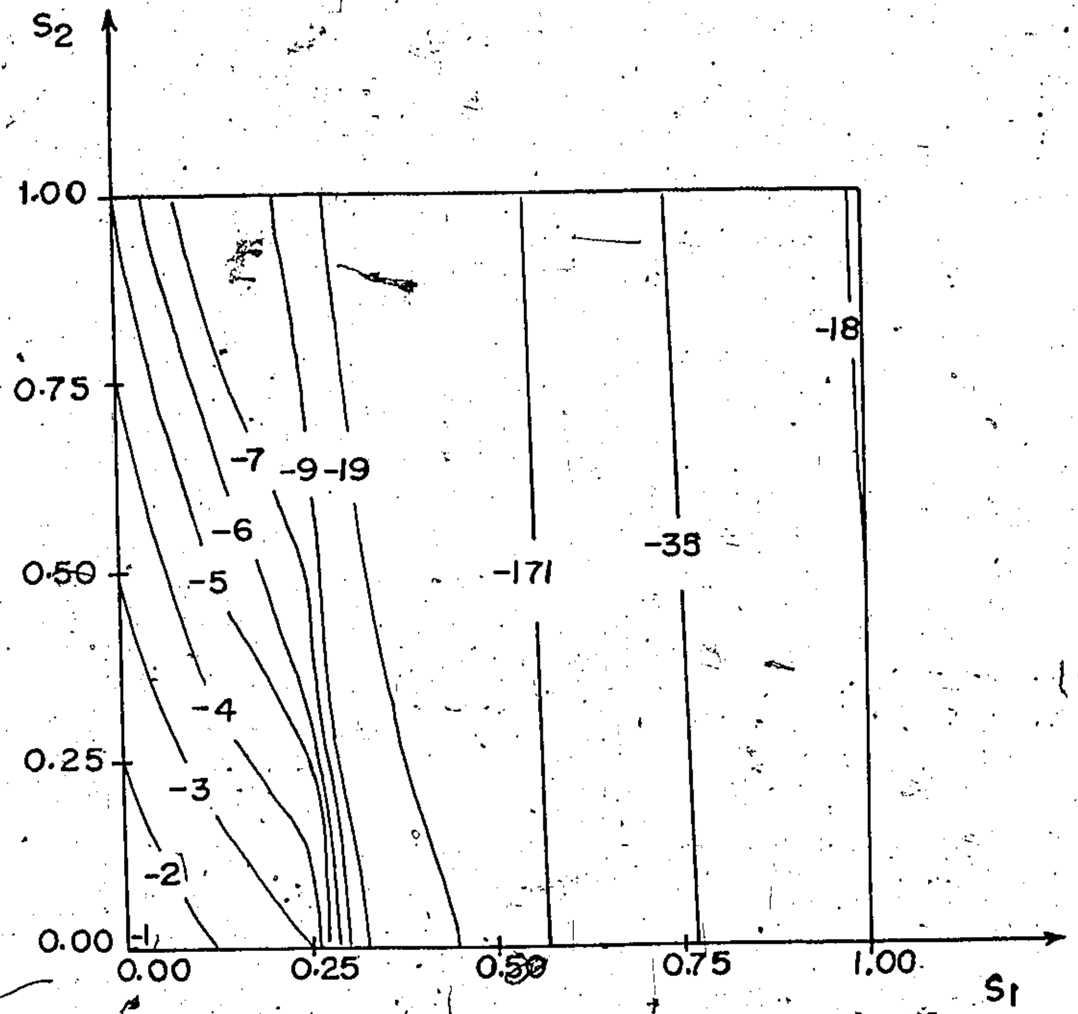

Figure 6.26. Stability Contours $(-C_2)$ for $C_1 = 0$ and $\rho_v = 170$.

APPENDIX B

Photographs

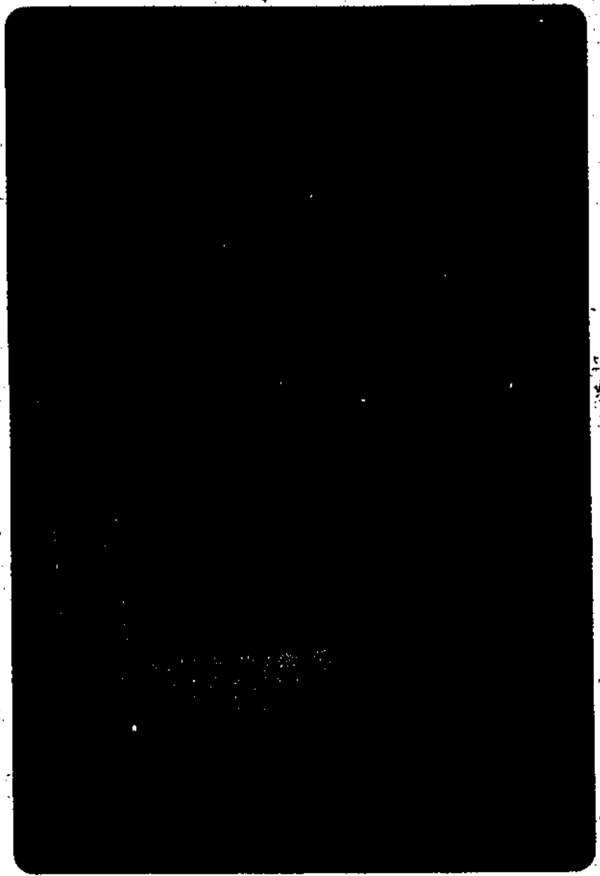

Photo 4.1 A view of the separation line and the wake zone.

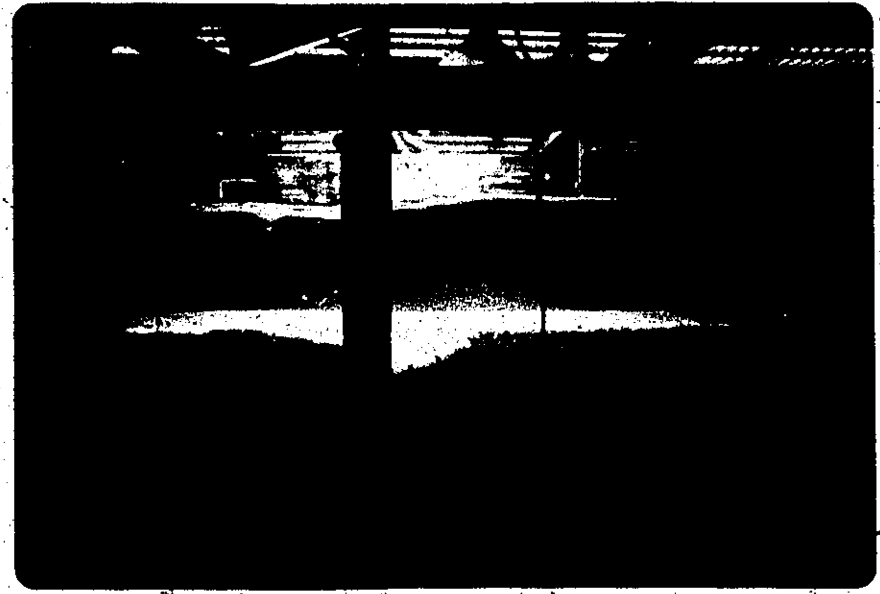

Photo 4.2 A front view of the vorticies and the development of the scour hole.

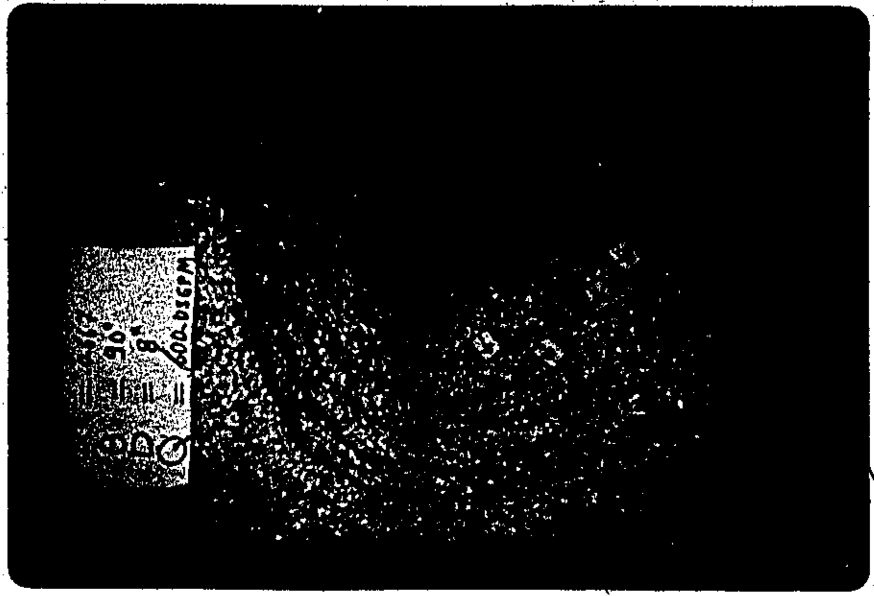

Photo 4.3 A top view of a typical experimental contour pattern with removal of the deposited material.

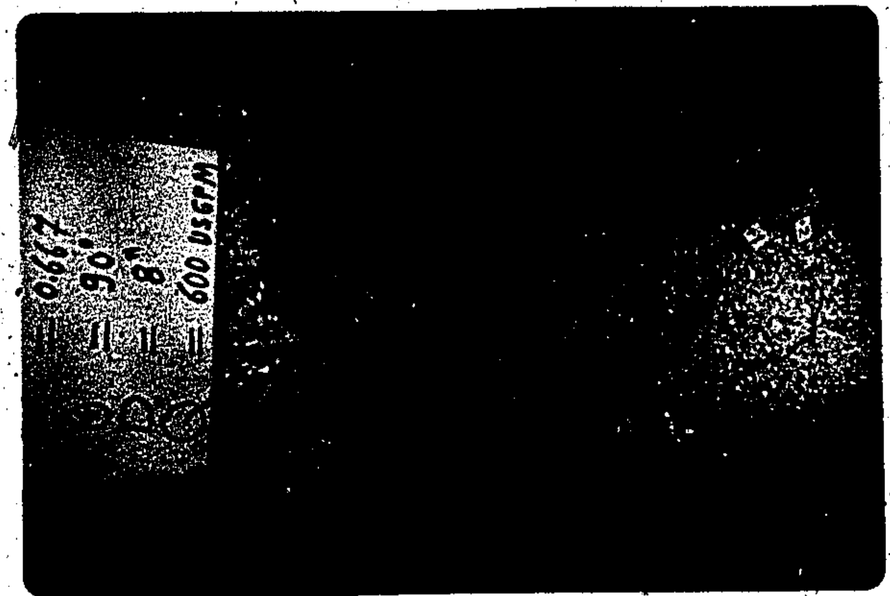

Photo 4.4 A top view of a typical experimental contour pattern without removal of the deposited material.

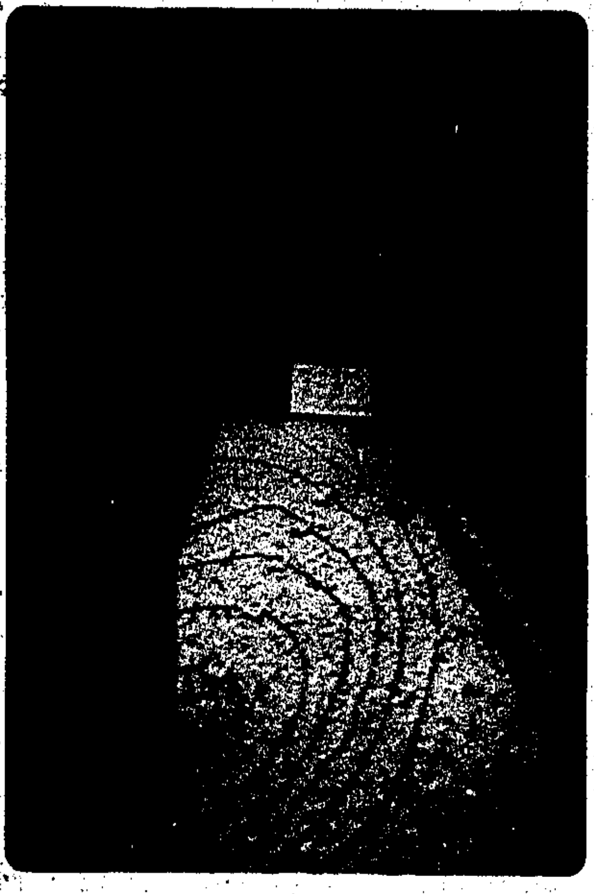

Photo 4.5 A view of the scour hole in the downstream direction.

Photo 4.6 A view of the scour hole in the upstream direction.

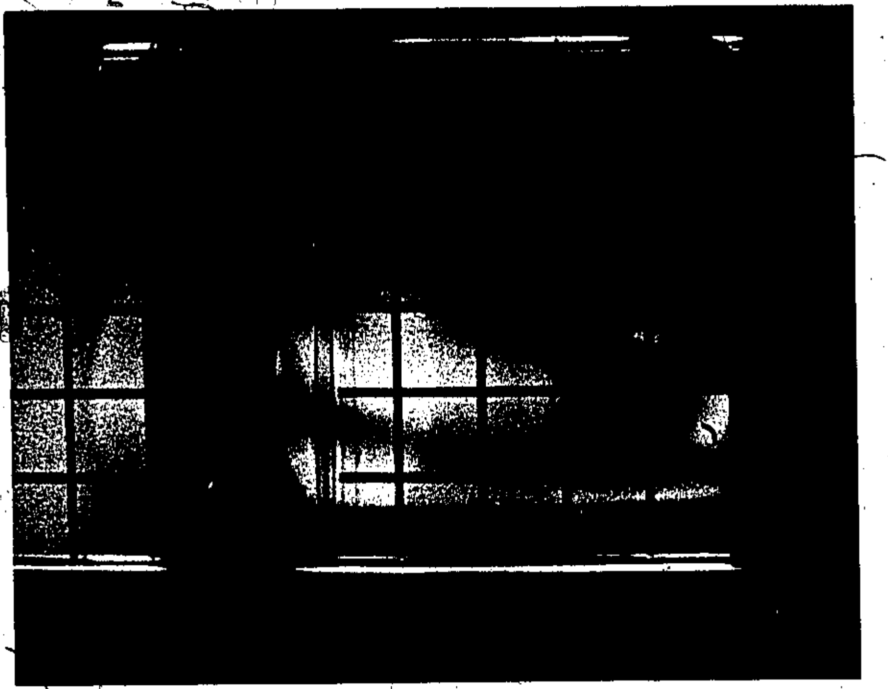

Photo 6.1 A flow visualization test for a laminar flow condition.

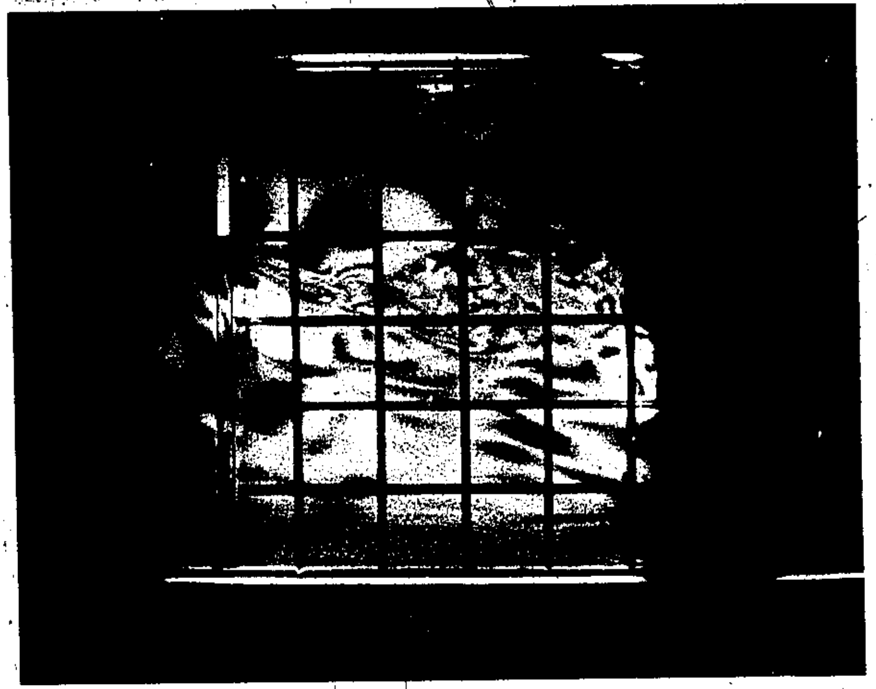

Photo 6.2 A flow visualization test for a turbulent flow condition.

APPENDIX C

Tables

TABLE 4.1

Effect of q on D_s

Upstream Water Depth H = 0.667 ft.

Test No.	q c.f.s./ft	α	D_s ft.	D_s/H	F
1	0.740	0.500	1.23	1.845	0.239
2	0.890	0.500	1.40	2.100	0.286
3	0.890	0.611	1.21	1.815	0.286
4	1.040	0.611	1.37	2.055	0.335
5	0.670	0.667	0.86	1.290	0.216
6	0.695	0.667	0.92	1.380	0.224
7	0.740	0.667	0.93	1.395	0.239
8	0.760	0.667	0.99	1.495	0.245
9	0.830	0.667	1.05	1.575	0.268
10	0.890	0.667	1.16	1.740	0.286
11	0.925	0.667	1.17	1.755	0.299
12	0.990	0.667	1.25	1.875	0.320
13	1.040	0.667	1.28	1.920	0.335
14	1.190	0.667	1.42	2.130	0.384
15	0.890	0.750	0.99	1.495	0.286
16	1.040	0.750	1.18	1.770	0.335
17	1.120	0.750	1.22	1.830	0.360
18	1.16	0.778	1.20	1.810	0.380
19	0.890	0.833	0.92	1.380	0.286
20	1.040	0.833	0.95	1.425	0.335
21	1.190	0.833	1.12	1.680	0.384
22	1.240	0.833	1.19	1.785	0.400
23	0.890	0.900	0.85	1.275	0.286
24	1.190	0.900	1.00	1.500	0.384
25	1.340	0.900	1.18	1.770	0.432
26	1.480	0.900	1.27	1.905	0.477

TABLE 4.2

Effect of H on D_s

opening ratio $\alpha = 0.667$

Test No.	q c.f.s./ft	H ft	v ft/sec	D_s ft	D_s/H	F
1	0.520	0.500	1.04	0.720	1.440	0.260
2	0.695	0.667	1.04	0.920	1.380	0.224
3	1.040	1.000	1.04	1.210	1.210	0.184
4	0.520	0.459	1.14	0.770	1.680	0.296
5	0.760	0.667	1.14	0.990	1.490	0.245
6	1.040	0.919	1.14	1.250	1.365	0.209
7	0.520	0.416	1.25	0.825	1.980	0.340
8	0.830	0.667	1.25	1.050	1.580	0.268
9	1.040	0.833	1.25	1.240	1.490	0.240
10	0.520	0.375	1.39	0.800	2.140	0.400
11	0.925	0.667	1.39	1.170	1.730	0.299
12	1.040	0.750	1.39	1.270	1.690	0.283

TABLE 4.3

Effect of α on D_s

Discharge $q = 0.89$ c.f.s./ft.

upstream water depth $H = 0.667$ ft.

Test No.	α	D_s	D_s/H
1	0.500	1.40	2.100
2	0.611	1.21	1.815
3	0.667	1.16	1.740
4	0.750	0.99	1.485
5	0.833	0.92	1.380
6	0.900	0.85	1.275

TABLE 4.4

Effect of θ on D_s

upstream water depth $H = 0.667$ ft.
opening ratio $\alpha = 0.667$
discharge $q = 0.89$ c.f.s./ft.

Test No.	θ degrees	θ radians	D_s ft.	D_s/H
1	30	0.523	1.180	1.770
2	45	0.785	1.170	1.755
3	60	1.045	1.160	1.740
4	90	1.570	1.158	1.737
5	120	2.090	1.125	1.688
6	135	2.355	1.085	1.628
7	150	2.615	0.950	1.425

APPENDIX D

Computer Programmes

```
C
C
C     **********************************************************************
C     THE TWO-DIMENSIONAL MODEL
C     **********************************************************************
C
C
C     SYMBOLS USED
C
C     X AND Y ARE SPACIAL COORDINATES
C     I AND J ARE INTEGERS IN THE DIRECTIONS X AND Y RESPECTIVELY
C     BSY(I,J)=STREAM-FUNCTION
C     U(I,J)=VELOCITY COMPONENT IN THE X-DIRECTION
C     V(I,J)=VELOCITY COMPONENT IN THE Y-DIRECTION
C     W(I,J,N)=VORTICITY FUNCTION
C     ALPHA(I),S(I),D(I),
C     ALPHA(I),S(I),D(I)=ARE MATRICES USED FOR THE GAUSS ELIMINATION
C     RN = REYNOLDS NUMBER
C     A = MESH SIZE
C     T = TIME INCREMENT
C
C
      DIMENSION BSY(70,19),V(70,19),U(70,37),W(70,37,2),ALPHA(70),S(70)
     1,D(70),WA(19,2)
      NS=15
      NS1=NS-1
      NS2=NS-3
      DO 2056 J=1,19
      DO 2056 N=1,2
      WA(J,N)=0.0
 2056 CONTINUE
      DO 36 I=1,70
      DO 36 J=1,19
      DO 36 NP1=1,2
      W(I,J,NP1)=0.0
   36 CONTINUE
      READ 1001,T,LL,RN
 1001 FORMAT (1F10.8,I10,1F10.2)
      PRINT 1002,T,LL,RN
 1002 FORMAT (5X,2HT=,F10.5,10X,3HLL=,I10,10X,3HRN=,1F10.2)
      READ 100,((BSY(I,J),J=1,19),I=1,70)
  100 FORMAT (16F5.3/3F5.3)
      ALT =1.0
      NJ=0.0
   51 NJ=NJ+1
      A=1./18.
      A2=A**2.
      RD =0.0
      AZ=(2.0*T)/A
      R=(2.0*T)/(A2*RN)
      R1=1.0-R
      R2=1.0+3.0*R
      A1=R
      C=R
      B=R2
      AL =-1.0
      K=1
      IF(NJ-1)49,49,50
   49 NP1=1
```

```
   50 CONTINUE
C     *************************************************************************
C     S.O.R. METHOD TO SOLVE FOR THE STREAM-FUNCTION
C     *************************************************************************
    6 AK=K
      OMEGA=1.7
      BIT=1.-OMEGA
      BO=OMEGA/4.
      IF(K-3)1000,1000,1100
 1100 IF((K/3)*3-K)2000,1000,1000
 1000 DO 1 I=2,69
      DO 1 J=2,18
      IF(I-26)8,17,8
   17 IF(J-NS)8,1,1
    8 X=(BSY(I-1,J)+BSY(I+1,J)+BSY(I,J+1)+BSY(I,J-1)+(A2*W(I,J,NP1)))
      X=(BIT*BSY(I,J))+(BO*X)
      D1=ABS(X-BSY(I,J))/BSY(1,19)
      BSY(I,J)=X
      IF(RD-D1)2,1,1
    2 RD=D1
    1 CONTINUE
      GO TO 3000
 2000 DO 4000 I=23,46
      DO 4000 J=8,18
      IF(I-26)5000,6000,5000
 6000 IF(J-NS)5000,4000,4000
 5000 X=(BSY(I-1,J)+BSY(I+1,J)+BSY(I,J+1)+BSY(I,J-1)+(A2*W(I,J,NP1)))
      X=(BIT*BSY(I,J))+(BO*X)
      D1=ABS(X-BSY(I,J))/BSY(1,19)
      BSY(I,J)=X
      IF(RD-D1)8000,4000,4000
 8000 RD=D1
 4000 CONTINUE
 3000 CONTINUE
      IF(RD-0.0002)11,7,7
    7 K=K+1
      RD =0.0
      IF(K-150)10,43,48
   10 GO TO 6
   11 CONTINUE
C     *************************************************************************
C     CALCULATION OF U AND V VELOCITY COMPONANTS
C     *************************************************************************
      DO 25 I=1,70
      DO 25 J=2,19
      U(I,2*J-2)=(BSY(I,J)-BSY(I,J-1))/A
   25 CONTINUE
      DO 24 I=1,69
      DO 24 J=1,19
      V(I,J)     =(BSY(I,J)-BSY(I+1,J))/A
   24 CONTINUE
      IF(NJ-1)41,41,42
   42 GO TO 43
   41 DO 30 I=2,69
      DO 30 J=2,18
      W(I,J,1)=(U(I,2*J-2)-U(I,2*J)+V(I,J)       -V(I-1,J))/A
   30 CONTINUE
   43 DO 56 J=NS,18
      DO 56 NN=1,2
      I=26
```

```
      W(I,J,NN)=-V(I-1,J)/(H/2.)
      WA(J,NN)=V(I,J)/(H/2.)
   56 CONTINUE
      ALT=AL*ALT
      IF(ALT)44,44,45
C     ****************************************************************
C     A.D.I.M. TO SOLVE FOR THE VORTICITY FUNCTION
C     ****************************************************************
C
C     ADVANCEMENT ALONG THE X-AXIS.
C
   44 NP1=2
      NM1=2
      N=1
      DO 200 J=NS,18
      DO 201 I=2,25
      G1             =((U(I,2*J)+U(I-1,2*J)+U(I-1,2*J-2)+U(I,2*J-2))*(W(I
     1,J,N)+W(I-1,J,N)))/8.0
      G2             =((U(I+1,2*J)+U(I,2*J)+U(I,2*J-2)+U(I+1,2*J-2))*(W(I+1
     1,J,N)+W(I,J,N)))/8.0
      G3             =((V(I,J)     +V(I-1,J)     +V(I-1,J-1)  +V(I,J-1))   *(W
     1(I,J,N)+W(I,J-1,N)))/8.0
      G4             =((V(I,   J+1)+V(I-1,   J+1)+V(I-1,J)     +V(I,J))     *(W(I
     1,J+1,N)+W(I,J,N)))/8.0
      IF(I-25)370,371,370
  371 IF(J-NS)370,372,370
  372 G2             =((U(I+1,2*J)+U(I,2*J)+U(I,2*J-2)+U(I+1,2*J-2))
     1*(0.5*(W(I+1,J,N)+WA(J,N))+W(I,J,N)))/8.0
      D(I)=R*(W(I,J-1,N)+W(I,J+1,N))+R1*W(I,J,NM1)+AZ*(G1-G2+G3-G4)
     1+R*0.5*(W(I+1,J,NP1)+WA(J,NP1))
      GO TO 201
  370 CONTINUE
      IF(I-2)201,310,311
  311 IF(I-25)312,313,201
  310 D(I)=R*(W(I,J-1,N)+W(I,J+1,N))+R1*W(I,J,NM1)+AZ*(G1-G2+G3-G4)+R*W(
     1I-1,J,NP1)
      GO TO 201
  312 D(I)=R*(W(I,J-1,N)+W(I,J+1,N))+R1*W(I,J,NM1)+AZ*(G1-G2+G3-G4)
      GO TO 201
  313 D(I)=R*(W(I,J-1,N)+W(J,J+1,N))+R1*W(I,J,NM1)+AZ*(G1-G2+G3-G4)+R*W(
     1I+1,J,NP1)
  201 CONTINUE
      ALPHA(2)=B
      S(2)=D(2)
      DO 215 I=3,25
      ALPHA(I)=B-((A1*C)/ALPHA(I-1))
      S(I)=D(I)+((A1*S(I-1))/ALPHA(I-1))
  215 CONTINUE
      W(25,J,NP1)=S(25)/ALPHA(25)
      DO 216 II=1,23
      I=25-II
      W(I,J,NP1)=(S(I)+(C*W(I+1,J,NP1)))/ALPHA(I)
  216 CONTINUE
      DO 314 I=27,69
      G1             =((U(I,2*J)+U(I-1,2*J)+U(I-1,2*J-2)+U(I,2*J-2))*(W(I
     1,J,N)+W(I-1,J,N)))/8.0
      G2             =((U(I+1,2*J)+U(I,2*J)+U(I,2*J-2)+U(I+1,2*J-2))*(W(I+1
     1,J,N)+W(I,J,N)))/8.0
      G3             =((V(I,J)     +V(I-1,J)     +V(I-1,J-1)  +V(I,J-1))   *(W
     1(I,J,N)+W(I,J-1,N)))/8.0
```

```
      G4          =((V(I,   J+1)+V(I-1,   J+1)+V(I-1,J)      +V(I,J))     *(W(I
     1,J+1,N)+W(I,J,N)))/8.0
      IF(I-27)373,374,373
  374 IF(J-NS)373,375,373
  375 G1                 =((U(I,2*J)+U(I-1,2*J)+U(I-1,2*J-2)+U(I,2*J-2))
     1*(W(I,J,N)+0.5*(W(I-1,J,N)+WA(J,N))))/8.0
      D(I)=R*(W(I,J-1,N)+W(I,J+1,N))+R1*W(I,J,NM1)+AZ*(G1-G2+G3-G4)
     1+R*0.5*(W(I-1,J,NP1)+WA(J,NP1))
      GO TO 314
  373 CONTINUE
      IF(I-27)314,315,316
  316 IF(I-69)317,318,314
  315 G1                 =((U(I,2*J)+U(I-1,2*J)+U(I-1,2*J-2)+U(I,2*J-2))*(W(I
     1,J,N)+WA(J,N))))/8.0
      D(I)=R*(W(I,J-1,N)+W(I,J+1,N))+R1*W(I,J,NM1)+AZ*(G1-G2+G3-G4)+R*WA
     1(J,NP1)
      GO TO 314
  317 D(I)=R*(W(I,J-1,N)+W(I,J+1,N))+R1*W(I,J,NM1)+AZ*(G1-G2+G3-G4)
      GO TO 314
  318 D(I)=R*(W(I,J-1,N)+W(I,J+1,N))+R1*W(I,J,NM1)+AZ*(G1-G2+G3-G4)+R*W(
     1I+1,J,NP1)
  314 CONTINUE
      ALPHA(27)=B
      S(27)=D(27)
      DO 217 I=28,69
      ALPHA(I)=B-((A1*C)/ALPHA(I-1))
      S(I)=D(I)+((A1*S(I-1))/ALPHA(I-1))
  217 CONTINUE
      W(69,J,NP1)=S(69)/ALPHA(69)
      DO 218 II=1,42
      I=69-II
      W(I,J,NP1)=(S(I)+(C*W(I+1,J,NP1)))/ALPHA(I)
  218 CONTINUE
  200 CONTINUE
      DO 319 J=2,NS1
      DO 320 I=2,69
      G1                 =((U(I,2*J)+U(I-1,2*J)+U(I-1,2*J-2)+U(I,2*J-2))*(W(I
     1,J,N)+W(I-1,J,N)))/8.0
      G2                 =((U(I+1,2*J)+U(I,2*J)+U(I,2*J-2)+U(I+1,2*J-2))*(W(I+1
     1,J,N)+W(I,J,N)))/8.0
      G3             =((V(I,J)      +V(I-1,J)      +V(I-1,J-1)  +V(I,J-1))   *(W
     1(I,J,N)+W(I,J-1,N)))/8.0
      G4          =((V(I,   J+1)+V(I-1,   J+1)+V(I-1,J)      +V(I,J))     *(W(I
     1,J+1,N)+W(I,J,N)))/8.0
      IF(J-NS1)360,361,360
  361 IF(I-26)360,362,360
  362 G4          =((V(I,   J+1)+V(I-1,   J+1)+V(I-1,J)      +V(I,J))     *
     1(0.5*(W(I,J+1,N)+WA(J+1,N))+W(I,J,N)))/8.0
      D(I)=R*(W(I,J-1,N)+0.5*(W(I,J+1,N)+WA(J+1,N)))+R1*W(I,J,NM1)
     1+AZ*(G1-G2+G3-G4)
      GO TO 320
  360 CONTINUE
      IF(I-2)320,321,322
  322 IF(I-69)323,324,320
  321 D(I)=R*(W(I,J-1,N)+W(I,J+1,N))+R1*W(I,J,NM1)+AZ*(G1-G2+G3-G4)+R*W(
     1I-1,J,NP1)
      GO TO 320
  323 D(I)=R*(W(I,J-1,N)+W(I,J+1,N))+R1*W(I,J,NM1)+AZ*(G1-G2+G3-G4)
      GO TO 320
  324 D(I)=R*(W(I,J-1,N)+W(I,J+1,N))+R1*W(I,J,NM1)+AZ*(G1-G2+G3-G4)+R*W(
```

```
     1I+1,J,NP1)
  320 CONTINUE
      ALPHA(2)=B
      S(2)=D(2)
      DO 213 I=3,69
      ALPHA(I)=B-((A1*C)/ALPHA(I-1))
      S(I)=D(I)+((A1*S(I-1))/ALPHA(I-1))
  213 CONTINUE
      W(69,J,NP1)=S(69)/ALPHA(69)
      DO 214 II=1,67
      I=69-II
      W(I,J,NP1)=(S(I)+(C*W(I+1,J,NP1)))/ALPHA(I)
  214 CONTINUE
  319 CONTINUE
      GO TO 800
C
C       ADVANCEMENT ALONG THE Y-AXIS
C
   45 NP1=1
      NM1=1
      N=2
      DO 219 I=2,25
      DO 220 J=2,18
      G1                  =((U(I,2*J)+U(I-1,2*J)+U(I-1,2*J-2)+U(I,2*J-2))*(W(I
     1,J,N)+W(I-1,J,N)))/3.0
      G2                  =((U(I+1,2*J)+U(I,2*J)+U(I,2*J-2)+U(I+1,2*J-2))*(W(I+1
     1,J,N)+W(I,J,N)))/3.0
      G3                  =((V(I,J)      +V(I-1,J)      +V(I-1,J-1)   +V(I,J-1))   *(W
     1(I,J,N)+W(I,J-1,N)))/8.0
      G4              =((V(I,   J+1)+V(I-1,   J+1)+V(I-1,J)      +V(I,J))      *(W(I
     1,J+1,N)+W(I,J,N)))/8.0
      IF(I-25)376,377,376
  377 IF(J-NS)376,378,376
  378 G2                  =((U(I+1,2*J)+U(I,2*J)+U(I,2*J-2)+U(I+1,2*J-2))
     1*(0.5*(W(I+1,J,N)+WA(J,N))+W(I,J,N)))/8.0
      D(J)=R*(W(I-1,J,N)+0.5*(W(I+1,J,N)+WA(J,N)))+R1*W(I,J,NM1)+
     1AZ*(G1-G2+G3-G4)
      GO TO 220
  376 CONTINUE
      IF(J-2)220,325,326
  326 IF(J-18)327,328,220
  325 D(J)=R*(W(I-1,J,N)+W(I+1,J,N))+R1*W(I,J,NM1)+AZ*(G1-G2+G3-G4)+R*W(
     1I,J-1,NP1)
      GO TO 220
  327 D(J)=R*(W(I-1,J,N)+W(I+1,J,N))+R1*W(I,J,NM1)+AZ*(G1-G2+G3-G4)
      GO TO 220
  328 D(J)=R*(W(I-1,J,N)+W(I+1,J,N))+R1*W(I,J,NM1)+AZ*(G1-G2+G3-G4)+R*W(
     1I,J+1,NP1)
  220 CONTINUE
      ALPHA(2)=B
      S(2)=D(2)
      DO 233 J=3,18
      ALPHA(J)=B-((A1*C)/ALPHA(J-1))
      S(J)=D(J)+((A1*S(J-1))/ALPHA(J-1))
  233 CONTINUE
      W(I,18,NP1)=S(18)/ALPHA(18)
      DO 234 JJ=1,16
      J=18-JJ
      W(I,J,NP1)=(S(J)+(C*W(I,J+1,NP1)))/ALPHA(J)
  234 CONTINUE
```

```
219 CONTINUE
    I=26
    DO 329 J=2,NS1
    G1             =(((U(I,2*J)+U(I-1,2*J)+U(I-1,2*J-2)+U(I,2*J-2))*(W(I
   1,J,N)+W(I-1,J,N)))/8.0
    G2            =(((U(I+1,2*J)+U(I,2*J)+U(I,2*J-2)+U(I+1,2*J-2))*(W(I+1
   1,J,N)+W(I,J,N)))/8.0
    G3            =(((V(I,J)      +V(I-1,J)     +V(I-1,J-1)   +V(I,J-1))  *(W
   1(I,J,N)+W(I,J-1,N)))/8.0
    G4            =(((V(I,    J+1)+V(I-1,    J+1)+V(I-1,J)     +V(I,J))    *(W(I
   1,J+1,N)+W(I,J,N)))/8.0
    IF(J-2)329,330,331
331 IF(J-NS1)332,333,329
330 D(J)=R*(W(I-1,J,N)+W(I+1,J,N))+R1*W(I,J,NM1)+AZ*(G1-G2+G3-G4)+R*W(
   1I,J-1,NP1)
    GO TO 329
332 D(J)=R*(W(I-1,J,N)+W(I+1,J,N))+R1*W(I,J,NM1)+AZ*(G1-G2+G3-G4)
    GO TO 329
333 G4            =(((V(I,    J+1)+V(I-1,    J+1)+V(I-1,J)     +V(I,J))    *
   1(0.5*(W(I,J+1,N)+WA(J+1,N))+W(I,J,N)))/8.0
    D(J)=R*(W(I-1,J,N)+W(I+1,J,N))+R1*W(I,J,NM1)+AZ*(G1-G2+G3-G4)
   1+R*0.5*(W(I,J+1,NP1)+WA(J+1,N))
329 CONTINUE
    ALPHA(2)=B
    S(2)=D(2)
    DO 236 J=3,NS1
    ALPHA(J)=B-((A1*C)/ALPHA(J-1))
    S(J)=D(J)+((A1*S(J-1))/ALPHA(J-1))
236 CONTINUE
    W(I,NS1,NP1)=S(NS1)/ALPHA(NS1)
    DO 237 JJ=1,NS2
    J=NS1-JJ
    W(I,J,NP1)=(S(J)+(C*W(I,J+1,NP1)))/ALPHA(J)
237 CONTINUE
    DO 334  I=27,69
    DO 335 J=2,18
    G1             =(((U(I,2*J)+U(I-1,2*J)+U(I-1,2*J-2)+U(I,2*J-2))*(W(I
   1,J,N)+W(I-1,J,N)))/8.0
    G2             =(((U(I+1,2*J)+U(I,2*J)+U(I,2*J-2)+U(I+1,2*J-2))*(W(I+1
   1,J,N)+W(I,J,N)))/8.0
    G3             =(((V(I,J)      +V(I-1,J)     +V(I-1,J-1)   +V(I,J-1))  *(W
   1(I,J,N)+W(I,J-1,N)))/8.0
    G4            =(((V(I,    J+1)+V(I-1,    J+1)+V(I-1,J)     +V(I,J))    *(W(I
   1,J+1,N)+W(I,J,N)))/8.0
    IF(I-27)335,336,337
336 IF(J-2)335,339,340
340 IF(J-NS)341,379,343
343 IF(J-18)342,344,335
339 D(J)=R*(W(I-1,J,N)+W(I+1,J,N))+R1*W(I,J,NM1)+AZ*(G1-G2+G3-G4)+R*W(
   1I,J-1,NP1)
    GO TO 335
341 D(J)=R*(W(I-1,J,N)+W(I+1,J,N))+R1*W(I,J,NM1)+AZ*(G1-G2+G3-G4)
    GO TO 335
379 G1              =(((U(I,2*J)+U(I-1,2*J)+U(I-1,2*J-2)+U(I,2*J-2))
   1*(W(I,J,N)+0.5*(W(I-1,J,N)+WA(J,N))))/8.0
    D(J)=R*(0.5*(W(I-1,J,N)+WA(J,N))+W(I+1,J,N))+R1*W(I,J,NM1)+
   1AZ*(G1-G2+G3-G4)
    GO TO 335
342 G1              =(((U(I,2*J)+U(I-1,2*J)+U(I-1,2*J-2)+U(I,2*J-2))*(W(I
   1,J,N)+WA(J,N)))/8.0
```

```
      D(J)=R*(WA(J,N    )+W(I+1,J,N))+R1*W(I,J,NM1)+AZ*(G1-G2+G3-G4)
      GO TO 335
  344 G1              =((U(I,2*J)+U(I-1,2*J)+U(I-1,2*J-2)+U(I,2*J-2))*(W(I
     1,J,N)+WA(J,N)))/8.0
      D(J)=R*(WA(J,N    )+W(I+1,J,N))+R1*W(I,J,NM1)+AZ*(G1-G2+G3-G4)+R*W(
     1I,J+1,NP1)
      GO TO 335
  337 CONTINUE
      IF(J-2)335,345,346
  346 IF(J-18)347,348,335
  345 D(J)=R*(W(I-1,J,N)+W(I+1,J,N))+R1*W(I,J,NM1)+AZ*(G1-G2+G3-G4)+R*W(
     1I,J-1,NP1)
      GO TO 335
  347 D(J)=R*(W(I-1,J,N)+W(I+1,J,N))+R1*W(I,J,NM1)+AZ*(G1-G2+G3-G4)
      GO TO 335
  348 D(J)=R*(W(I-1,J,N)+W(I+1,J,N))+R1*W(I,J,NM1)+AZ*(G1-G2+G3-G4)+R*W(
     1I,J+1,NP1)
  335 CONTINUE
      ALPHA(2)=B
      S(2)=D(2)
      DO 349 J=3,18
      ALPHA(J)=B-((A1*C)/ALPHA(J-1))
      S(J)=D(J)+((A1*S(J-1))/ALPHA(J-1))
  349 CONTINUE
      W(I,18,NP1)=S(18)/ALPHA(18)
      DO 350 JJ=1,16
      J=18-JJ
      W(I,J,NP1)=(S(J)+(C*W(I,J+1,NP1)))/ALPHA(J)
  350 CONTINUE
  334 CONTINUE
  800 CONTINUE
       IF(NJ-500)70,71,72
   70 IF(NJ-450)73,71,72
   73 IF(NJ-400)74,71,72
   74 IF(NJ-380)75,71,72
   75 IF(NJ-360)76,71,72
   76 IF(NJ-340)77,71,72
   77 IF(NJ-320)78,71,72
   78 IF(NJ-300)79,71,72
   79 IF(NJ-280)82,71,72
   82 IF(NJ-260)83,71,72
   83 IF(NJ-240)84,71,72
   84 IF(NJ-220)85,71,72
   85 IF(NJ-200)86,71,72
   86 IF(NJ-150)87,71,72
   87 IF(NJ-100)88,71,72
   88 IF(NJ-80 )89,71,72
   89 IF(NJ-60 )90,71,72
   90 IF(NJ-40 )91,71,72
   91 IF(NJ-20 )92,71,72
   92 IF(NJ-10 )93,71,72
   93 IF(NJ-5  )71,71,72
   71 PRINT 15,K,NJ
   15 FORMAT (1H1/5X,23HNO. OF ITERATION BSY =,I10,10X,3HNJ=,I10)
      PRINT 16,((BSY(I,J),J=1,19),I=1,70)
   16 FORMAT (5X,19F6.3)
      PRINT 500,NJ,((U(I,2*J-2),J=2,19),I=1,70)
  500 FORMAT (1H1/5X,10HVELOCITY U,10X,3HNJ=,I10/(5X,18F6.3))
      PRINT 400,NJ,((V(I,J),J=1,19),I=1,69)
  400 FORMAT (1H1/5X,10HVELOCITY V,10X,3HNJ=,I10/(5X,19F6.3))
```

```
      IF(NJ-1)80,80,81
   80 PRINT 600,NJ,(((W(I,J,NP1),J=1,19),I=1,70),NP1=1,1)
  600 FORMAT (1H1/5X,11HVORTICITY W,10X,3HNJ=,I10/(5X,19F6.3))
   81 CONTINUE
      PRINT 700,NJ,(((W(I,J,NP),J=2,18),I=1,26),NP=NP1,NP1)
  700 FORMAT (1H1/5X,10HADVANCED W,10X,3HNJ=,I10/(2X,17F7.2))
      PRINT 701,((W(J,N),J=13,18),N=NP1,NP1)
  701 FORMAT (79X,6F7.2)
      PRINT 702,(((W(I,J,NP),J=2,18),I=27,70),NP=NP1,NP1)
  702 FORMAT (2X,17F7.2)
   72 IF(NJ-LL)47,1800,1800
   47 GO TO 51
   48 PRINT 1900
 1900 FORMAT (2X,37HNO. OF ITERATION EXCEEDED 150 CYCLES )
 1800 STOP
      END
```

```
C
C
C     ***********************************************************************
C     THE THREE-DIMENSIONAL MODEL
C     ***********************************************************************
C
C
C     SYMPOLS USED
C
C     X AND Y ARE SPACIAL COORDINATES
C     I AND J ARE INTEGERS IN THE DIRECTIONS X AND Y RESPECTIVELY
C     BSY(I,J) = THE 3-D STREAM-FUNCTION
C     U(I,J) = DEPTH-AVERAGED VELOCITY COMPONENT IN THE X-DIRECTION
C     V(I,J) = DEPTH-AVERAGED VELOCITY COMPONENT IN THE Y-DIRECTION
C     VR(I,J) = RESULTANT VELOCITY
C     W(I,J) = THE VORTICITY FUNCTION
C     Z(I,J) = THE DEPTH FUNCTION
C     TW(I,J) = THE SHEAR STRESS FUNCTION
C     TWC = THE CRITICAL SHEAR STRESS
C     C1 = CHEZY COEFFICIENT
C     A = MESH SIZE
C     B = CHANNEL WIDTH
C
C     SUBROUTINES USED
C
C     (1) CORRE : CORRECTION FOR THE RESULTANT VELOCITY ALONG THE
C     SEPARATION LINE
C     (2) RAISE : CORRECTION FOR THE RESULTANT VELOCITY NEAR THE
C     NOSE OF THE DIKE
C     (3) SCAN : TURBULENCE CORRECTION FOR THE SHEAR FUNCTION
C     (4) SHED : SHEDDING CORRECTION TO THE VORTICITY FUNCTION
C     (5) NOSE : FOR DEPTH ADJUSTEMENT OF THE POINTS ON THE DIKES
C     NOSE AND THE ONE U/S OF IT IN THE DIAGONAL DIRECTION
C     (6) CONE : FOR DEPTH ADJUSTEMENTS OF ALL THE POINTS D/S THE
C     DIKE THAT HAS THE CONDITION TW(I,J)>TWC
C
C
      DIMENSION BSY(70,19),V(70,19),U(70,37),W(70,19),Z(70,19),VR(70,19)
     1,WA(10),TW(70,19)
      COMMON BSY,TW,U,V,W,Z,KKK,C1,C2,RW,ZO,CK,TWC,ZMAX,IO,JO,VR,WA,WWW
     1,WAAA,DMAX
      NS=15
      NK=60
      PW=0.5
      READ 250,LL,CK,TWC,UI,ZO
  250 FORMAT (I10,4F10.5)
      PRINT 260,LL,CK,TWC,UI,ZO
  260 FORMAT (2X,3HLL=,I10,2X,3HCK=,F10.5,2X,4HTWC=,F10.5,2X,3HUI=,F10.5
     1,2X,3HZ0=,F10.5)
      C=91.5
      C1=(62.4/(C**2))
      A=1./12.
      A2=A**2
      B=1.5
      READ 100, ((BSY(I,J),J=1,19),I=1,70)
  100 FORMAT (5F15.10/5F15.10/5F15.10/4F15.10)
      DO 36 I=1,70
      W(I,1)=0.0
      W(I,19)=0.0
```

```
 36 CONTINUE
    DO 60 I=1,70
    DO 60 J=1,19
    BSY(I,J)=BSY(I,J)*UI*D*ZO
    Z(I,J)=ZO
 60 CONTINUE
    PRINT 16,((BSY(I,J),J=1,19),I=1,70)
    DO 61 I=1,70
    DO 61 J=2,19
    U(I,2*J-2)=(BSY(I,J)-BSY(I,J-1))/(A*ZO)
 61 CONTINUE
    PRINT 500,NJ,((U(I,2*J-2),J=2,19),I=1,70)
    DO 62 I=1,69
    DO 62 J=1,19
    V(I,J)=(BSY(I,J)-BSY(I+1,J))/(A*ZO)
 62 CONTINUE
    PRINT 400,NJ,((V(I,J),J=1,19),I=1,69)
    DO 315 I=2,69
    DO 315 J=2,18
    W(I,J)=(U(I,2*J-2)-U(I,2*J)+V(I,J)-V(I-1,J))/A
315 CONTINUE
    I=26
    J=NS
    W(I,J)=(V(I,J)-V(I-1,J))/A
    DO 316 J=2,18
    W(1,J)=0.0
    W(70,J)=0.0
316 CONTINUE
    WAAA=W(26,NS)
    NJ=0.0
 51 NJ=NJ+1
C   ****************************************************************
C   CALCULATION OF THE SHEAR FUNCTION TW(I,J)
C   ****************************************************************
    CK=0.60
    IF(NJ-5)2505,2505,2506
2506 IF(NJ-10)2500,2500,2501
2501 IF(NJ-30)2502,2502,2503
2500 CK=0.85
    GO TO 2505
2502 CK=1.0
    GO TO 2505
2503 CK=1.2
2505 CONTINUE
    DO 340 I=2,69
    DO 340 J=2,18
    VR(I,J)=(((U(I,2*J-2)+U(I,2*J))/2.0)**2)+(((V(I,J)+V(I-1,J))/2.0)*
   1*2)
340 CONTINUE
    DO 341 I=1,70
    J=1
    VR(I,J)=U(I,2*J)**2
    J=19
    VR(I,J)=U(I,2*J-2)**2
341 CONTINUE
    DO 342 J=2,18
    I=1
    VR(I,J)=((U(I,2*J-2)+U(I,2*J))/2.0)**2
    I=70
    VR(I,J)=((U(I,2*J-2)+U(I,2*J))/2.0)**2
```

```
  342 CONTINUE
      DO 343 I=26,65
      DO 344 J=2,18
      IF(BSY(I,J)-BSY(1,19))344,5344,5344
 5344 I2=I
      J2=J
      CALL CORRE(I2,J2)
      J2=J-1
      CALL CORRE(I2,J2)
      J2=J+1
      CALL CORRE(I2,J2)
      GO TO 343
  344 CONTINUE
  343 CONTINUE
      DO 77 I=27,31
      DO 75 J=2,18
      I4=I
      J4=J
      IF(BSY(I,J)-BSY(1,19))75,76,76
   76 CALL RAISE(I4,J4)
      GO TO 77
   75 CONTINUE
   77 CONTINUE
      DO 66 I=1,70
      DO 66 J=1,19
      TW(I,J)=C1*VR(I,J)*((1.0+ABS((RW*W(I,J))/WAAA      ))**2)
   66 CONTINUE
      DO 320 I=27,69
      DO 170 J=1,18
      I1=I
      J1=J
      IF(BSY(I,J)-BSY(1,19))170,322,322
  322 IF(I-31)325,326,327
  327 IF(I-36)326,328,329
  329 IF(I-41)328,330,331
  331 IF(I-46)330,332,333
  333 IF(I-51)332,334,334
  325 KKK=0
      C2=0.2
      CALL SCAN (I1,J1)
      GO TO 320
  326 KKK=1
      CALL SCAN (I1,J1)
      GO TO 320
  328 KKK=2
      C2=0.1
      CALL SCAN (I1,J1)
      GO TO 320
  330 KKK=3
      CALL SCAN (I1,J1)
      GO TO 320
  332 KKK=4
      CALL SCAN (I1,J1)
      GO TO 320
  334 KKK=5
      CALL SCAN (I1,J1)
      GO TO 320
  170 CONTINUE
  320 CONTINUE
C
```

```
C       ***************************************************************
C       CALCULATION OF THE DEPTH FUNCTION Z(I,J)
C       ***************************************************************
        DO 350 I=2,69
        DO 350 J=2,18
        IF(I-29)3350,3350,3351
   3350 TWC=0.075
        GO TO 3352
   3351 TWC=0.090
   3352 CONTINUE
        Z(I,J)=Z(I,J)+(CK*(TW(I,J)-TWC))
        IF(Z(I,J)-ZO)41,41,42
     41 Z(I,J)=ZO
     42 CONTINUE
    350 CONTINUE
        Z(25,NS-1)=Z(26,NS)
        I5=25
        J5=NS-1
        DMAX=Z(I5,J5)
        CALL NOSE(I5,J5)
        I5=26
        J5=NS
        DMAX=Z(I5,J5)
        CALL NOSE(I5,J5)
        DO 5002 I=27,69
        DO 540 J=1,18
        IF(I-29)5540,5540,5541
   5540 TWC=0.075
        GO TO 5542
   5541 TWC=0.090
   5542 CONTINUE
        IF(BSY(I,J)-BSY(1,19))540,5001,5001
   5001 IF(TW(I,J)-TWC-0.001)540,540,520
    520 IO=I
        JO=J
        ZMAX=Z(IO,JO)
        CALL CONE
        JO=J-1
        ZMAX=Z(IO,JO)
        CALL CONE
        JO=J+1
        ZMAX=Z(IO,JO)
        CALL CONE
        GO TO 5002
    540 CONTINUE
   5002 CONTINUE
C       ***************************************************************
C       SOLUTION OF THE STREAM-FUNCTION BSY(I,J)
C       ***************************************************************
        RD=0.0
        K=1
      6 AK=K
        IF(K-3)1000,1000,1100
   1100 IF((K/3)*3-K)2000,1000,1000
   1000 DO 1 I=2,69
        DO 1 J=2,18
        IF(I-26)8,17,8
     17 IF(J-NS)8,1,1
      8 Z1=(Z(I,J)+Z(I,J-1))
        Z2=(Z(I,J+1)+Z(I,J))
```

```
      Z3=(Z(I+1,J)+Z(I,J))
      Z4=(Z(I,J)+Z(I-1,J))
      ZB=(1./Z1)+(1./Z2)+(1./Z3)+(1./Z4)
      X   =    ((BSY(I,J-1)/Z1)+(BSY(I,J+1)/Z2)+(BSY(I+1,J)/Z3)+(BSY(I-1
     1,J)/Z4)+(0.5*A2*W(I,J)))/ZB
      D1=ABS(X-BSY(I,J))/BSY(1,19)
      BSY(I,J)=X
      IF(RD-D1)2,1,1
    2 RD=D1
    1 CONTINUE
      GO TO 3000
 2000 DO 4000 I=23,46
      DO 4000 J=8,18
      IF(I-26)5000,6000,5000
 6000 IF(J-NS)5000,4000,4000
 5000 Z1=(Z(I,J)+Z(I,J-1))
      Z2=(Z(I,J+1)+Z(I,J))
      Z3=(Z(I+1,J)+Z(I,J))
      Z4=(Z(I,J)+Z(I-1,J))
      ZB=(1./Z1)+(1./Z2)+(1./Z3)+(1./Z4)
      X   =    ((BSY(I,J-1)/Z1)+(BSY(I,J+1)/Z2)+(BSY(I+1,J)/Z3)+(BSY(I-1
     1,J)/Z4)+(0.5*A2*W(I,J)))/ZB
      D1=ABS(X-BSY(I,J))/BSY(1,19)
      BSY(I,J)=X
      IF(RD-D1)8000,4000,4000
 8000 RD=D1
 4000 CONTINUE
 3000 CONTINUE
      IF(RD-0.0002)11,7,7
    7 K=K+1
      RD =0.0
      IF(K-150)10,48,48
   10 GO TO 6
   11 CONTINUE
C     ******************************************************************
C     CALCULATION OF THE VELOCITY COMPONENTS U(I,J) AND V(I,J)
C     AND THE VORTICITY FUNCTION W(I,J)
C     ******************************************************************
      DO 25 I=1,70
      DO 25 J=2,19
      U(I,2*J-2)=((BSY(I,J)-BSY(I,J-1))/A)*(2.0/(Z(I,J)+Z(I,J-1)))
   25 CONTINUE
      DO 24 I=1,69
      DO 24 J=1,19
      V(I,J)=((BSY(I,J)-BSY(I+1,J))/A)*(2.0/(Z(I,J)+Z(I+1,J)))
   24 CONTINUE
      DO 30 I=2,69
      DO 30 J=2,18
      W(I,J)=(U(I,2*J-2)-U(I,2*J)+V(I,J)-V(I-1,J))/A
   30 CONTINUE
      I=26
      J=NS
      W(I,J)=(V(I,J)-V(I-1,J))/A
      IF(NJ.EQ.1)GO TO 1151
      IF((NJ/NK)*NK-NJ)1150,1151,1151
 1151 CONTINUE
      PRINT 505,NJ,((VR(I,J),J=1,19),I=1,70)
  505 FORMAT (1H1/5X,21HRESULTANT VELOCITY VR,10X,3HNJ=,I10/(5X,19F6.3))
      PRINT 800,NJ,((TW(I,J),J=1,19),I=1,70)
  800 FORMAT (1H1/5X,21HSHEAR STRESS FORCE TW,10X,3HNJ=,I10/(5X,19F6.3))
```

```
      PRINT 510,((Z(I,J),J=1,19),I=1,70)
  510 FORMAT (1H1/5X,23HEXCAVATED SCOUR DEPTH Z/(5X,19F6.3))
      PRINT 5,K,NJ
    5 FORMAT (1H1/ 5X,23HNO. OF ITERATION BSY =,I10,10X,3HNJ=,I10 )
      PRINT 16,((BSY(I,J),J=1,19),I=1,70)
   16 FORMAT (5X,19F6.3)
      PRINT 600,NJ,((W(I,J),J=2,18),I=1,70)
  600 FORMAT (1H1/5X,11HVORTICITY W,10X,3HNJ=,I10/(5X,17F7.3))
 1150 CONTINUE
      IF(NJ-LL)150,151,151
  150 GO TO 51
   48 PRINT 50
   50 FORMAT (30HNO. OF ITERATION EXCEEDED 150 )
  151 CONTINUE
      STOP
      END
C     ..............................................................
      SUBROUTINE CORRE(I2,J2)
C     ..............................................................
      DIMENSION BSY(70,19),TW(70,19),U(70,37),V(70,19),W(70,19),Z(70,19)
     1,VR(70,19),WA(10)
      COMMON BSY,TW,U,V,W,Z,KKK,C1,C2,RW,ZO,CK,TWC,ZMAX,IO,JO,VR,WA,WWW
     1,WAAA,DMAX
      I=I2
      J=J2
      WA(1)=U(I,2*J)**2+V(I-1,J)**2
      WA(2)=U(I,2*J)**2+V(I,J)**2
      WA(3)=U(I,2*J-2)**2+V(I,J)**2
      WA(4)=U(I,2*J-2)**2+V(I-1,J)**2
      RD=0.0
      DO 4 K=1,4
      D=ABS(WA(K)-0.0)
      IF(RD-D)3,4,4
    3 RD=D
    4 CONTINUE
      VR(I,J)=RD
      RETURN
      END
C     ..............................................................
      SUBROUTINE FALSE (I4,J4)
C     ..............................................................
      DIMENSION BSY(70,19),TW(70,19),U(70,37),V(70,19),W(70,19),Z(70,19)
     1,VR(70,19),WA(10)
      COMMON BSY,TW,U,V,W,Z,KKK,C1,C2,RW,ZO,CK,TWC,ZMAX,IO,JO,VR,WA,WWW
     1,WAAA,DMAX
      I=I4
      J=J4
      VR(I,J)=1.3*VR(I,J)
      RETURN
      END
C     ..............................................................
      SUBROUTINE SCAN (I1,J1)
C     ..............................................................
      DIMENSION BSY(70,19),TW(70,19),U(70,37),V(70,19),W(70,19),Z(70,19)
     1,VR(70,19),WA(10)
      COMMON BSY,TW,U,V,W,Z,KKK,C1,C2,RW,ZO,CK,TWC,ZMAX,IO,JO,VR,WA,WWW
     1,WAAA,DMAX
      I=I1
      J=J1
      II=J-KKK
```

```
      JJ=J+KKK
      IF(JJ-18)15,15,16
   16 JJ=18
   15 CONTINUE
      IF(II-2)17,18,18
   17 II=2
   18 CONTINUE
      DO 20 J=II,JJ
      TW(I,J)=C1*VR(I,J)*((1.0+ABS((RW*W(I,J))/WAAA      )+C2)**2)
   20 CONTINUE
      I=I1
      J=J1
      I3=I
      J3=J
      IF(I-28)25,25,26
   26 CONTINUE
      CALL SHED (I3,J3)
      TW(I,J)=C1*VR(I,J)*((1.0+ABS((RW*WWW)/WAAA      )+C2)**2)
      I3=I
      J3=J-1
      CALL SHED (I3,J3)
      I=I3
      J=J3
      TW(I,J)=C1*VR(I,J)*((1.0+ABS((RW*WWW)/WAAA      )+C2)**2)
   25 CONTINUE
      RETURN
      END
C     ..................................................................
      SUBROUTINE SHED (I3,J3)
C     ..................................................................
      DIMENSION BSY(70,19),TW(70,19),U(70,37),V(70,19),W(70,19),Z(70,19)
     1,VR(70,19),WA(10)
      COMMON BSY,TW,U,V,W,Z,KKK,C1,C2,RW,ZO,CK,TWC,ZMAX,IO,JO,VR,WA,WWW
     1,WAAA,DMAX
      I=I3
      J=J3
      AI=I3
      WWW=W(I,J)+(0.5*W(26,13)*((1.0-((AI-26.0)/39.0))**2))
      RETURN
      END
C     ..................................................................
      SUBROUTINE NOSE(I5,J5)
C     ..................................................................
      DIMENSION BSY(70,19),TW(70,19),U(70,37),V(70,19),W(70,19),Z(70,19)
     1,VR(70,19),WA(10)
      COMMON BSY,TW,U,V,W,Z,KKK,C1,C2,RW,ZO,CK,TWC,ZMAX,IO,JO,VR,WA,WWW
     1,WAAA,DMAX
      IO=I5
      JO=J5
      K=JO+1
      KK=IO+1
      DO 1 I=IO,70
      DX=(I-IO)/12.0
      DO 2 J=JO,19
      DY=(J-JJ)/12.0
      X=DMAX-(((DX**2+DY**2)/3.0)**0.5)
      IF(Z(I,J)-X)3,3,2
    3 Z(I,J)=X
    2 CONTINUE
      DO 4 JJ=1,JO
```

```
      J=K-JJ
      DY=(J-JO)/12.0
      X=DMAX-(((DX**2+DY**2)/3.0)**0.5)
      IF(Z(I,J)-X)5,5,4
    5 Z(I,J)=X
    4 CONTINUE
    1 CONTINUE
      DO 6 II=1,IO
      I=KK-II
      DX=(I-IO)/12.0
      DO 7 J=JO,19
      DY=(J-JO)/12.0
      X=DMAX-(((DX**2+DY**2)/3.0)**0.5)
      IF(Z(I,J)-X)8,8,7
    8 Z(I,J)=X
    7 CONTINUE
      DO 9 JJ=1,JO
      J=K-JJ
      DY=(J-JO)/12.0
      X=DMAX-(((DX**2+DY**2)/3.0)**0.5)
      IF(Z(I,J)-X)10,10,9
   10 Z(I,J)=X
    9 CONTINUE
    6 CONTINUE
      RETURN
      END
C     ..............................................................
      SUBROUTINE CONE
C     ..............................................................
      DIMENSION BSY(70,19),TW(70,19),U(70,37),V(70,19),W(70,19),Z(70,19)
     1,VR(70,19),WA(10)
      COMMON BSY,TW,U,V,W,Z,KKK,C1,C2,RW,ZO,CK,TWC,ZMAX,IO,JO,VR,WA,WWW
     1,WAAA,DMAX
      IMAX=20.76*(ZMAX-ZO)+0.5+IO
      JMAX=20.76*(ZMAX-ZO)+0.5+JO
      A=1./12.
      DO 1 I=IO,IMAX
      IF(I-70)16,16,17
   17 GO TO 1
   16 CONTINUE
      DX=(I-IO)*A
      DO 2 J=JO,JMAX
      DY=(J-JO)*A
      X=ZMAX-SQRT((DX**2+DY**2)*0.3333)
      IF(J-19)18,18,19
   19 GO TO 4
   18 CONTINUE
      IF(Z(I,J)-X)3,3,4
    3 Z(I,J)=X
    4 JP=2*JO-J
      IF(JP-1)20,21,21
   20 GO TO 2
   21 CONTINUE
      IF(Z(I,JP)-X)5,5,6
    5 Z(I,JP)=X
    6 IF(Z(I,JP)-ZO)1,1,2
    2 CONTINUE
    1 CONTINUE
      RETURN
      END
```

APPENDIX E

REFERENCES

1. Ahmad, M., Experiments on Design and Behaviour of Spur-Dikes, Proceedings, Minnesota International Hydraulics Convention, Minneapolis, Minnesota, Sept., 1953.

2. Ahmed, N., Mechanism of Erosion Below Hydraulic Works, Proceedings, Minnesota International Hydraulic Convention, Minneapolis, Minnesota, Sept., 1953.

3. Awazu, S., On Scour Around Spur-Dike, Proc. 12th Congress of the International Association for Hydraulic Research, Sept., 1967.

4. Blench, T., Regime Behaviour of Canals and Rivers, Butterworths Scientific Publications, London, 1957.

5. Chee, S.P., and Zaghloul, N., Effect of Engineering Structures on the Regime of Waterways, 8th American Water Resources Conference, St. Louis, Missouri, U.S.A., 1972.

6. Chow, V.T., Open-Channel Hydraulics, McGraw-Hill Book Company, Inc., New York, N.Y., 1959.

7. Chow, V.T., Handbook of Applied Hydrology, McGraw-Hill Book Company, Inc., New York, N.Y., 1964.

8. DeWiest, R.J.M., Geohydrology, John Wiley and Sons, Inc., New York, N.Y., 1967.

9. Doddiah, D., Albertson, M., and Thomas, R., Scour From Jets, Proceedings, Minnesota International Hydraulic Convention, Minneapolis, Minnesota, Sept., 1953.

10. DuBoys, P., LeRhone et Les Rivieres a Lit Affouillable, Annals des Pouts et Chaussees, Series 5, Vol. 18, 1879.

11. Einstein, H.A., The Bed-Load Function for Sediment Transportation in Open Channel Flows, United States Department of Agriculture, Soil Conservation Service, Washington, D.C., Technical Bulletin 1026, September 1950.

12. Flaxman, E.M., Channel Stability in Undisturbed Cohesive Soils, Journal of Hydr. Div., Vol. 89, HY2, March, 1963.

13. Frankel, S., Convergence Rates of Iterative Treatments of Partial Differential Equations, Math. Tables Aids Computations, Vol. 4, 1950

14. Fromm, J.E., A Method for Computing Nonsteady, Incompressible, Viscous Fluid Flows, Los Alamos Scientific Laboratory, University of California, Los Alamos, New Mexico, 1963.

15. Gill, M.A., Erosion of Sand Beds Around Spur-Dikes, Journal of the Hyd. Div., ASCE, Vol. 98, HY9, Sept., 1972.

16. Grade, R.J., Subramanya, K., and Nambudripad, K.D., Study of Scour Around Spur-Dikes, Journal of the Hyd. Div., ASCE, Vol. 87, HY6, Nov., 1961.

17. Graf, W.H., Hydraulics of Sediment Transport, McGraw-Hill Book Co., Inc., New York, N.Y., 1971.

18. Griffith, W.M., A Theory of Silt Transportation, Transactions, ASCE, Vol. 104, 1939.

19. Henderson, F.M., Open Channel Flow, The MacMillan Company, New York, N.Y., 1966.

20. Hinze, J.O., Turbulence, McGraw-Hill Book Co., Inc., New York, N.Y., 1959.

21. Johnson, C.O., Similarity in Scour Below a Spillway, Thesis presented at the University of Minnesota, Minneapolis, Minnesota, in 1950, in partial fulfillment of the requirements of Master of Science.

22. Khosla, A.N., Design of Weir on Permeable Foundations, Central Board of Irrigation, India Publication No. 12, 1936.

23. Kindsvater, C.E., Carter, R.W., and Tracey, H.J., Computations of Peak Discharge at Contractions, U.S. Geological Survey, Circular No. 284, 1953.

24. Kindsvater, C.E., and Carter, R.W., Tranquil Flow Through Open-Channel Constrictions, Transactions, ASCE, Vol. 120, 1955.

25. Lacey, G., A General Theory of Flow in Alluvium, Journal of Institute of Civil Engineers, Vol. 27, 1939.

26. Langhaar, H.L., Dimensional Analysis and Theory of Models, John Wiley and Sons, Inc., New York, N.Y., 1951.

27. Laursen, E.M., Observations on the Nature of Scour, Proc. 5th Hydr. Conf., State University of Iowa, Iowa City, Iowa, Bulletin 34, June, 1952.

28. Laursen, E.M., and Toch, A., A Generalized Model Study of Scour Around Bridge Piers and Abutments, Proceedings, Minnesota International Hydraulic Convention, Minneapolis, Minnesota, Sept., 1953.

29. Laursen, E.M., Scour at Bridge Crossings, Journal of Hydr. Div., ASCE, Vol. 86, HY2, Feb., 1960.

30. Laursen, E.M., An Analysis of Relief Bridge Scour, Journal of Hydr. Div., ASCE, Vol. 89, HY3, May, 1963.

31. Liu, H.K., and Skinner, M.M., Laboratory Observations of Scour at Bridge Abutments, Highway Research BD., Bulletin No. 242, 1960.

32. Neville, A.M., and Kennedy, J.B., Basic Statistical Methods for Engineers and Scientists, International Textbook Co., Scranton, Pa., 1964.

33. O'Brien, G.G., Hyman, M.A., and Kaplan, S., A Study of the Numerical Solution of Partial Differential Equations, J. Math. Physics, Vol. 29, 1951.

34. Peaceman, D.W., and Rachford, H.H., The Numerical Solution of Parapolic and Elliptic Differential Equations, The American Mathematical Society, Vol. 3, March, 1955.

35. Richardson, E.V., and Simons, D.B., Resistance of Flow in Sand Channels, Proc. 12th Congress of the International Association for Hydraulic Research, Vol. 1, Sept., 1967.

36. Rouse, H., Fluid Mechanics for Hydraulic Engineers, McGraw-Hill Book Company, Inc., New York, N.Y., 1938.

37. Rouse, H., Criteria for Similarity in the Transportation of Sediment, Proceedings of 1st Hydraulic Conference, State University of Iowa, Iowa City, Iowa, Bulletin 20, March, 1940.

38. Rouse, H., Engineering Hydraulics, John Wiley and Sons, Inc., New York, 1958.

39. Schneible, D.E., An Investigation of the Effect of Bridge Pier Shape on the Relative Depth of Scour, Thesis presented at the State University of Iowa, Iowa, in 1951, in partial fulfillment of the requirements for the degree of Master of Science.

40. Shen, H.W., Schneider, V.R., and Karaki, S., Local Scour Around Bridge Piers, Journal of Hydr. Div., ASCE, Vol. 95, HY6, Nov., 1969.

41. Shields, A., Anwendung der Aehnlichkeitsmechanik und der Turbulenz forschung auf die Geschiebebewegung, (Application of Similarity Principles and Turbulence Research to Bed-Load Movement), Mitteilungen der Preuss. Versuchsanst fur Wasserbau und Schiffbau, Berlin, No. 26, 1936. Available also in translation by Ott, W.P., and Van Uchelen, J.C., U.S.C.S. Cooperative Laboratory, California Institute of Technology, Pasadena, California.

42. Simons, D.B., and Albertson, M.L., Uniform Water Conveyance Channels in Alluvial Material, Proceedings, ASCE, Vol. 86, HY5, May, 1960.

43. Smith, G.D., Numerical Solution of Partial Differential Equations, Oxford University Press, London, 1965.

44. Straub, L.G., Effect of Channel Contraction Works Upon Regime of Movable Beds, Transactions, American Geophysical Union, Part II, 1934.

45. Straub, L.G., Approaches to the Study of the Mechanics of Bed Movement, Proceedings, 1st Hydraulics Conference of Iowa Studies in Engineering, Iowa City, Iowa, 1940.

46. Straub, L.G., Missouri River Report, House Document 238, Corps of Engineers, U.S. Department of the Army, to 73rd U.S. Congress, 2nd session, 1946.

47. Tanaka, S., and Yano, M., Local Scour Around a Circular Cylinder, Colorado International Hydraulic Convention, Vol. 3, Fort Collins, Colorado, Sept., 1967.

48. Tarapore, Z.S., Scour Below a Submerged Sluice Gate, Thesis presented at the University of Minnesota, Minneapolis, Minnesota, in 1956, in partial fulfillment of the requirements of Master of Science.

49. Tarapore, Z.S., Determination of the Depth of Scour Around an Obstruction in an Alluvial Channel, Proceedings, Colorado International Hydraulic Convention, Vol. 3, Fort Collins, Colorado, Sept., 1967.

50. Thomas, Z., An Interesting Hydraulic Effect Occurring at Local Scour, Proceedings, Colorado International Hydraulic Convention, Vol. 3, Fort Collins, Colorado, Sept. 1967.

51. Tracy, H.J., and Carter, R.J., Backwater Effects of Open-Channel Constrictions, Transactions, ASCE, Vol. 120, 1955.

52. Trutt, F.C., Erdelyi, E.A., and Jackson, R.F., The Nonlinear Potential Equation and Its Numerical Solution for Highly Saturated Electric Machines, IEEE Trans. AS-1, 1963.

53. Vallentine, H.R., Applied Hydrodynamics, Butterworths Scientific Publications, London, 1959.

54. Young, D., Iterative Methods for Solving Partial Difference Equations of Elliptic Type, Trans. Amer. Math. Soc., Vol. 76, 1954.

55. Young, D., The Numerical Solution of Elliptic and Parabolic Partial Differential Equations, Chap. 11, Survey of Numerical Analysis, ed. J. Todd, McGraw-Hill Book Company, Inc., 1962.

56. Young, D., and Wheeler, M.F., Alternating Direction Methods for Solving Partial Difference Equations, in Nonlinear Problems in Engineering, ed. W.F. Ames, Academic Press, New York, N.Y., 1964.

APPENDIX F

NOMENCLATURE

A	Fourier coefficient
a	mesh size
B	channel width
b	size of obstruction
C	constants
c	Chezy coefficient
C_1, C_2	dimensionless velocity gradients
C_c	coefficient of contraction
D	water depth
D_s	maximum scour depth
D_{ji}	deformation tensor
d	mean size of bed material
d_{85}	full diameter (85% finer by weight)
F	Froude number
F_i	external body force
$f( )$	function
g	acceleration due to gravity
H	upstream water depth
i, j, k	indices
k	superscripts indicating iteration cycles
k_1, k_2, k_3	constants

M,N	maximum node number
N	a numerical exponent
n	Manning's roughness coefficient
n	superscript indicating time
O(-)	order of the error
p,q	subscripts
$\bar{P}$	ensemble average
Q	total discharge
q	discharge per unit width
R	error ratio
R_N	Reynolds number
r	$= \frac{2(\nu+\xi)\ \delta t}{a^2}$
r_1	$= \frac{2\ \delta t}{a}$
S	channel slope
S_s	specific gravity
T	temperature
t	time
δt	time step
$\delta t'$	dimensionless time step
U_i, u_i, u_j	velocity tensor
u,v	x and y velocity components
u', v'	x and y dimensionless velocity components
u'', v''	x and y depth average velocity components
v	mean approaching velocity
V_R	average velocity

v_s	particle fall velocity
$\forall$	unit volume
w	over relaxation factor
x,y,z	cartesian coordinates
Δz	eroded depth increment
α	opening ratio
α_1	constant
γ	specific weight
δ_{ji}	kronecker delta
$\varepsilon_{i,j,n}$	error
θ	angle of attack
λ	eddy viscosity
μ	dynamic viscosity
ν	kinematic viscosity
ξ	kinematic eddy viscosity
ρ	$= 1/r = \frac{a^2}{2\ \delta t(\nu+\xi)}$
ρ_f	fluid density
Σ	summation
σ_{ji}	stress tensor
τ	shear stress
τ_c	critical shear stress
ϕ	function
ψ	stream function
ψ'	dimensionless stream function
ψ''	depth average stream function
ψ_o	reference stream function
ω	vorticity

ω'	dimensionless vorticity
ω_o	reference vorticity

VITA AUCTORIS

1945	Born on the 22nd of March in Damanhour, Egypt.
1961	Matriculated from Orman High School, Cairo, Egypt.
1966	Graduated with a Bachelor of Science in Civil Engineering, Ein Shams University, Cairo, Egypt.
1966	Appointed as an instructor of Civil Engineering at Ein Shams University, Cairo, Egypt.
1970	Obtained a Master of Applied Science in Civil Engineering, University of Windsor, Windsor, Ontario, Canada.
1970	Registered as a Ph.D. candidate in Civil Engineering at the University of Windsor, Windsor, Ontario, Canada.